Title
Applying Effective Theories to Collider Phenomenology

Author
Ovanesyan, Grigol

Publication Date
2010

Peer reviewed|Thesis/dissertation

Applying Effective Theories to Collider Phenomenology

by

Grigol Gagikovich Ovanesyan

A dissertation submitted in partial satisfaction of the

requirements for the degree of

Doctor of Philosophy

in

Physics

in the

Graduate Division

of the

University of California, Berkeley

Committee in charge:

Professor Christian Bauer, Co-Chair

Professor Yasunori Nomura, Co-Chair

Professor Hitoshi Murayama

Professor Nicolai Reshetikhin

Fall 2010

Applying Effective Theories to Collider Phenomenology

Abstract

Applying Effective Theories to Collider Phenomenology

by

Grigol Gagikovich Ovanesyan

Doctor of Philosophy in Physics

University of California, Berkeley

Professor Christian Bauer, Co-Chair

Professor Yasunori Nomura, Co-Chair

Collinear fields in soft collinear effective theory (SCET) can be made invariant under collinear gauge transformations by multiplying them with collinear Wilson lines. We discuss how we can quantize SCET directly in terms of these gauge invariant fields, allowing to directly calculate S matrix elements using the gauge invariant collinear fields. We also show how for each collinear direction SCET can be written in terms of fields whose interactions are given by the usual QCD Lagrangian, and how external operators coupling these different directions can be constructed.

Using SCET, which provides a unified framework for factorization, resummation of logarithms, and incorporation of universal nonperturbative functions in hard-scattering QCD cross-sections, we present a new prediction of angularity distributions in e^+e^- annihilation. Angularities τ_a are an infinite class of event shapes which vary in their sensitivity to the substructure of jets in the final state, controlled by a continuous parameter $a < 2$. We calculate angularity distributions for all $a < 1$ to first order in the strong coupling α_s and resum large logarithms in these distributions to next-to-leading logarithmic (NLL) accuracy. Our expressions for the next-to-leading order (NLO) $\mathcal{O}(\alpha_s)$ partonic jet and soft functions in the factorization theorem for angularity distributions are given for the first time. We employ a model for the nonperturbative soft function with a gap parameter which cancels the renormalon ambiguity in the partonic soft function. We explore the relation between the SCET approach to resummation and past approaches in QCD, and discuss the advantages of the effective theory approach. In addition, we draw from the NLO calculations of the jet and soft functions an intuitive lesson about how factorization breaks down in the effective theory as $a \to 1$.

A matching calculation for SCET is performed using exotic external states, which mimic the topology of Drell-Yan amplitude. It is found that for the consistency of effective theory, more specifically for the fact that the matching coefficient C_2 is independent of external states involved in the matching, a new mode needs to be added to SCET, which is the Glauber mode. Connections with Coleman-Norton theorem and Landau equations are discussed.

To the memory of my father,

Gagik Ovanesyan

Contents

List of Figures

List of Tables

Acknowledgments

I want to thank all my collaborators at UC Berkeley which include Christian Bauer, Oscar Cata, Marat Freytsis, Andrew Hornig, Björn Lange, Chris Lee, and Jesse Thaler. My views and approach to physics have been influenced by these people. Especially I want to thank my advisor Christian Bauer for always being helpful and for being a great advisor.

Also I want to thank the entire Department of Physics of UC Berkeley for being so supportive all five years that I have spent here. Special thanks to Anne Takizawa and Donna Sakima for their help and for having answers to all my numerous questions that I had for them.

I want to thank my fiance Olga Serafimova, brother Zaven Ovanesyan and my mother Rita Bagdasarova for their constant encouragement. I also want to say a special thanks to my grandmother Zina Galustyan for everything that she has done for me.

Chapter 1

Introduction

The Standard Model (SM) has proven to be a very successful theory, withstanding all experimental tests over the past forty years. One of the most important tasks in the modern stage of Particle Physics is finding New Physics (NP), especially since the Large Hadron Collider (LHC) is already running and gathering data. Consequently, it is extremely important to work on strategies to identify which one, if any, of the Beyond the Standard Model (BSM) theories is the right description of Nature. In order to discover a BSM theory in a high energy experiment, one should have a thorough understanding of the SM backgrounds. Gaining such an understanding is a challenge because most backgrounds are dominated by strong interactions, for which the Perturbation Theory (PT) is poorly convergent.

Nevertheless, powerful tools have been developed to make reliable predictions for QCD cross-sections at high energies. There are three key concepts for such predictions: asymptotic freedom, factorization, and universality of non-perturbative physics. The basic idea is that at high energies the cross-section factorizes into long distance (non-perturbative) and short distance (perturbative) parts. The latter is pertubatively calculable due to asymptotic freedom, whereas the former is often universal and can be extracted from one process and used in another.

Historically, first proofs of factorization used pinch analysis of Feynman diagrams. In this approach one finds all the infrared singularities of an amplitude to all orders in PT. This can be done for example via use of Landau Equations [117]. Then the leading behavior of an amplitude is studied by approximating it with contributions coming from pinched surfaces. All such leading contributions are shown to factorize order by order in PT. This is the famous Collins-Soper-Sterman type approach to factorization (see for example [142] and the references therein).

More recently the ideas of factorization have been revisited from the point of view of Effective Field Theory (EFT). The simplest effective theory is the four-Fermi theory, where one integrates out the heavy particle, in this case the $W-$boson. However, to prove factorization theorems more complex effective theories are used, such as Non-Relativistic QCD (NRQCD), Heavy Quark Effective Theory (HQET) and Soft Collinear Effective Theory (SCET). In such theories one integrates out of the QCD Lagrangian kinematically suppressed modes for a certain process, and constructs an effective Lagrangian, including only the relevant long-distance modes. Factorization arises in a natural and intuitive way in the language of EFT.

Another benefit coming from the use of Effective field theories is clean resummation of large logarithms which can be achieved for all ratios of physical energy scales in the problem. These

are the famous Sudakov logarithms of the ratios of the physical energy scales. Such logarithms arise at any order in PT and need to be resummed in order to have a reliable prediction. Here we describe how the EFT allows the resummation of large logarithms. EFT approach relies on the hierarchy of physical scales in the problem: $Q_1 >> Q_2$.... Then one matches the full theory above the scale Q_1 onto effective theory below the scale Q_1. At this step all other scales are set to zero. If the effective theory correctly reproduces the infrared physics of the full theory, then the matching coefficient contains only ultraviolet divergences which one obtains as a result of the matching calculation. This UV terms should be renormalized into counterterms and they define the anomalous dimension of the matching coefficient. This allows to run down using RGE to the scale Q_2 and calculate the matching coefficient there. And then again integrate out the scale Q_2 in the similar fashion. Thus the final cross-section becomes a product of matching coefficients and matrix elements of effective theory operators, which we can all evaluate at some common IR scale, at which we know the matrix elements of the operators and where all the large logarithms are resummed in the kernels of RGE from running between the energy scales. In other words the flexibility of EFT to have multiple renormalization scales as opposed to the traditional approach, where you have just one renormalization scale, allows the EFT approach to achieve resummation of all Large logarithms.

Among other advantages of the EFT approach is the straightforward way to incorporate power-suppressed processes, enhanced symmetries because of the power counting, absence of spurious Landau poles in the final expression for the resummed cross-section [126, 31, 101], which are inevitable in the traditional approach.

SCET is an effective theory for QCD [12, 14, 25, 21] which describes interactions of highly energetic particles. In this effective theory one integrates out of the full theory all the modes except the ones that are collinear quarks, gluons and soft gluons. These are the important low energy modes that carry all the infrared dynamics of QCD at high energies. In Chapter 2 we explicitly derive the effective Lagrangian of SCET as a result of integrating out the hard modes in QCD at the functional integral method. With the advance of SCET many processes have been recalculated in this approach and in many cases the theory prediction has improved significantly compared to the old ways of classical QCD approach. The best example is the extraction of the strong coupling α_s from the combined LEP data on event shape observable Thrust. The recent analysis [1] of this data comparing it to SCET higher order prediction leads to one of the best extractions of α_s, which is even competitive with the combined world average from Particle Data Group. Another example is the prediction for Angularities cross-section [101], which is some generalization of Thrust, and we describe this calculation in Chapter 3.

While for e^+e^- annihilation into hadrons the SCET predictions for Event shapes (thrust, angularities, etc) are well known in the literature, similar predictions for pp are in the development stage. Of course with the LHC running and producing data it is extremely important to have a reliable control over QCD cross-sections of hadron collisions. In this paragraph we discuss the main complications which we face as we go from a lepton to hadron collider. There are three such complications. First, unlike the lepton collider, where the initial state colliding particles fully annihilate, in the hadronic collider there are unmeasurable remnants of the protons. This fact makes usual event shapes, like Thrust, which are fully inclusive, not the best candidates for hadronic event shape observables. Consequently, inventing new hadronic event shape observables is of great importance. Since in hadronic collision the initial states are strongly interacting, new soft functions are needed in the SCET factorization formula. This leads to new non-perturbative

effects in the cross-section. This problem can be solved by introducing a model for non-perturbative physics, using a technique called "Shape Function". The basic idea is to fix the first few moments of the unknown function and to extract their values from the fit to data. The third complication is the fact that initial state radiation of the colliding protons plays an important role for certain observables. A first step in treating this physics has recently been introduced through so-called "Beam Function", which essentially describes the initial state radiation by treating active parton inside the proton as an initial state jet. Thus, in hadron collisions we have to deal for certain observables with two additional jets in the initial state, in addition to jets in the final state.

This Thesis is based on the following work: Chapter 2 is based on [9], Chapter 3 on [102, 101], and Chapter 4 on work in progress [16]. In Chapter 2 we consider three different formulations of SCET: with gauge non-invariant fields ξ_n, A_n, with gauge invariant quark field and non gauge invariant gluon field χ_n, A_n and finally with both gauge invariant fields $\chi_n, \mathcal{B}_n$.[1] The difference between different formulations is trivial via field redefinition in the Lagrangian. However it is instructive to know how exactly the equivalence works in terms of the Feynman rules. The non-trivial part of our analysis is in the gauge sector of QCD. We find that the calculations with the gauge invariant collinear gluon field $\mathcal{B}_n$ are equivalent to that of the non-gauge invariant field A_n but in one particular gauge: in the light cone gauge.

In Chapter 3 we perform complete phenomenology of event shapes in e^+e^- annihilation to hadrons using SCET. The event shape that we consider is called Angularity, and it has a continuous real parameter. By varying this parameter one changes the sensitivity of the observable to narrower or wider jets. Thus makes Angularities a powerful tool to study the substructure of the jets. We work at fixed next-to-leading order(NLO) in Perturbation Theory and resum large logarithms to next-to-leading logarithmic order (NLL). In the peak region where the angularity value goes to zero, we are in the region of back to back jets. In this limit the effective theory reproduces the full theory, however physical scales(hard, jet and soft) become widely separated. Resummation of large logarithms is thus essential to have a reliable prediction. Besides large logarithms in the peak region, there is also non-perturbative physics affecting this region of the parameter space. This physics can be conveniently incorporated into effective theory analysis using "Shape Function" described above. We generalize the Shape Function used for thrust to all angularities, using the proven universality of non-perturbative corrections for Angularities [119].

In Chapter 4 we switch to hadron collisions, namely the Exclusive Drell-Yan process. The question we ask is: are we sure that we have all the necessary low energy modes incorporated in SCET to properly describe the infrared behavior of Drell-Yan amplitude? The reason we should worry is buried in the original analysis of all order factorization of the Drell-Yan cross-section, where it is shown that in addition to soft and collinear pinch surfaces, for this amplitude additional Glauber pinch is present, which breaks the factorization of the exclusive(in the sense that we measure the transverse momentum of the lepton pair) Drell-Yan process. This Glauber mode has large transverse momentum and small longitudinal ones, it arises in the interaction between the spectators of the colliding hadrons [44, 65]. We perform a consistency check on SCET by doing a matching calculation for two back to back jet operator $\mathcal{O}_2$ with special external states, namely $\langle\gamma\gamma|$ and $|q\bar{q}\rangle$. This choice of external states involves Drell-Yan like amplitudes in the calculation. A consistency check on effective theory is that the matching coefficient C_2 is independent from the choice of the external states. We find that this is not true for SCET without Glauber modes,

[1] We mean collinear gauge invariance here.

while in effective theory which is SCET expanded with a Glauber mode this cross-check is satisfied. We conclude that for correct description of the Infrared physics of Drell-Yan amplitude one needs to expand SCET with a Glauber mode. We further discuss the reconciliation of the apparently off-shell Glauber mode with Coleman-Norton theorem and Landau Equations.

Chapter 2

Different Formulations of SCET

1 Introduction

Soft collinear effective theory (SCET) [12, 14, 25, 21] is by now a rather mature effective field theory with wide applications in B physics and collider physics. SCET describes QCD in the kinematic regime where the energy of particles is far in excess of their (invariant) mass. Short distance physics is contained in Wilson coefficients which are determined order by order in perturbation theory. Long distance physics on the other hand is described by separate collinear fields for each light-like direction, together with Wilson lines Y_n describing the usoft physics interactions between the different collinear directions. Since there are no direct interactions between collinear fields in different directions, gauge invariance requires the presence of Wilson lines to render collinear fermions and gauge bosons gauge invariant.

There are several equivalent versions of SCET used in the literature. The original formulation of SCET [12, 14] described the interactions between the gauge dependent collinear quark ξ_n and gluon A_n fields, with the leading order Lagrangian given by[1]

$$\begin{aligned}\mathcal{L}_I^n(\xi_n, A_n) &= \bar{\xi}_n \left[in\cdot D_n + i\not{D}_n^\perp \frac{1}{i\bar{n}\cdot D_n} i\not{D}_n^\perp \right] \frac{\not{\bar{n}}}{2} \xi_n \\ &\quad -\frac{1}{2}\mathrm{Tr}\, F_{\mu\nu}^n F_n^{\mu\nu}\,, \end{aligned} \tag{2.1}$$

with the standard definition of the covariant derivative and the field strength tensor

$$iD_n^\mu = i\partial_n^\mu + g_s A_n^\mu\,, \qquad F_n^{\mu\nu} = \frac{i}{g_s}[D_n^\mu, D_n^\nu]\,, \tag{2.2}$$

where the partial derivative ∂_n is given in terms of the label operator introduced in [25]

$$i\partial_n^\mu = \bar{n}\cdot\mathcal{P}\frac{n^\mu}{2} + \mathcal{P}_\perp^\mu + in\cdot\partial\frac{\bar{n}^\mu}{2}\,. \tag{2.3}$$

In order to construct gauge invariant operators containing collinear fermions, these fermions are required to appear in the gauge invariant combination

$$\chi_n = W_n^\dagger \xi_n\,, \tag{2.4}$$

[1] We here omit any reference to gauge-fixing and potential ghost terms. We will address the quantization of gauge fields later on.

where W_n is the collinear Wilson line [25]

$$W_n = \mathrm{P}\exp\left[-ig_s\int_0^\infty \mathrm{d}s\ \bar{n}\cdot A_n(\bar{n}s+x)\right]. \tag{2.5}$$

Using a simple field redefinition, one can easily obtain the collinear Lagrangian in terms of these gauge invariant combinations

$$\begin{aligned}\mathcal{L}^n_{II}(\chi_n, A_n) &= \bar{\chi}_n W_n^\dagger\left[in\cdot D_n + i\not{D}^\perp_n\frac{1}{i\bar{n}\cdot D_n}i\not{D}^\perp_n\right]\frac{\not{\bar{n}}}{2}W_n\chi_n \\ &\quad -\frac{1}{2}\mathrm{Tr}\,F^n_{\mu\nu}F^{\mu\nu}_n\,.\end{aligned} \tag{2.6}$$

Since the fields χ_n are gauge invariant, the combination $W_n^\dagger D_n^\mu W_n$ has to be gauge invariant as well. Thus, we can define [4]

$$\mathcal{D}^\mu_n = W_n^\dagger D^\mu_n W_n\,. \tag{2.7}$$

The gauge invariant derivative operator $\mathcal{D}^\mu_n$ can be written in terms of the partial derivative and a gauge invariant gluon field $\mathcal{B}^\mu_n$

$$i\mathcal{D}^\mu_n = i\partial^\mu_n + g_s\mathcal{B}^\mu_n\,, \tag{2.8}$$

where

$$\mathcal{B}^\mu_n = \left[\frac{1}{\bar{n}\cdot\partial}\left[i\bar{n}\cdot\mathcal{D}_n, i\mathcal{D}^\mu_n\right]\right] = \frac{1}{g_s}\left[W_n^\dagger iD^\mu_n W_n\right], \tag{2.9}$$

and the derivatives only act within the square brackets. In terms of these fields, the Lagrangian reads

$$\begin{aligned}\mathcal{L}^n_{III}(\chi_n, \mathcal{B}_n) &= \bar{\chi}_n\left[in\cdot\mathcal{D}_n + i\not{\mathcal{D}}^\perp_n\frac{1}{i\bar{n}\cdot\partial}i\not{\mathcal{D}}^\perp_n\right]\frac{\not{\bar{n}}}{2}\chi_n \\ &\quad -\frac{1}{2}\mathrm{Tr}\,\mathcal{F}^n_{\mu\nu}\mathcal{F}^{\mu\nu}_n\,,\end{aligned} \tag{2.10}$$

where we have defined

$$\mathcal{F}^{\mu\nu}_n = \frac{i}{g_s}[\mathcal{D}^\mu_n, \mathcal{D}^\nu_n]\,. \tag{2.11}$$

A sample of Feyman rules for the three different formulations of SCET is shown in Fig. 2.1.

It is well known that the dynamics of SCET with a single collinear direction is identical to full QCD. This is of course expected, since one can perform a simple Lorentz boost along the direction n to make all momentum components of the collinear field similar in magnitude. Since this eliminates any large ratio of scales, the interactions have to be those of full QCD. This implies that for example the wave function renormalization in SCET is equivalent to that of full QCD, as was first shown in [12, 14]. This equivalence has been used in the literature in order to simplify perturbative calculations in SCET (*vid.*, for instance, [28]).

It is the purpose of this Chapter to study the relationship between different formulations of SCET. We work out the relationship between SCET using gauge dependent and gauge invariant degrees of freedom, as well as the relationship between full QCD and collinear fields in a single direction further. One of the features of the original formulation of SCET is that collinear gluons are coupled to the quark fields in a non-linear way. This means that there are an infinite number of

$$V^{(1)}_{\mathcal{L}_I} = \quad = igT^A\Big[n^\mu + \frac{\gamma^\mu_\perp \not{p}_\perp}{\bar n\cdot p} + \frac{\not{p}'_\perp \gamma^\mu_\perp}{\bar n\cdot p'} - \frac{\not{p}'_\perp \not{p}_\perp}{\bar n\cdot p' \bar n\cdot p}\bar n^\mu\Big]\frac{\not{\bar n}}{2}$$

$$V^{(2)}_{\mathcal{L}_I} = \quad = ig^2\Big[\frac{T^AT^B}{\bar n\cdot(p-q)}\gamma^\mu_\perp\gamma^\nu_\perp + \frac{T^BT^A}{\bar n\cdot(q+p')}\gamma^\nu_\perp\gamma^\mu_\perp\Big]\frac{\not{\bar n}}{2} + (\ldots)$$

$$V^{(1)}_{\mathcal{L}_{II}} = \quad = V^{(1)}_{\mathcal{L}_I} + igT^A\Big[\frac{1}{\bar n\cdot(p-p')}\Big(\frac{p^2}{\bar n\cdot p} - \frac{p'^2}{\bar n\cdot p'}\Big)\bar n^\mu\Big]\frac{\not{\bar n}}{2}$$

$$V^{(2)}_{\mathcal{L}_{II}} = \quad = V^{(2)}_{\mathcal{L}_I} + (\ldots)$$

$$V^{(1)}_{\mathcal{L}_{III}} = \quad = igT^A\Big[n^\mu + \frac{\gamma^\mu_\perp \not{p}_\perp}{\bar n\cdot p} + \frac{\not{p}'_\perp \gamma^\mu_\perp}{\bar n\cdot p'}\Big]\frac{\not{\bar n}}{2}$$

$$V^{(2)}_{\mathcal{L}_{III}} = \quad = ig^2\Big[\frac{T^AT^B}{\bar n\cdot(p-q)}\gamma^\mu_\perp\gamma^\nu_\perp + \frac{T^BT^A}{\bar n\cdot(q+p')}\gamma^\nu_\perp\gamma^\mu_\perp\Big]\frac{\not{\bar n}}{2}$$

$$\Delta_{\mathcal{L}_{III}} = \quad = -i\frac{\delta^{AB}}{k^2+i\epsilon}\Big(g_{\mu\nu} - \frac{\bar n_\mu k_\nu + \bar n_\nu k_\mu}{\bar n\cdot k}\Big)$$

Figure 2.1: A subset of Feynman rules for the three different formulations of SCET. The (...) denote terms which do not contribute to the tadpole diagram of Fig. 2.2b) in Feynman gauge.

vertices consisting of quark-antiquark and an arbitrary number of collinear gluons, whose Feynman rules get increasingly complicated. This makes the theory particularly unfriendly for computations beyond the one-loop order.

We will show how to quantize SCET directly in terms of the gauge invariant degrees of freedom, and write the theory as a path integral over these gauge invariant fields. We will also discuss how to re-express the theory using only the interactions of full QCD. This first gives a precise field theoretical understanding of the well known property of SCET that the dynamics in a given collinear direction are equivalent to that of full QCD. Our formulation using directly the generating functional will extend this result to include interactions between different collinear directions through local operators. One can hope that these results will simplify the perturbative calculation of matching coefficients in the future, since much of the SCET calculations are now identical to the corresponding QCD results. It will prove instructive, however, to first illustrate this equivalence between different formulations of SCET using a simple one-loop calculation. We do it in the next section.

2 One loop jet function in three different formulations

Consider the two point correlator of two gauge invariant fermion fields

$$\langle 0|T\chi_n(x)\bar\chi_n(y)|0\rangle = \langle 0|TW_n^\dagger(x)\xi_n(x)\bar\xi_n(y)W_n(y)|0\rangle\,. \tag{2.12}$$

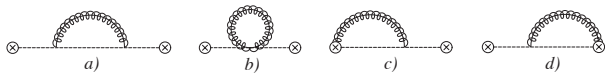

Figure 2.2: Diagrams contributing to the gauge invariant jet function at one loop.

The Fourier transform of this correlator is what is known in the literature as the jet function, and plays a crucial role in any process containing external collinear particles. In the original formulation of SCET in terms of ξ_n and A_n fields there are four diagrams contributing at one loop, which are shown in Fig. 2.2. The first two diagrams are entirely built out of interactions contained in the Lagrangian of the theory, while in the last two diagrams one of the gluon couplings comes from the Wilson lines W_n or $W_n^\dagger$. Using the Feynman rules given in Fig. 2.1, one can easily obtain the result

$$D_{I,a} = g_s^2 \frac{\not{n}}{2} \frac{\bar{n}\cdot p}{p^2} C_F (2-D) \int \frac{d^D k}{(2\pi)^D} \left[\frac{1}{2} \frac{1}{(k^2+i\epsilon)((k+p)^2+i\epsilon)} - \frac{\bar{n}\cdot p}{p^2} \frac{1}{(k^2+i\epsilon)\bar{n}\cdot(k+p)} \right], \tag{2.13}$$

$$D_{I,b} = g_s^2 \frac{\not{n}}{2} \left(\frac{\bar{n}\cdot p}{p^2} \right)^2 C_F (2-D) \int \frac{d^D k}{(2\pi)^D} \frac{1}{(k^2+i\epsilon)\bar{n}\cdot(k+p)}, \tag{2.14}$$

$$D_{I,c} = D_{I,d} = g_s^2 \frac{\not{n}}{2} \frac{\bar{n}\cdot p}{p^2} C_F (n\cdot\bar{n}) \int \frac{d^D k}{(2\pi)^D} \frac{\bar{n}\cdot(k+p)}{(k^2+i\epsilon)((k+p)^2+i\epsilon)\bar{n}\cdot k}. \tag{2.15}$$

Note that the tadpole diagram is canceled exactly against the second term in the first diagram. Performing the remaining integrals and summing the diagrams one obtains the well known result [126]

$$D_I = i \frac{\alpha_s C_F}{4\pi} \frac{\not{n}}{2} \frac{\bar{n}\cdot p}{p^2} \left(\frac{\mu^2}{-p^2} \right)^\epsilon \left[\frac{4}{\epsilon^2} + \frac{3}{\epsilon} + 7 - \frac{\pi^2}{3} \right]. \tag{2.16}$$

We can repeat this calculation using the formulation of SCET in terms of χ_n and A_n fields. This removes the last two diagrams of Fig. 2.2, since there are no Wilson lines in the definition of the correlator when written in terms of χ_n fields. However, the extra Wilson lines in the collinear Lagrangian change the Feynman rules in the way shown in Fig. 2.1. While this does not change the result for the second diagram, the first diagram is now

$$\begin{aligned} D_{II,a} &= g_s^2 \frac{\not{n}}{2} \frac{\bar{n}\cdot p}{p^2} C_F \int \frac{d^D k}{(2\pi)^D} \left[(2-D) \left(\frac{1}{2} \frac{1}{(k^2+i\epsilon)((k+p)^2+i\epsilon)} - \frac{\bar{n}\cdot p}{p^2} \frac{1}{(k^2+i\epsilon)\bar{n}\cdot(k+p)} \right) \right. \\ &\quad \left. + 2 n\cdot\bar{n} \frac{\bar{n}\cdot(k+p)}{(k^2+i\epsilon)((k+p)^2+i\epsilon)\bar{n}\cdot k} - (n\cdot\bar{n})^2 \frac{\bar{n}\cdot p}{p^2} \frac{1}{(k^2+i\epsilon)\bar{n}\cdot k} \right]. \end{aligned} \tag{2.17}$$

The first two terms reproduce the result for $D_{I,a}$, and the third reproduces $D_{I,c} + D_{I,d}$. Finally, the fourth term in $D_{II,a}$ vanishes, since it is odd as $k \to -k$. Thus, the sum of all diagrams is identical in both versions of the theory.

Showing that we can reproduce this result using the fully gauge invariant χ_n and $\mathcal{B}_n$ fields is a little more tricky. This is because now there are no Wilson lines whatsoever, neither in the definition of the correlator nor in the Lagrangian of Eq. (2.10). Thus, it is not immediately obvious how the contributions from diagrams D_c and D_d are reproduced in this case. However, care has to

be taken when deriving the gluon propagator. The $\mathcal{B}_n$ field is by construction explicitly invariant under collinear gauge transformations, and the usual procedure of adding an arbitrary gauge-fixing term to the Lagrangian is not valid. However, from the definition of $\mathcal{B}_n^\mu$ in Eq. (2.9) one easily verifies the constraint $\bar{n}\cdot\mathcal{B}_n = 0$ (see Eqs. (2.29) and (2.30) below). Thus, the propagator of a $\mathcal{B}_n$ field has to satisfy the condition $\bar{n}_\mu \Delta_{\mathcal{B}}^{\mu\nu} = 0$. As we will discuss in more detail later, the propagator takes the form [8, 147]

$$(\Delta_{\mathcal{B}})^{ab}_{\mu\nu}(k) = \frac{-i\delta^{ab}}{k^2 + i\epsilon}\left(g_{\mu\nu} - \frac{\bar{n}_\mu k_\nu + \bar{n}_\nu k_\mu}{\bar{n}\cdot k}\right) . \tag{2.18}$$

Using this propagator for the gauge invariant gluon field one can easily verify that

$$D_{III,a} = D_{II,a}\,, \quad D_{III,b} = D_{II,b}\,. \tag{2.19}$$

Thus, the three formulations of SCET give identical results to one another for the two point correlator of two gauge invariant collinear fermion fields.

3 Path integral derivation of SCET Lagrangian from QCD

In order to generalize this discussion to any matrix element, we quantize the theory directly in terms of the various fields. This is achieved by using the path integral formulation, working directly with the generating functional of the theory

$$Z[J] = \int \mathcal{D}\bar{\xi}_n \mathcal{D}\xi_n \mathcal{D}A_n^\mu \exp\left[i\int d^4x\, \mathcal{S}_I(\xi_n, A_n^\mu, J_n)\right] , \tag{2.20}$$

where we have defined

$$\begin{aligned}\mathcal{S}_I \;=\; & \sum_n \big[\mathcal{L}_I^n + \bar{J}_n^\xi \xi_n + \bar{\xi}_n J_n^\xi + \bar{J}_n^\chi W_n^\dagger \xi_n + \bar{\xi}_n W_n J_n^\chi \\ & + J_{n\mu}^A A_n^\mu + J_{n\mu}^{\mathcal{B}} \mathcal{B}_n^\mu(A_n) \\ & + \sum_k J_k \mathcal{O}_k\left(W_n^\dagger \xi_n, \mathcal{B}_n^\mu(A_n)\right) . \end{aligned} \tag{2.21}$$

A few comments are in order to understand our notation. First, the integration in Eq. (2.20) is over all fields with different directions n. Second, the subscripts I, II, III indicate which version of SCET we are using, with Lagrangians given in Eqs. (2.1), (2.6) and (2.10) above. Third, we have added separate currents for the gauge invariant fields $\chi_n = W_n^\dagger \xi_n$ and $\mathcal{B}_n^\mu = \mathcal{B}_n^\mu(A_n) = \frac{1}{g_s}[W_n^\dagger i D_n^\mu W_n]$, as well as for the gauge dependent fields ξ_n and A_n. This allows us to calculate correlators with gauge invariant fields, such as the jet function, as well as those with gauge dependent fields, as is often done in matching calculations to QCD. Finally, we have indicated currents J_k for any local operator in SCET. Such operators are typically written in terms of the gauge invariant fields, and an example would be the production current for two collinear fields in opposite directions, $\mathcal{O}_2 = \bar{\chi}_n \Gamma \chi_{\bar{n}}$.

In order to obtain the generating functional with the Lagrangian written in terms of χ_n fields, we make the field redefinition given in Eq. (2.4), which just amounts to a change in the

integration variable in the generating functional. Since $W_n^\dagger W_n = 1$, one can easily show that the integration measure is the same when written in terms of the χ_n fields

$$\mathcal{D}\xi_n \mathcal{D}\bar{\xi}_n \mathcal{D}A_n^\mu = \mathcal{D}\chi_n \mathcal{D}\bar{\chi}_n \mathcal{D}A_n^\mu \,. \tag{2.22}$$

Thus, the generating functional can be written as

$$Z[J] = \int \mathcal{D}\bar{\chi}_n \mathcal{D}\chi_n \mathcal{D}A_n^\mu \exp\left[i \int d^4x \, \mathcal{S}_{II}(\chi_n, A_n^\mu, J_n) \right] , \tag{2.23}$$

with

$$\begin{aligned} \mathcal{S}_{II} \;=\; & \sum_n \big[\mathcal{L}_{II}^n + \bar{J}_n^\xi W_n \chi_n + \bar{\chi}_n W_n^\dagger J_n^\xi + \bar{J}_n^\chi \chi_n + \bar{\chi}_n J_n^\chi \\ & + J_{n\mu}^A A_n^\mu + J_{n\mu}^{\mathcal{B}} \mathcal{B}_n^\mu(A_n) \big] \\ & + \sum_k J_k \mathcal{O}_k(\chi_n, \mathcal{B}_n(A_n)) \,. \end{aligned} \tag{2.24}$$

In other words, any matrix element written in terms of ξ_n and A_n fields is identical to the matrix element written in terms of χ_n and A_n fields, as long as the interactions between the fields are given by the Lagrangian $\mathcal{L}_{II}$ instead of $\mathcal{L}_I$.

4 Relation between A_n and B_n and gauge fixing

Next, we discuss the relation between the gauge dependent gluon field A_n and the gauge invariant field $\mathcal{B}_n$. The Yang Mills action is given by

$$Z_{\rm YM} = \int \mathcal{D}A_n^\mu \, e^{iS_{\rm YM}[A_n]} \,, \tag{2.25}$$

where

$$S_{\rm YM}[A] = -\frac{1}{2} \int d^4x \, \sum_n {\rm Tr}\, F_{\mu\nu}^n F_n^{\mu\nu} \,. \tag{2.26}$$

Recall that the relation between these two fields is given by

$$\mathcal{B}_n^\mu = \frac{1}{g_s} \left[W_n^\dagger i D_n^\mu W_n \right] , \tag{2.27}$$

where ∂_n^μ acts only within the square brakets. Since the Wilson lines W_n are unitary, the Yang-Mills action can be written in terms of the $\mathcal{B}_n^\mu$ fields as

$$S_{\rm YM}[\mathcal{B}] = -\frac{1}{2} \int d^4x \, \sum_n {\rm Tr}\, \mathcal{F}_{\mu\nu}^n \mathcal{F}_n^{\mu\nu} \,, \tag{2.28}$$

where $\mathcal{F}_n^{\mu\nu}$ is given in Eq. (2.11). However, in order to write the generating functional in terms of the fields $\mathcal{B}_n$ requires changing the integration measure as well, and that is where additional care has to be taken. From the definition of the $\mathcal{B}_n$ field we can immediately see that

$$\bar{n}\cdot\mathcal{B}_n = 0 \,, \tag{2.29}$$

which follows from the well known relation of Wilson lines

$$\bar{n}\cdot D_n\, W_n = W_n\, \bar{n}\cdot\partial_n\,. \tag{2.30}$$

Thus, while there are four components of the A_n^μ field, there are only three components for the $\mathcal{B}_n^\mu$ field, making the Jacobian for the change in the integration measure singular.

Of course, the fact that the $\mathcal{B}_n^\mu$ field has less independent components than the A_n^μ field is not unexpected, given that the former is gauge independent, while the latter contains all the gauge redundancy. The only way one can obtain a meaningful definition of a Jacobian factor is by removing the gauge redundancy and thus considering only three of the four components of the A_n^μ field. This can be achieved using the usual Faddeev-Popov procedure, by inserting a representation of unity into the path integral (2.25) in the following form

$$1 = \int \mathcal{D}\alpha(x)\,\delta[G(A_n^\alpha)]\,\det\left(\frac{\delta G(A_n^\alpha)}{\delta\alpha}\right)\,, \tag{2.31}$$

where $G(A_n^\alpha)$ is some gauge-fixing function linear in the gauge field. Here $\alpha(x)$ defines a specific gauge transformation and A_n^α denotes the (infinitesimally) gauge transformed field

$$(A_n^\mu)^\alpha = A_n^\mu + \frac{1}{g_s} D_n^\mu \alpha\,. \tag{2.32}$$

Note that for infinitesimal gauge transformations (from which all finite transformations can be constructed), the determinant of $\delta G/\delta\alpha$ is in general a function of $(A_n^\mu)^\alpha$ but independent of α.

Following the standard treatment, the gauge invariance of both the action and the integration measure allows one to write

$$Z_{\rm YM} = \int \mathcal{D}\alpha \int \mathcal{D}A_n^\mu\,\delta[G(A_n)]\,E_G[A_n]\,, \tag{2.33}$$

where we have defined

$$E_G[A_n] = \det\left(\frac{\delta G(A_n^\alpha)}{\delta\alpha}\right)[A_n]\, e^{iS_{\rm YM}[A_n]}\,. \tag{2.34}$$

One should remember that the determinant $\det(\delta G/\delta\alpha)$ is independent of α and therefore the integral over the gauge freedom is just a global factor that can be safely ignored. The important feature of this way of writing the path integral is that the integration measure $\mathcal{D}A_n^\mu\,\delta[G(A_n)]$ contains only three components of the A_n^μ field, and can thus be related to the integration measure of the $\mathcal{B}_n^\mu$ field. This allows us to formally write

$$\mathcal{D}A_n^\mu\,\delta[G(A_n)] = J_G[\mathcal{B}_n]\,\mathcal{D}\mathcal{B}_n^\mu\,\delta[\bar{n}\cdot\mathcal{B}_n]\,, \tag{2.35}$$

where the Jacobian factor for the change of the integration measure $J_G[\mathcal{B}_n]$ depends on the choice of the gauge-fixing condition G. Combining these results together we find

$$Z_{\rm YM} = \int \mathcal{D}\mathcal{B}_n^\mu\;\delta[\bar{n}\cdot\mathcal{B}_n]\,J_G[\mathcal{B}_n]\,E_G[A_n(\mathcal{B}_n)]\,. \tag{2.36}$$

Everything in this generating functional is known, except for the explicit form of the Jacobian $J_G[\mathcal{B}_n]$ and the determinant inside $E_G[A_n(\mathcal{B}_n)]$. Due to the non-linear nature of Eq. (2.27), their

expressions for a general gauge-fixing condition G are very difficult to derive. However, from the Faddeev-Popov procedure it is obvious that the generating functional is identical for all choices of the gauge-fixing condition G, since it was introduced as an arbitrary function in Eq. (2.31). Thus, any choice of $G(A_n)$ will do, and the easiest choice is light-cone gauge, which uses

$$G(A_n) \equiv G_{\rm LC}(A_n) = \bar{n}\cdot A_n \,. \tag{2.37}$$

In this case, we have $\bar{n}\cdot A_n = 0$, which immediately implies $W_n = 1$, making the relation between the A_n^μ and $\mathcal{B}_n^\mu$ fields trivial:

$$\mathcal{B}_n^\mu = A_n^\mu \,. \tag{2.38}$$

Thus, in this particular gauge we find

$$J_{G_{\rm LC}}[\mathcal{B}_n] = 1 \,, \qquad E_{G_{\rm LC}}[\mathcal{B}_n] = \det(\bar{n}\cdot\partial)\, e^{iS_{\rm YM}[\mathcal{B}_n]} \,, \tag{2.39}$$

and we obtain the final form of the generating fuctional in terms of $\mathcal{B}_n^\mu$ fields as

$$Z_{\rm YM} = \int \mathcal{D}\mathcal{B}_n^\mu\, \delta[\bar{n}\cdot\mathcal{B}_n]\, \det(\bar{n}\cdot\partial)\, e^{iS_{\rm YM}[\mathcal{B}_n]} \,. \tag{2.40}$$

In other words, the Yang-Mills action in terms of the gauge invariant gluon field $\mathcal{B}_n^\mu$ is identical to the one in terms of the field A_n^μ in the light-cone gauge. Therefore, all Feynman rules for the $\mathcal{B}_n^\mu$ fields are identical to Feynman rules for the A_n^μ fields in the light-cone gauge. In particular, this justifies Eq. (2.18) as the right form of the gluon propagator for the $\mathcal{B}_n^\mu$ fields. Incidentally, notice also that the determinant in Eq. (2.40) is independent of the gauge field and therefore can be ignored, meaning that the formulation with $\mathcal{B}_n^\mu$ fields is ghost-free. This obviously complies with the well known fact that the light-cone gauge is unitary and ghost fields decouple (see, for instance, [144]).

5 External operators in SCET

Having worked out how one can quantize SCET directly in terms of the gauge invariant degrees of freedom, we next ask whether it is possible to write the generating functional of SCET in terms of fields, whose interactions are given by the interactions of full QCD. As we will show, this is indeed possible if we restrict ourselves to leading order in the power counting, but requires separate fields for each different collinear direction. We will also show how to construct external operators coupling these different fields to one another, such that any leading order correlation function in SCET can be reproduced using only fields whose coupling to other fields is described by the Lagrangian of full QCD. We do want to emphasize that *this by no means implies* that SCET as an effective theory is useless. The power of SCET comes from understanding the interactions between fields in different directions, and while we can reproduce any leading order operator using fields that resemble full QCD, we can neither easily implement power corrections, nor can we derive the form of the leading order operators without the construction of SCET. However, we can use this equivalence to calculate matrix elements in SCET using the familiar Feynman rules of QCD, which will in general simplify the required calculations at higher orders in perturbation theory.

We start by making the Ansatz

$$Z[J] = \int \mathcal{D}\bar{\psi_n}\mathcal{D}\psi_n\mathcal{D}A_n^\mu \exp\left[i\int d^4x\, S_{\rm QCD}(\psi_n, A_n, J)\right], \tag{2.41}$$

where $S_{\rm QCD}$ is defined by

$$\begin{aligned} S_{\rm QCD} &= \sum_n \big[\mathcal{L}_n^{\rm QCD} + \bar{J}_n^\xi \mathcal{M}_n^\xi \psi_n + \bar{\psi}_n \bar{\mathcal{M}}_n^\xi J_n^\xi + \bar{J}_n^\chi \mathcal{M}_n^\chi \psi_n \\ &\quad + \bar{\psi}_n \bar{\mathcal{M}}_n^\chi J_n^\chi + J_{n\mu}^A A_n^\mu + J_{n\mu}^{\mathcal{B}} \mathcal{B}_n^\mu(A_n)\big] \\ &\quad + \sum_k J_k \mathcal{Q}_k(\psi_n, A_n)\,, \end{aligned} \tag{2.42}$$

with

$$\mathcal{L}_n^{\rm QCD} = \bar{\psi}_n\, i\not{D}\psi_n\,. \tag{2.43}$$

The set of operators $\mathcal{Q}_k$ couple k fields in different directions $n_1, ..., n_k$. Our goal is to find expressions for $\mathcal{M}_n$ and $\mathcal{Q}_k$, such that the generating functional in Eq. (2.41) is equivalent to the generating functional of SCET.

Let's begin by setting all currents in the action to zero, leaving only the Lagrangian $\mathcal{L}_n^{\rm QCD}$. One can write

$$\psi_n(x) = (P_n + P_{\bar{n}})\,\psi_n(x)\,, \tag{2.44}$$

with the projection operators P_n and $P_{\bar{n}}$ defined by

$$P_n = \frac{\not{n}\bar{\not{n}}}{4}\,, \qquad P_{\bar{n}} = \frac{\bar{\not{n}}\not{n}}{4}\,, \tag{2.45}$$

and define

$$\xi_n \equiv P_n\psi_n\,, \qquad \phi_n \equiv P_{\bar{n}}\psi_n\,. \tag{2.46}$$

This allows us to write

$$\begin{aligned} Z[J=0] &= \int \mathcal{D}\bar{\xi}_n\mathcal{D}\xi_n\mathcal{D}\bar{\phi}_n\mathcal{D}\phi_n\mathcal{D}A_n^\mu \\ &\quad \times\exp\left[\sum_n i\int d^4x\,(\bar{\xi}_n + \bar{\phi}_n) i\not{D}(\xi_n + \phi_n)\right]. \end{aligned} \tag{2.47}$$

Using the well-known formula for Gaussian integration,

$$\begin{aligned} &\int \mathcal{D}\phi\mathcal{D}\bar{\phi}\, \exp\left[i\int d^4x(\bar{\phi}M\phi + \bar{J}\phi + \bar{\phi}J)\right] \\ &\qquad = \det(-iM)\exp\left[-i\int d^4x \bar{J}\frac{1}{M}J\right], \end{aligned} \tag{2.48}$$

it is straightforward to perform the integrals over ϕ_n explicitly. We find

$$Z[J=0] = \int \mathcal{D}\bar{\xi}_n\mathcal{D}\xi_n\mathcal{D}A_n^\mu \exp\left[i\int d^4x\,\sum_n \mathcal{L}_n^{\rm SCET}\right], \tag{2.49}$$

where

$$\mathcal{L}_n^{\rm SCET} = \bar\xi_n \left[in\cdot D + i\not{D}_\perp \frac{1}{i\bar n\cdot D} i\not{D}_\perp \right] \frac{\bar{n}\!\!\!/}{2} \xi_n \,. \tag{2.50}$$

Note that in getting to Eqs. (2.49) and (2.50) no expansion has been made, only integration of modes in the generating functional. Also note that in Eq.(2.49) we have omitted the determinant factor in Eq. (2.48). Indeed it is easy to show that

$$\begin{aligned} \det\left(\frac{n\!\!\!/}{2}\bar n\cdot D\right) &= \int \mathcal{D}\eta_n \mathcal{D}\bar\eta_n \, \exp\left[-\int d^4x \, \bar\eta_n \left(\frac{n\!\!\!/}{2}\bar n\cdot D\right)\eta_n \right] \\ &= \int \mathcal{D}\eta_n' \mathcal{D}\bar\eta_n' \, \exp\left[-\int d^4x \, \bar\eta_n' \left(\frac{n\!\!\!/}{2} W_n^\dagger \bar n\cdot D W_n\right)\eta_n' \right] \\ &= \det\left(\frac{n\!\!\!/}{2}\bar n\cdot\partial\right), \end{aligned} \tag{2.51}$$

where we have defined $\eta_n' = W_n^\dagger \eta_n$. Thus the determinant is just an overall constant and can be ignored.

We can now move on and consider the addition of current terms in the action. Keeping the currents $\bar J_n \mathcal{M}_n$ and $\bar{\mathcal{M}}_n J_n$ for the fields ψ_n and $\bar\psi_n$, but still neglecting the currents J_k for the local operators $\mathcal{Q}_k$, and again performing the integrals over ϕ_n and $\bar\phi_n$ gives

$$Z[J_k=0] = \int \mathcal{D}\bar\xi_n \mathcal{D}\xi_n \mathcal{D}A_n^\mu \exp\left[i\int d^4x \, S^{\rm SCET}(J_k=0)\right] , \tag{2.52}$$

with

$$\begin{aligned} S^{\rm SCET}(J_k=0) \;=\; & \sum_n \mathcal{L}_I^n + \bar J_n^\xi \mathcal{M}_n^\xi \mathcal{R}_n \xi_n + \bar\xi_n \bar{\mathcal{R}}_n \bar{\mathcal{M}}_n^\xi J_n^\xi + \bar J_n^\chi \mathcal{M}_n^\chi \mathcal{R}_n \xi_n + \bar\xi_n \bar{\mathcal{R}}_n \bar{\mathcal{M}}_n^\chi J_n^\chi + J_{n\mu}^A A_n^\mu + J_{n\mu}^{\mathcal{B}} \mathcal{B}_n^\mu(A_n) \\ & - \left(\bar J_n^\xi \mathcal{M}_n^\xi + \bar J_n^\chi \mathcal{M}_n^\chi\right) \frac{1}{i\bar n\cdot D} \frac{\bar{n}\!\!\!/}{2} \left(\bar{\mathcal{M}}_n^\xi J_n^\xi + \bar{\mathcal{M}}_n^\chi J_n^\chi\right) . \end{aligned} \tag{2.53}$$

Here we have defined

$$\mathcal{R}_n = \left[1 + \frac{1}{i\bar n\cdot D} i\not{D}_\perp \frac{\bar{n}\!\!\!/}{2} \right] . \tag{2.54}$$

In order for this action to be equal to the action of SCET given in Eq. (2.21) (still with $J_k=0$), requires

$$\mathcal{M}_n^\xi \mathcal{R}_n \xi_n \equiv \xi_n \,, \qquad \mathcal{M}_n^\chi \mathcal{R}_n \chi_n \equiv W_n^\dagger \xi_n \,, \tag{2.55}$$

in addition to having the second line in Eq. (2.53), corresponding to contact terms arising when taking two derivatives of the generating functional with respect to the currents $J_n^{\xi/\chi}$, vanish. There are two possible solutions for each of the $\mathcal{M}_n^\xi$ and $\mathcal{M}_n^\chi$ to satisfy Eq. (2.55), namely

$$\begin{aligned} &\mathcal{M}_n^\xi = \mathcal{R}_n^{-1} && \text{or} \qquad \mathcal{M}_n^\xi = P_n \,, \\ &\mathcal{M}_n^\chi = W_n^\dagger \mathcal{R}_n^{-1} && \text{or} \qquad \mathcal{M}_n^\chi = W_n^\dagger P_n \,. \end{aligned} \tag{2.56}$$

While both of these solutions for $\mathcal{M}_n$ give the same answer, the second choice is in practice much easier to use. This is because choosing $\mathcal{M}_n^\xi = \mathcal{R}_n^{-1}$ in Eq. (2.42) adds couplings between fermions and gluons to the current terms, complicating perturbative calculations significantly. Furthermore, for the second solution the second line in Eq. (2.53) vanishes as desired. Therefore, for $\mathcal{M}_n^\xi = P_n$ and $\mathcal{M}_n^\chi = W_n^\dagger P_n$ we obtain for $J_k = 0$ the desired result $S^{\rm SCET} = S_I$, where S_I is defined in Eq. (2.21).

Finally, we add the currents for the local operators $\mathcal{Q}_k$ back to the action. Since these operators couple fields with different n's to one another, integrating out the ϕ_n fields is very complicated. However, there is a simple choice for the operators $\mathcal{Q}_k$ that will directly reproduce the form $\sum_k J_k \mathcal{O}_k$ present in the final answer, Eq. (2.21). This is achieved by taking

$$\mathcal{Q}_k(\psi_n, A_n) = \mathcal{O}_k(W_n^\dagger P_n \psi_n, \mathcal{B}_n(A_n))\,, \tag{2.57}$$

with P_n defined in Eq. (2.45). Since $P_n \psi_n = \xi_n$, this choice eliminates any dependence on ϕ_n in $\mathcal{Q}_k$. Thus, the integrals over ϕ_n can be performed as before and we therefore find

$$\mathcal{Q}_k(\psi_n, A_n) = \mathcal{O}_k(W_n^\dagger \xi_n, \mathcal{B}_n(A_n))\,. \tag{2.58}$$

In conclusion, the generating functional in terms of QCD fields

$$Z[J] = \int \mathcal{D}\bar\psi_n \mathcal{D}\psi_n \mathcal{D}A_n^\mu \exp\left[i\int d^4x\, S_{\rm QCD}(\psi_n, A_n, J)\right]\,, \tag{2.59}$$

with $S_{\rm QCD}$ defined by

$$\begin{aligned} S_{\rm QCD} \;=\; & \sum_n \big[\mathcal{L}_n^{\rm QCD} + \bar J_n^\xi P_n \psi_n + \bar\psi_n P_{\bar n} J_n^\xi + \bar J_n^\chi W_n^\dagger P_n \psi_n \\ & + \bar\psi_n P_{\bar n} W_n J_n^\chi + J_{n\mu}^A A_n^\mu + J_{n\mu}^{\mathcal{B}} \mathcal{B}_n^\mu(A_n)\big] \\ & + \sum_k J_k \mathcal{O}_k(W_n^\dagger P_n \psi_n, \mathcal{B}_n(A_n))\,, \end{aligned} \tag{2.60}$$

is identical to the generating functional defined in Eqs. (2.20) and (2.21) in terms of SCET fields. This proves that the collinear sector of SCET is equivalent to a theory containing multiple copies of QCD, where the only interactions between them are contained in the local operators $\mathcal{O}_k$.

So far we have only considered the collinear sector of SCET, but of course it is well known that usoft degrees of freedom are required in order to reproduce the long distance dynamics of QCD. On the other hand, it is also well known that at leading order in the effective theory the interactions between usoft and collinear particles can be removed to all orders in perturbation theory by using the field redefinition [21]

$$\xi_n \to Y_n \xi_n\,, \tag{2.61}$$

where

$$Y_n = \mathrm{P}\exp\left[ig\int_0^\infty \mathrm{d}s\; n\cdot A(ns+x)\right]\,. \tag{2.62}$$

Thus, we can include the interactions with the usoft gluons by making a similar field redefinition on the fields ψ_n. This implies that the action given in Eq. (2.42), but now with

$$\mathcal{L}_n^{\rm QCD} = \bar\psi_n \left(i\not{D} + g n\cdot A_{us}\frac{\bar{\not{n}}}{2}\right)\psi_n \tag{2.63}$$

reproduces both the collinear and usoft interactions of the collinear fields.

6 Conclusions

We have shown how SCET can be quantized either in terms of gauge dependent or gauge invariant fields. In practice, most calculations in the literature are performed using the gauge dependent degrees of freedom, whereas the external operators have to depend on the gauge invariant fields. Using our results, one can perform the calculations directly in terms of the gauge invariant fields, reducing the number of Feynman diagrams significantly. We have then moved on to show how the collinear sector of SCET is equivalent to a theory constructed out of multiple decoupled copies of full QCD, in the sense that each copy describes the interactions of fields in a given direction and the different copies do not interact with one another. We have also shown in detail how to construct the local operators describing precisely the interactions between the different copies of QCD, such that any SCET correlator at leading order can be reproduced.

Chapter 3

Event Shapes(Angularities) in e^+e^- annihilation

1 Introduction

Event shapes probe the hadronic final states produced in hard scattering processes for jet-like structure [71]. Two-jet event shapes e in hadronic e^+e^- annihilations are constructed so that one of the kinematic endpoints corresponds to the limit of two back-to-back perfectly collimated jets. Different event shapes vary in their sensitivity to particles close to or far away from the jet axis and thus used in tandem probe the substructure of jets [3, 2]. Some examples of two-jet event shapes are the familiar thrust [47, 86], jet masses [58, 53, 59], and jet broadening [49], and the more recently introduced angularities [37]. The shape of the distributions in these variables depend on several energy scales, namely, the scale Q of the hard scattering, the scale of the invariant mass or typical transverse momentum of the jet μ_J, and the scale $\Lambda_{\rm QCD}$ of soft radiation from the jets involved in color recombination occurring during hadronization. Event shapes thus probe the behavior of QCD over a large range of energy scales, and indeed have been the source of some of the most precise extractions of the strong coupling constant α_s [32, 76, 42].

Dependence on strong interactions at soft scales near $\Lambda_{\rm QCD}$ where QCD is nonperturbative would render predictive calculations impossible, without the use of factorization. Factorization separates an observable into pieces depending on each individual relevant energy scale. Those pieces depending on large scales can be calculated perturbatively, while those depending on soft scales remain nonperturbative. If these soft functions are, however, universal among different observables or physical processes, then calculations of the factorized observables become predictive. A large number of two-jet event shape distributions in e^+e^- annihilation can be factorized into hard, jet, and soft functions:

$$\frac{1}{\sigma_{\rm tot}}\frac{\mathrm{d}\sigma}{\mathrm{d}e} = H(Q;\mu)\int \mathrm{d}e_1\,\mathrm{d}e_2\,\mathrm{d}e_s\,J_1(e_1;\mu)J_2(e_2;\mu)S(e_s;\mu)\delta(e-e_1-e_2-e_s)\,, \tag{3.1}$$

where $H(Q;\mu)$ is the hard coefficient dependent only on the hard scattering $e^+e^-\to q\bar{q}$ at center-of-mass energy Q, $J_{1,2}$ are jet functions describing the perturbative evolution of the initially produced partons $q,\bar{q}$ into collimated jets of lower-energy partons, and finally $S(e_s;\mu)$ is the soft function describing the color exchange between the two jets leading to the hadronization of their constituent

partons. This description introduces dependence on a factorization scale μ, at which the cross-section is factorized, into each of the individual functions. This dependence must cancel in the whole combination in Eq. (3.1). The full distribution and the individual jet and soft functions contain terms of the form $(1/e)\alpha_s^n \ln^m e$ which become large in the two-jet limit $e \to 0$. The dependence of the hard, jet, and soft functions on the factorization scale μ can be determined from renormalization group equations, which can be used to resum the large logarithms [69].

The formidable achievements of proofs of factorization theorems for hard scattering cross-sections in QCD span a long and monumental history [63, 142]. More recently many of these theorems were reformulated in the language of soft-collinear effective theory (SCET) [12, 14, 25, 21]. This was done for two-jet event shapes for light quark jets in the series of papers [19, 17, 119, 11] and for top quark jets in [88, 87]. Some of the relations between the full and effective theory formulations of factorization were explored in [119, 11]. Equivalent results can be formulated in either language, although our discussion below will be in the context of SCET, which we find advantageous for its intuitive framework for separating physics at hard, collinear, and soft scales and its explicit Lagrangian for interactions between collinear and soft modes. These features facilitate the implementation of factorization and resummation of logarithms of ratios of all the relevant energy scales. At the same time that the effective theory provides us an intuitive framework in which to analyze the behavior of event shape distributions, the properties of the angularities themselves will in turn illuminate properties of the effective theory, and in particular, the conditions under which it is valid for the observables under consideration.

To describe the conditions under which the distribution in a particular event shape factorizes as in Eq. (3.1), it is useful to write event shapes in a generic form. Many event shapes can be written in the form,

$$e(X) = \frac{1}{Q} \sum_{i \in X} \left| \mathbf{p}_\perp^i \right| f_e(\eta_i) \,, \tag{3.2}$$

where the sum is over all particles i in the final state X, $\mathbf{p}_\perp^i$ is the transverse momentum of the ith particle and η_i its rapidity relative to the thrust axis. Each choice of the weight function f_e determines a different event shape. For example, for the thrust and jet broadening, $f_{1-T}(\eta) = \mathrm{e}^{-|\eta|}$ and $f_B(\eta) = 1$. A continuous set of event shapes which generalize the thrust and jet broadening are the *angularities* τ_a [37], corresponding to the choice

$$f_{\tau_a}(\eta) = \mathrm{e}^{-|\eta|(1-a)} \,, \tag{3.3}$$

where a is any real number $a < 2$. For $a \geq 2$, the function in Eq. (3.3) weights particles collinear to the thrust axis too strongly and makes the quantity Eq. (3.2) sensitive to collinear splitting, and thus not infrared-safe. The factorization theorem Eq. (3.1), however, is valid only for $a < 1$. At $a = 1$, the distribution of events in τ_1 is dominated by jets with invariant mass of order $\Lambda_{\rm QCD}$. Thus, the jet and soft scales coincide, and the distribution cannot be divided into separately infrared-safe jet and soft functions, at least in the traditional form of the factorization theorem. This breakdown can be seen in the uncontrollable growth of a number of nonperturbative power corrections as $a \to 1$ [37, 119], or in the failure to cancel infrared divergences in the perturbative calculation of the jet or soft functions in the same limit, as we have recently explored in Ref. [102]. We review this breakdown of factorization in the explicit perturbative calculations we perform below. Any choice of weight function f_e that sets a jet scale at or lower than the soft scale will ruin the factorization Eq. (3.1).

The distributions for which the factorization in Eq. (3.1) breaks down might still factorize in a different form, by distinguishing collinear and soft modes not by their invariant mass, but by their rapidity, as proposed in [129]. We do not, however, pursue such a strategy here, and focus only on angularities with strictly $a < 1$.[1]

The soft function evaluated at a scale $\mu_s \sim \Lambda_{\rm QCD}$ is nonperturbative. Evaluated at a higher scale, however, it can be calculated in perturbation theory. An appropriate model for the soft function should interpolate between these two regimes. In our analysis we adopt a model like that proposed for hemisphere jet masses in [100] and for b-quark distributions in [121], in which the soft function is a convolution,

$$S(e_s;\mu) = \int \mathrm{d}e'_s\, S^{\rm PT}(e_s - e'_s;\mu) f^{\rm exp}(e'_s - \Delta_e)\,, \tag{3.4}$$

where $S^{\rm PT}$ is the partonic soft function calculated in perturbation theory, and $f^{\rm exp}$ is a nonperturbative model function. The gap parameter Δ_e, proposed in Ref. [100], enters $f^{\rm exp}$ through a theta function $\theta(e_s - \Delta_e)$ so that the minimum possible value of an event shape e of final states is Δ_e, which is zero in the partonic distribution, but is nonzero due to hadronization in the actual distribution. The full soft function $S(e_s;\mu)$ inherits its scale dependence from $S^{\rm PT}(e_s;\mu)$ and thus has a well-defined running with the scale μ.

The partonic soft function $S^{\rm PT}(e_s;\mu)$ contains a renormalon ambiguity due to the behavior of the perturbative series at high orders. This ambiguity should not be present in the full physical distribution or the soft function, so the ambiguity in $S^{\rm PT}$ is canceled by a corresponding ambiguity in Δ_e. Shifting from Δ_e to a renormalon-free gap parameter $\bar{\Delta}_e(\mu) = \Delta_e - \delta_e(\mu)$ removes the ambiguity from the entire soft function Eq. (3.4). This greatly reduces the uncertainty in the predicted distribution due to such renormalon ambiguities. These features were demonstrated in [100] for jet mass and thrust distributions. In this Chapter, we extend the soft function model and demonstrate that a similar cancellation occurs for angularities τ_a.

Many studies of nonperturbative soft power corrections in event shape distributions have been based on the behavior of the perturbative expansions of the distributions, either the behavior of their renormalon ambiguities [130, 34] or their dependence on a postulated "infrared" effective coupling α_s at low scales [79, 80, 81]. In particular, they led to the proposal of a universal soft power correction to the mean values of event shape distributions in the form [80, 81]

$$\langle e\rangle = \langle e\rangle_{\rm PT} + \frac{c_e \mathcal{A}}{Q}\,, \tag{3.5}$$

where $\langle e\rangle_{\rm PT}$ is the mean value of the partonic distribution, and the coefficient of the $1/Q$ power correction is an exactly-calculable number c_e dependent on the choice of event shape multiplied by an unknown nonperturbative parameter $\mathcal{A}$ which is universal for numerous event shape distributions. In [119] the operator definition of the soft function in the factorization theorem Eq. (3.1) was used to prove the relation Eq. (3.5) to all orders in α_s. For angularities, $c_{\tau_a} = 2/(1-a)$. This scaling of the power correction with a was observed in [40] based on the behavior of the resummed perturbative series for angularity distributions after imposing an IR cutoff on the scale in $\alpha_s(\mu)$ and in [39] based on analysis of the distributions using dressed gluon exponentiation [91]. Below

[1] Even though traditional factorization breaks down for $a = 1$ (jet broadening), the resummation of jet broadening in QCD was performed in [49, 77] and nonperturbative effects were discussed in [78].

we will review the proof of the scaling in [119] based on the operator definition of the soft function independently of its perturbative expansion, and later use the scaling rule to constrain the nonperturbative model we adopt for the soft function in angularity distributions.

The history of calculating event shape distributions using perturbation theory in QCD goes all the way back to QCD's earliest years. The thrust distribution for light quark jets to $\mathcal{O}(\alpha_s)$ was calculated in [74], to which our fixed-order results for $\mathrm{d}\sigma/\mathrm{d}\tau_a$ reduce at $a = 0$. The resummation of the thrust distribution to NLL was performed in QCD in [48, 50] and to LL in SCET in [24, 140] (and later extended to $\mathrm{N^3LL}$ in [32]). Our results are consistent with these SCET results at the appropriate orders for $a = 0$. The jet mass distribution for top quark jets was calculated and resummed to the same order in [87], with which we agree on the SCET jet and soft functions for $a = 0$ in the limit $m_t = 0$. The jet and soft functions for thrust or jet mass distributions can be derived easily from the "ordinary" SCET jet function $J(k^+)$, and the hemisphere soft function $S(k^+, k^-)$, because the thrust and jet mass depend only on a single light-cone component of the total four-momentum in each hemisphere (cf. [48]). These standard jet and soft functions were calculated to two-loop order in [29, 28, 98]. Angularities for arbitrary a, however, depend on *both* light-cone components $k^\pm$ in *each* hemisphere, thus requiring the new calculations we perform below.

In the original introduction of the angularities τ_a [37] the resummation of logarithms was achieved to the same next-to-leading-logarithmic (NLL) order that we achieve below, but without full inclusion of next-to-leading-order (NLO) jet and soft functions for the τ_a-distribution, which we calculate explicitly here for the first time. This improves the accuracy of our result for small τ_a. Our result is also improved in this region by adopting the soft function model Eq. (3.4) which cures unphysical behavior of the point-by-point distribution $\mathrm{d}\sigma/\mathrm{d}\tau_a$ as $\tau_a \to 0$ due to renormalon ambiguities. The results of [37] converted to the traditional form of an NLL resummed event shape distribution [48] were subsequently matched to fixed-order QCD at $\mathcal{O}(\alpha_s^2)$ numerically in [40], improving the accuracy of the large-τ_a region. We perform this fixed-order matching only at $\mathcal{O}(\alpha_s^1)$.

Comparing our result to those of [37, 40] elucidates the relation between SCET and traditional QCD-based approaches to resumming logarithms more generally. While the advantages of SCET in achieving factorization or resummation of logarithms through renormalization group evolution can of course be formulated without the explicit language of the effective theory (see, e.g., [37, 69]), the effective theory nevertheless unifies these concepts and methods in an intuitive framework that, we have found, allows us greater facility in improving the precision and reliability of our predictions of event shape distributions. Even though we do not go beyond the existing NLL resummation of logarithms of τ_a [37, 40], the flexibility in the effective theory to vary the scales $\mu_{H,J,S}$, where logarithms in the hard, jet, and soft functions are small and from which we run each function to the factorization scale μ, allows additional improvements. For example, we are able to avoid any spurious Landau pole singularities which the traditional approaches usually encounter. (For previous discussions on how the effective theory avoids spurious Landau poles present in the traditional approach, see Refs. [126, 27, 30].)

The plan of the Chapter is as follows. In Sec. 2, we review the demonstration of factorization of event shape distributions in the formalism of SCET that was presented in [11], recalling the introduction of the event shape operator $\hat{e}$ that returns the value of an event shape e of a final state X, constructed from the energy-momentum tensor. In Sec. 3, we calculate the jet and soft

functions appearing in the factorization theorem for angularity distributions for $a < 1$ to one-loop order in α_s. We recall the observations of [102] about how the breakdown of factorization as $a \to 1$ is observed in the infrared behavior of these functions in perturbation theory. In Sec. 4 we solve the renormalization group equations obeyed by the hard, jet, and soft functions and resum leading and next-to-leading logarithms of τ_a in the perturbative expansions of these functions, and explain how we match the resummed distributions onto the fixed-order prediction of QCD at $\mathcal{O}(\alpha_s)$. In Sec. 5 we construct a model for the soft function in angularity distributions for all $a < 1$, based on existing models for hemisphere and thrust soft functions which contain a nonperturbative gap parameter introduced in [100], which cancels the renormalon ambiguity in the perturbative series for the soft function. In Sec. 6 we present plots of our final predictions of angularity distributions using all the results of Secs. 3–5. In Sec. 7 we compare and contrast the SCET approach to predicting resummed angularity distributions to those based on factorization and RG evolution in full QCD [37] and to the traditional approach to resummation [40, 48]. In Sec. 8 we present our conclusions, and in the Appendices, we verify a consistency relation among the hard, jet, and soft anomalous dimensions for arbitrary a, provide some technical details necessary for the solution of the RG equations for the jet and soft functions, and explain our procedure to calculate angularity distributions at fixed-order in QCD at $\mathcal{O}(\alpha_s)$, noting the hitherto unnoticed property of the angularities that they fail to separate two- and three-jet-like events for values of $a \lesssim -2$, and so cease to behave exactly as "two-jet" event shapes.

2 Review of Factorization of Event Shape Distributions

We begin by reviewing the factorization of event shape distributions in the formalism of SCET, presented in [11].

2.1 Event shape distributions in full QCD

The full QCD distribution of events in $e^+e^- \to$ hadrons in an event shape variable e is given, to leading-order in electroweak couplings, by

$$\frac{\mathrm{d}\sigma}{\mathrm{d}e} = \frac{1}{2Q^2} \sum_X \int \mathrm{d}^4x \, \mathrm{e}^{iq\cdot x} \sum_{i=V,A} L^i_{\mu\nu} \langle 0| \, j_i^{\mu\dagger}(x) \, |X\rangle \langle X| \, j_i^{\nu}(0) \, |0\rangle \, \delta(e - e(X)) \,, \tag{3.6}$$

where $q = (Q, \mathbf{0})$ is the total four-momentum in the center-of-mass frame, the sum is over final states X, and $e(X)$ is the value of the event shape e of the state X. The final state is produced by the vector and axial currents,

$$j_i^\mu = \sum_{f,a} \bar{q}_f^a \Gamma_i^\mu q_f^a \,, \tag{3.7}$$

where $\Gamma_V^\mu = \gamma^\mu$ and $\Gamma_A^\mu = \gamma^\mu\gamma^5$ and the sum is over quark flavors f and colors a. The leptonic tensor, which includes contributions from an intermediate photon and Z boson, is given by

$$L^V_{\mu\nu} = -\frac{e^4}{3Q^2} \left(g_{\mu\nu} - \frac{q_\mu q_\nu}{Q^2} \right) \left[Q_f^2 - \frac{2Q^2 v_e v_f Q_f}{Q^2 - M_Z^2} + \frac{Q^4 (v_e^2 + a_e^2) v_f^2}{(Q^2 - M_Z^2)^2} \right] \tag{3.8a}$$

$$L^A_{\mu\nu} = -\frac{e^4}{3Q^2} \left(g_{\mu\nu} - \frac{q_\mu q_\nu}{Q^2} \right) \frac{Q^4 (v_e^2 + a_e^2) a_f^2}{(Q^2 - M_Z^2)^2} \,, \tag{3.8b}$$

where Q_f is the electric charge of f in units of e, and v_f, a_f are the vector and axial charges of f,

$$v_f = \frac{1}{2\sin\theta_W\cos\theta_W}(T_f^3 - 2Q_f\sin^2\theta_W)\,, \quad a_f = \frac{1}{2\sin\theta_W\cos\theta_W}T_f^3. \tag{3.9}$$

As shown in [11], the sum over hadronic final states remaining in Eq. (3.6) can be performed by introducing an operator $\hat{e}$ that gives the event shape $e(X)$ of a final state X. This operator can be constructed from a momentum flow operator, which in turn is constructed from the energy-momentum tensor. That is,

$$\hat{e}\,|X\rangle \equiv e(X)\,|X\rangle = \frac{1}{Q}\int_{-\infty}^{\infty}\mathrm{d}\eta\, f_e(\eta)\mathcal{E}_T(\eta;\hat{t})\,|X\rangle\ , \tag{3.10}$$

where $\hat{t}$ is the operator yielding the thrust axis of final state X, and $\mathcal{E}_T(\eta;\hat{t})$ is the transverse momentum flow operator, yielding the total transverse momentum flow in the direction given by rapidity η, measured with respect to the thrust axis, in a final state X,

$$\mathcal{E}_T(\eta;\hat{t})\,|X\rangle \equiv \frac{1}{\cosh^3\eta}\int_0^{2\pi}\mathrm{d}\phi\lim_{R\to\infty}R^2\int_0^{\infty}\mathrm{d}t\,\hat{n}_i T_{0i}(t,R\hat{n})\,|X\rangle = \sum_{i\in X}\left|\mathbf{p}_\perp^i\right|\delta(\eta-\eta_i)\,|X\rangle\ , \tag{3.11}$$

which is closely related to the energy flow operator proposed in [114]. The thrust axis operator $\hat{t}$ can be constructed explicitly, as shown in [11]. After matching onto SCET, however, an explicit construction is not necessary, as the thrust axis is simply given by the jet axis $\mathbf{n}$ labeling the two-jet current. The difference between the two axes introduces power corrections in λ which are subleading, as long as $a < 1$ [37, 11]. Using the operator $\hat{e}$, we perform the sum over X in Eq. (3.6), leaving

$$\frac{\mathrm{d}\sigma}{\mathrm{d}e} = \frac{1}{2Q^2}\int\mathrm{d}^4x\,\mathrm{e}^{iq\cdot x}\sum_{i=V,A}L_{\mu\nu}^i\,\langle 0|\,j_i^{\mu\dagger}(x)\delta(e-\hat{e})j_i^{\nu}(0)\,|0\rangle\ . \tag{3.12}$$

2.2 Factorization of event shape distributions in SCET

To proceed to a factorized form of the distribution Eq. (3.12), we match the current j^μ and the operator $\hat{e}$ onto operators in SCET. To reproduce the endpoint region of the two-jet event shape distribution, we match the QCD currents j_i^μ onto SCET operators containing fields in just two back-to-back collinear directions,

$$j_i^\mu(x) \;=\; \sum_{\mathbf{n}}\sum_{\tilde{p}_n,\tilde{p}_{\bar{n}}} C_{n\bar{n}}(\tilde{p}_n,\tilde{p}_{\bar{n}};\mu)\mathcal{O}_{n\bar{n}}(x;\tilde{p}_n,\tilde{p}_{\bar{n}})\,, \tag{3.13}$$

summing over the direction $\mathbf{n}$ of the light-cone vectors $n,\bar{n} = (1,\pm\mathbf{n})$, and label momenta $\tilde{p}_n,\tilde{p}_{\bar{n}}$. The two-jet operators [17, 13], after the BPS field redefinition [21] with soft Wilson lines, are

$$\mathcal{O}_{n\bar{n}}(x;\tilde{p}_n,\tilde{p}_{\bar{n}}) = e^{i(\tilde{p}_n-\tilde{p}_{\bar{n}})\cdot x}\bar{\chi}_{n,p_n}(x)Y_n(x)\Gamma_i^\mu\overline{Y}_{\bar{n}}(x)\chi_{\bar{n},p_{\bar{n}}}(x)\,, \tag{3.14}$$

where $\Gamma_V^\mu = \gamma_\perp^\mu$ and $\Gamma_A^\mu = \gamma_\perp^\mu\gamma_5$. The soft Wilson lines are the path-ordered exponentials of soft gluons,

$$Y_n(x) = P\exp\left[ig\int_0^\infty n\cdot A_s(ns+x)\right]\,, \qquad \overline{Y}_{\bar{n}}(x) = P\exp\left[ig\int_0^\infty \bar{n}\cdot\bar{A}_s(\bar{n}s+x)\right]\,, \tag{3.15}$$

with $A_s, \bar{A}_s$ respectively in the fundamental or anti-fundamental representation. The jet fields $\chi_n = W_n^\dagger \xi_n$ and $\chi_{\bar{n}} = W_{\bar{n}}^\dagger \xi_{\bar{n}}$ are combinations of collinear quark fields made invariant under collinear gauge transformations by Wilson lines of collinear gluons [14, 25], where

$$W_n(x) = \sum_{\text{perms}} \exp\left[-g\frac{1}{\bar{\mathcal{P}}}\bar{n}\cdot A_{n,q}(x)\right], \tag{3.16}$$

where q is the label momentum of the collinear gluon field A_n, and $\bar{\mathcal{P}}$ is a label momentum operator which acts as $\bar{\mathcal{P}}A_{n,q} = (\bar{n}\cdot q)A_{n,q}$ [25]. Recall that, in SCET, collinear momenta $p_c^\mu = \tilde{p}^\mu + k^\mu$ are divided into a large label piece, $\tilde{p}^\mu = (\bar{n}\cdot\tilde{p})n^\mu/2 + \tilde{p}_\perp^\mu$, and a residual piece, k^μ, where $\bar{n}\cdot\tilde{p}$ is $\mathcal{O}(Q)$, $\tilde{p}_\perp$ is $\mathcal{O}(Q\lambda)$, and k is $\mathcal{O}(Q\lambda^2)$. The residual momenta are the same size as soft momenta, k_s, of $\mathcal{O}(Q\lambda^2)$. Below, however, we will see how the natural scaling of the collinear modes varies with the choice of observable τ_a. The integral over x in Eq. (3.12) enforces that the label momenta of the jet fields in the two-jet operator satisfy $\bar{n}\cdot\tilde{p}_n = -n\cdot\tilde{p}_{\bar{n}} = Q$ and $\tilde{p}_n^\perp = \tilde{p}_{\bar{n}}^\perp = 0$.

We must also match the operator $\hat{e}$ in full QCD onto SCET. To do so we simply replace the QCD energy-momentum tensor $T^{\mu\nu}$ appearing in the definition Eq. (3.11) with the energy-momentum tensor in SCET, and, as noted above, set the thrust axis equal to the jet axis $\mathbf{n}$ in the two-jet operator $\mathcal{O}_{n\bar{n}}$. After the BPS field redefinition, to leading order in λ the SCET energy-momentum tensor is a direct sum over contributions from fields in the $n, \bar{n}$ collinear and soft sectors, since the Lagrangian splits into these separate sectors with no interactions between them. (Beyond leading order in λ, there are power-suppressed terms in the SCET Lagrangian in which interactions between collinear and soft fields do not decouple following the BPS field redefintion [20, 54, 136, 22].) Then the event shape operator $\hat{e}$ splits into separate collinear and soft operators,

$$\hat{e} = \hat{e}_n + \hat{e}_{\bar{n}} + \hat{e}_s\,, \tag{3.17}$$

where each $\hat{e}_i$ is constructed only from the energy-momentum tensor of sector i of the effective theory. So, finally, the event shape distribution in SCET factorizes into purely hard, collinear and soft functions,

$$\frac{1}{\sigma_0}\frac{\mathrm{d}\sigma}{\mathrm{d}e} = H(Q;\mu)\int \mathrm{d}e_n\,\mathrm{d}e_{\bar{n}}\,\mathrm{d}e_s\,\delta(e - e_n - e_{\bar{n}} - e_s)J_n(e_n;\mu)J_{\bar{n}}(e_{\bar{n}};\mu)S(e_s;\mu)\,, \tag{3.18}$$

where the hard coefficient is the squared amplitude of the two-jet matching coefficient,

$$H(Q;\mu) = |C_{n\bar{n}}(Qn/2, -Q\bar{n}/2;\mu)|^2\,, \tag{3.19}$$

and the jet and soft functions are given by the matrix elements of collinear and soft operators,

$$S(e_s;\mu) = \frac{1}{N_C}\mathrm{Tr}\,\langle 0|\,\overline{Y}_{\bar{n}}^\dagger(0)Y_n^\dagger(0)\delta(e_s - \hat{e}_s)Y_n(0)\overline{Y}_{\bar{n}}(0)\,|0\rangle\,, \tag{3.20}$$

and

$$J_n(e_n;\mu) = \int\frac{\mathrm{d}l^+}{2\pi}\mathcal{J}_n(e_n, l^+;\mu)\,, \quad J_{\bar{n}}(e_{\bar{n}};\mu) = \int\frac{\mathrm{d}k^-}{2\pi}\mathcal{J}_{\bar{n}}(e_{\bar{n}}, k^-;\mu)\,, \tag{3.21}$$

where

$$\mathcal{J}_n(e_n, l^+;\mu)\left(\frac{\bar{n}\!\!\!/}{2}\right)_{\alpha\beta} = \frac{1}{N_C}\mathrm{Tr}\int \mathrm{d}^4x\,\mathrm{e}^{il\cdot x}\,\langle 0|\,\chi_{n,Q}(x)_\alpha\delta(e_n - \hat{e}_n)\bar{\chi}_{n,Q}(0)_\beta\,|0\rangle \tag{3.22a}$$

$$\mathcal{J}_{\bar{n}}(e_{\bar{n}}, k^-;\mu)\left(\frac{n\!\!\!/}{2}\right)_{\alpha\beta} = \frac{1}{N_C}\mathrm{Tr}\int \mathrm{d}^4x\,\mathrm{e}^{ik\cdot x}\,\langle 0|\,\bar{\chi}_{\bar{n},-Q}(x)_\beta\delta(e_{\bar{n}} - \hat{e}_{\bar{n}})\chi_{\bar{n},-Q}(0)_\alpha\,|0\rangle\,. \tag{3.22b}$$

In Eqs. (3.20), (3.22a), and (3.22b), the traces are over colors. Also, in Eq. (3.18), we have divided the distribution by the total Born cross-section for $e^+e^- \to q\bar{q}$,

$$\sigma_0 = \frac{4\pi\alpha^2 N_C}{3Q^2} \sum_f \left[Q_f^2 - \frac{2Q^2 v_e v_f Q_f}{Q^2 - M_Z^2} + \frac{Q^4 (v_e^2 + a_e^2)(v_f^2 + a_f^2)}{(Q^2 - M_Z^2)^2} \right] . \tag{3.23}$$

The n-collinear jet function J_n depends only on the $l^+ \equiv n \cdot l$ component of the residual momentum, and $J_{\bar{n}}$ on $k^- \equiv \bar{n} \cdot k$, as only the $n \cdot \partial$ derivative appears in the n-collinear Lagrangian, and $\bar{n} \cdot \partial$ in the $\bar{n}$-collinear Lagrangian, at leading order in λ [14]. In angularity distributions, the jet functions are independent of the residual transverse momenta $k_\perp, l_\perp$ as long as $a < 1$ [11].

In Secs. 3 and 4 we calculate the above hard, jet, and soft functions for angularity distributions to next-to-leading order in α_s, and solve for their dependence on μ through the renormalization group equations, which will allow us to sum large logarithms of τ_a.

2.3 Universal first moment of the soft function

As shown in [119], the behavior of the soft function Eq. (3.20) under Lorentz boosts in the $\mathbf{n}$ direction implies a universal form for its first moment. The vacuum $|0\rangle$ and the Wilson lines $Y_{n,\bar{n}}(0), \overline{Y}_{n,\bar{n}}(0)$ are all invariant under such boosts, while the transverse momentum flow operator $\mathcal{E}_T(\eta)$ appearing in the definition of $\hat{e}_s$ transforms as $\mathcal{E}_T(\eta) \to \mathcal{E}_T(\eta')$ under a boost by rapidity $\eta' - \eta$. These properties imply that the first moment of $S(e_s; \mu)$ is given by

$$\int \mathrm{d}e_s \, e_s \, S(e_s; \mu) = \frac{c_e \mathcal{A}(\mu)}{Q} , \tag{3.24}$$

where

$$c_e = \frac{1}{Q} \int_{-\infty}^{\infty} \mathrm{d}\eta \, f_e(\eta) \tag{3.25}$$

$$\mathcal{A}(\mu) = \frac{1}{N_C} \mathrm{Tr} \, \langle 0 | \, \overline{Y}_{\bar{n}}^\dagger(0) Y_n^\dagger(0) \mathcal{E}_T(0) Y_n(0) \overline{Y}_{\bar{n}}(0) \, | 0 \rangle \ . \tag{3.26}$$

The coefficient c_e is exactly calculable from the definition of the event shape e in Eq. (3.2) while $\mathcal{A}(\mu)$ is not fully calculable due to the contribution of nonperturbative effects, but is completely independent of the choice of variable e. The first moment Eq. (3.24) is universal for all event shapes of the form Eq. (3.2) in this sense. For angularities, using Eq. (3.3) and Eq. (3.25),

$$c_a = \int_{-\infty}^{\infty} \mathrm{d}\eta \, \mathrm{e}^{-|\eta|(1-a)} = \frac{2}{1-a} . \tag{3.27}$$

This scaling of the first moment of the soft function for angularities will constrain the parameterization of the nonperturbative model for the soft function that we introduce in Sec. 5.

3 Fixed-order Perturbative Calculations of Hard, Jet, and Soft Functions

In this section we calculate at next-to-leading order, that is, $\mathcal{O}(\alpha_s)$, in perturbation theory the hard, jet, and soft functions, $H(Q; \mu)$, $J_a^{n,\bar{n}}(\tau_a^{n,\bar{n}}; \mu)$, and $S_a(\tau_a^s; \mu)$, in the factorization theorem

for angularity distributions, which is given by Eq. (3.18) with $e = \tau_a$.[2]

3.1 Hard function at NLO

The hard function $H(Q;\mu)$, given by Eq. (3.19), is the squared amplitude of the two-jet matching coefficient $C_{n\bar{n}}(Q,-Q;\mu)$. This matching coefficient was calculated, for example, in [126] in the context of DIS and in [17] for e^+e^- annihilation, to NLO. It is found by calculating a matrix element of the QCD current Eq. (3.7) and SCET current Eq. (3.13) (for example, $\langle q(p_q)\bar{q}(p_{\bar{q}})|\, j_i^\mu\, |0\rangle$), and requiring that the two match. Since the matching of the currents is independent of the observable being calculated, we do not need to repeat the matching calculation here, and simply quote the result. The matching coefficient $C_{n\bar{n}}(\tilde{p}_n,\tilde{p}_{\bar{n}};\mu)$ in the SCET current Eq. (3.13) is given by

$$C_{n\bar{n}}(\tilde{p}_n,\tilde{p}_{\bar{n}};\mu) = 1 - \frac{\alpha_s C_F}{4\pi}\left[8 - \frac{\pi^2}{6} + \ln^2\left(\frac{\mu^2}{2\tilde{p}_n\cdot\tilde{p}_{\bar{n}}}\right) + 3\ln\left(\frac{\mu^2}{2\tilde{p}_n\cdot\tilde{p}_{\bar{n}}}\right)\right]. \tag{3.28}$$

Here and in the remainder of this section, $\alpha_s \equiv \alpha_s(\mu)$. The hard function $H(Q;\mu)$ in Eq. (3.19) is thus

$$H(Q;\mu) = 1 - \frac{\alpha_s C_F}{2\pi}\left(8 - \frac{7\pi^2}{6} + \ln^2\frac{\mu^2}{Q^2} + 3\ln\frac{\mu^2}{Q^2}\right). \tag{3.29}$$

The additional contribution to the coefficient of π^2 in going from Eq. (3.28) to Eq. (3.29) is due to the sign of $2\tilde{p}_n\cdot\tilde{p}_{\bar{n}} = -Q^2$, following the conventions of [25].

The bare SCET two-jet operators in Eq. (3.14) are renormalized by the relation

$$\mathcal{O}^{(0)}_{n\bar{n}}(x;\tilde{p}_n,\tilde{p}_{\bar{n}}) = Z_{\mathcal{O}}(\tilde{p}_n,\tilde{p}_{\bar{n}};\mu)\mathcal{O}_{n\bar{n}}(x;\tilde{p}_n,\tilde{p}_{\bar{n}}), \tag{3.30}$$

where the renormalization constant, calculated using dimensional regularization to regulate the UV divergences in $d = 4-2\epsilon$ dimensions, is given by

$$Z_{\mathcal{O}}(\tilde{p}_n,\tilde{p}_{\bar{n}};\mu) = 1 + \frac{\alpha_s C_F}{4\pi}\left[\frac{2}{\epsilon^2} + \frac{2}{\epsilon}\ln\left(\frac{\mu^2}{2\tilde{p}_n\cdot\tilde{p}_{\bar{n}}}\right) + \frac{3}{\epsilon}\right]. \tag{3.31}$$

Matching the QCD current Eq. (3.7) onto only two-jet operators in SCET is sufficient to describe accurately the two-jet region near $\tau_a = 0$ of angularity distributions. To calculate accurately also the tail region to $\mathcal{O}(\alpha_s)$, where the jets broaden and an additional jet begins to form, we would need to include a basis of three-jet operators in Eq. (3.13) as well [24, 133]. But since we are mainly interested in obtaining the correct shape of the two-jet region, we do not pursue this approach here. We will simply calculate the whole distribution in SCET with only two-jet operators, and then match the tail region numerically onto the fixed-order prediction of full QCD. This will be described more precisely in Sec. 4.4.

3.2 Cutting rules for weighted matrix elements

The jet and soft functions that typically appear in factorizations of hard cross-sections in SCET are defined in terms of matrix elements of the products of collinear and soft fields, which

[2] Note that here and below a superscript n on a quantity is not a power but denotes "n-collinear" just as $\bar{n}$ denotes "$\bar{n}$-collinear" and s denotes "soft".

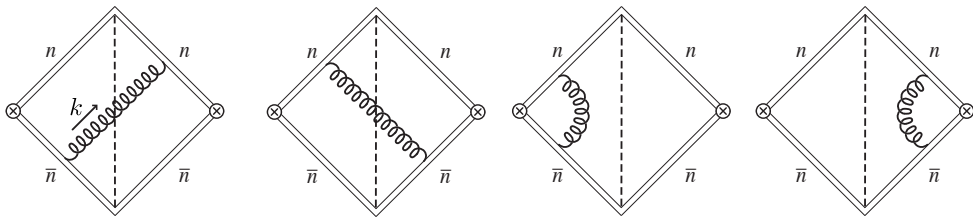

Figure 3.1: The (A), (B) real and (C), (D) virtual contributions to the soft function. The gluons all have momentum k.

are related to the imaginary part of the matrix element of a time-ordered product of the fields according to the optical theorem,

$$\int \mathrm{d}^4x\, \mathrm{e}^{iq\cdot x} \big\langle 0\big|\phi(x)\phi^\dagger(0)\big|0\big\rangle = \mathrm{Disc}\left[\int \mathrm{d}^4x\, \mathrm{e}^{iq\cdot x} \big\langle 0\big|\mathrm{T}\,\phi(x)\phi^\dagger(0)\big|0\big\rangle\right] . \tag{3.32}$$

The right-hand side is then related to the sum of all cuts of the relevant Feynman diagrams using the standard Cutkosky cutting rules.

However, for more generic jet observables such as angularities for $a \neq 0$, the jet and soft functions that appear in factorization proofs contain matrix elements in which additional operators are inserted between the collinear and soft fields in the definition of the traditional jet and soft functions [15]. For the matrix elements involving the extra insertion of such operators, we need to generalize the cutting rules for calculating these matrix elements from Feynman diagrams.

For the case of angularities, the jet and soft functions given in Eqs. (3.20), (3.22a), and (3.22b) differ from the traditional jet and soft functions by the insertion of the delta function operator $\delta(\tau_a - \hat{\tau}_a)$. We denote the appropriate generalized prescription for calculating the new matrix element from the Feynman diagrams of time-ordered perturbation theory as the "τ_a-discontinuity,"

$$\int \mathrm{d}^4x\, \mathrm{e}^{iq\cdot x} \big\langle 0\big|\phi(x)\,\delta(\tau_a - \hat{\tau}_a)\,\phi^\dagger(0)\big|0\big\rangle \equiv \mathrm{Disc}_{\tau_a}\left[\int \mathrm{d}^4x\, \mathrm{e}^{iq\cdot x} \big\langle 0\big|\mathrm{T}\phi(x)\phi^\dagger(0)\big|0\big\rangle\right] . \tag{3.33}$$

The Disc_{τ_a} prescription is to cut the diagrams contributing to the matrix element of time-ordered operators just as for the usual matrix elements in Eq. (3.32) but to insert an additional factor of $\delta(\tau_a - \tau_a(X))$ for each cut, where X is the final state created by the cut.[3] This prescription corresponds to reinserting a sum over a complete set of final states between the delta function operator and $\phi^\dagger(0)$ in Eq. (3.33), and is precisely how we would calculate the full differential cross-section as written in Eq. (3.6). In the next two subsections we illustrate extensively the use of the Disc_{τ_a} prescription.

3.3 Calculation of the soft function to NLO

The diagrams that contribute to the soft function are shown in Fig. 3.1. From Eqs. (3.3), (3.10), and (3.11), the contribution to the angularity from an on-shell soft gluon with momentum

[3]The operator-based method that was developed in [135] for calculating weighted cross-sections can be used to relate matrix elements such as in the left-hand side of Eq. (3.33) directly to the ordinary discontinuity of matrix elements of time-ordered products of fields. However, for the scope of this paper, we choose simply to apply the prescription Eq. (3.33).

k is

$$\tau_a^s = \frac{|\mathbf{k}_\perp|}{Q} e^{-\frac{1-a}{2}\left|\ln\frac{k^+}{k^-}\right|} = \begin{cases} \frac{1}{Q}\,|k^+|^{1-\frac{a}{2}}\,|k^-|^{\frac{a}{2}} & \text{for} \quad k^- \geq k^+ \\ \frac{1}{Q}\,|k^-|^{1-\frac{a}{2}}\,|k^+|^{\frac{a}{2}} & \text{for} \quad k^+ \geq k^- \end{cases} . \tag{3.34}$$

Since cutting a gluon puts it on shell, the operator $\hat{\tau}_a^s$ returns these values when acting on a cut soft gluon. When no gluon is in the final state cut, the operator $\hat{\tau}_a^s$ simply returns zero. The real and virtual diagrams then contain delta functions, which we denote δ_R and δ_V, respectively,

$$\begin{aligned} \delta_R \equiv \delta_R(\tau_a^s, k) &= \theta(k^- - k^+)\,\delta\Big(\tau_a^s - \frac{1}{Q}\,|k^+|^{1-\frac{a}{2}}\,|k^-|^{\frac{a}{2}}\Big) \\ &\quad + \theta(k^+ - k^-)\,\delta\Big(\tau_a^s - \frac{1}{Q}\,|k^-|^{1-\frac{a}{2}}\,|k^+|^{\frac{a}{2}}\Big)\,, \end{aligned} \tag{3.35a}$$

$$\delta_V \equiv \delta_V(\tau_a^s) = \delta(\tau_a^s)\,. \tag{3.35b}$$

In terms of these delta functions, the (bare) perturbative soft function can be written

$$S_a^{\mathrm{PT}(0)}(\tau_a^s;\mu) = \delta(\tau_a^s) + 2 \quad \delta_R + 2 \quad \delta_V\,, \tag{3.36}$$

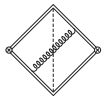

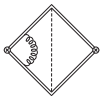

where we used that the tree-level contribution is just $\delta(\tau_a^s)$ and that the two real and the two virtual diagrams in Fig. 3.1 give identical contributions.

In pure dimensional regularization, the virtual contributions are scaleless and hence vanish so we only need to evaluate the real diagrams. They add to

$$2 \quad \delta_R = 2g^2\mu^{2\epsilon} C_F\, n\cdot\bar{n} \int \frac{\mathrm{d}^d k}{(2\pi)^d} \frac{1}{k^-}\frac{1}{k^+} 2\pi\delta(k^- k^+ - |\mathbf{k}_\perp|^2)\,\theta(k^-)\delta_R(\tau_a^s, k)\,. \tag{3.37}$$

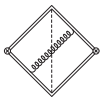

Performing the k integrals gives

$$S_a^{\mathrm{PT}(0)}(\tau_a^s;\mu) = \delta(\tau_a^s) + \theta(\tau_a^s)\frac{\alpha_s C_F\, n\cdot\bar{n}}{\pi(1-a)} \left(\frac{4\pi\mu^2}{Q^2}\right)^{\epsilon} \frac{1}{\Gamma(1-\epsilon)}\frac{1}{\epsilon}\left(\frac{1}{\tau_a^s}\right)^{1+2\epsilon} . \tag{3.38}$$

Nonzero values of τ_a^s regulate the IR divergences, and so here the $1/\epsilon$ pole is of UV origin, $\epsilon = \epsilon_{\mathrm{UV}}$.

Applying the distribution relation (valid for $\epsilon < 0$)

$$\frac{\theta(x)}{x^{1+2\epsilon}} = -\frac{\delta(x)}{2\epsilon} + \left[\frac{\theta(x)}{x}\right]_+ - 2\epsilon\left[\frac{\theta(x)\ln x}{x}\right]_+ + \mathcal{O}(\epsilon^2)\,, \tag{3.39}$$

where

$$\left[\frac{\theta(x)\ln^n(x)}{x}\right]_+ \equiv \lim_{\beta\to 0}\left[\frac{\theta(x-\beta)\ln^n(x)}{x} + \frac{\ln^{n+1}\beta}{n+1}\delta(x-\beta)\right], \tag{3.40}$$

to Eq. (3.38) we obtain the final result for the (bare) angularity soft function,

$$S_a^{\mathrm{PT}(0)}(\tau_a^s;\mu) = \int \mathrm{d}\tau_a^{s'}\, Z_S(\tau_a^s - \tau_a^{s'};\mu) S_a(\tau_a^{s'};\mu)\,, \tag{3.41}$$

where to NLO the renormalized soft function, $S_a^{\rm PT}$, is given by

$$S_a^{\rm PT}(\tau_a^s;\mu) = \delta(\tau_a^s)\left[1 - \frac{\alpha_s C_F}{\pi(1-a)}\left(\frac{1}{2}\ln^2\frac{\mu^2}{Q^2} - \frac{\pi^2}{12}\right)\right] + \frac{2\alpha_s C_F}{\pi(1-a)}\left[\frac{\theta(\tau_a^s)}{\tau_a^s}\ln\frac{\mu^2}{(Q\tau_a^s)^2}\right]_+ , \qquad (3.42)$$

and the renormalization factor, Z_S, is given by

$$Z_S(\tau_a^s;\mu) = \delta(\tau_a^s)\left[1 - \frac{\alpha_s C_F}{\pi(1-a)}\left(\frac{1}{\epsilon^2} + \frac{1}{\epsilon}\ln\frac{\mu^2}{Q^2}\right)\right] + \frac{1}{\epsilon}\frac{2\alpha_s C_F}{\pi(1-a)}\left[\frac{\theta(\tau_a^s)}{\tau_a^s}\right]_+ . \qquad (3.43)$$

3.4 IR structure of the soft function

While the mathematical identity in Eq. (3.39) allowed us to arrive at our final result, Eq. (3.42), the origin of the $1/\epsilon$ poles became obscured through its use. In fact, the use of Eq. (3.39) is only valid for $\epsilon < 0$ which suggests that the $1/\epsilon$ pole on the right-hand side of Eq. (3.39) is of IR origin. The virtual diagrams, while formally zero in pure dimensional regularization, play the role of converting this IR divergence into a UV divergence by adding a quantity proportional to $(1/\epsilon_{\rm UV} - 1/\epsilon_{\rm IR})$ to the coefficient of $\delta(\tau_a^s)$, if the final result is in fact free of IR divergences. Naïvely it seems that this conversion cannot possibly occur for arbitrary a, because the $1/\epsilon$ poles in the real diagrams have a-dependent coefficients (see Eq. (3.43)), while the virtual diagrams contain no apparent a dependence. Nevertheless, by carefully examining the contribution of both the real and virtual diagrams, we will show that, for $a < 1$, the virtual diagrams play precisely this role and convert each IR divergence in the real graphs into UV, but that for $a \geq 1$, this cancellation is incomplete. This is accomplished through an analysis of integration regions in the loop momentum integrals that avoids the use of explicit IR regulators. Our presentation here complements our discussion of these issues in [102].

Using that $\int_0^1 {\rm d}x\,[\ln^n(x)/x]_+ = 0$, the contribution to the coefficient of $\delta(\tau_a^s)$ can be isolated by integrating the diagrams over τ_a^s from 0 to 1. We find that the contribution from the real diagrams can be written as

$$\int_0^1 {\rm d}\tau_a^s \left[2 \quad \delta_R\right] = \frac{\alpha_s C_F\, n\cdot\bar n}{2\pi}\frac{\left(4\pi\mu^2\right)^\epsilon}{\Gamma(1-\epsilon)}\int_{\mathcal R} {\rm d}k^+ {\rm d}k^- (k^+k^-)^{-1-\epsilon}\,, \qquad (3.44)$$

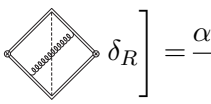

where $\mathcal{R}$ is given by the region of positive k^+ and k^- such that

$$\begin{aligned} (k^-)^{\frac{a}{2}}(k^+)^{1-\frac{a}{2}} &< Q \quad \text{for} \quad k^- \geq k^+ \\ (k^+)^{\frac{a}{2}}(k^-)^{1-\frac{a}{2}} &< Q \quad \text{for} \quad k^- \leq k^+ \,. \end{aligned} \qquad (3.45)$$

This region is plotted in Fig. 3.2A for various values of a.

The contribution of the virtual diagrams to the coefficient of $\delta(\tau_a^s)$ sums to

$$\begin{aligned} \int_0^1 {\rm d}\tau_a^s \left[2 \quad \delta_V\right] &= 2g^2\mu^{2\epsilon} C_F\, n\cdot\bar n \int \frac{{\rm d}^d k}{(2\pi)^d}\frac{1}{k^- - i0^+}\frac{1}{k^+ + i0^+}\frac{i}{k^+k^- - |\mathbf{k}_\perp|^2 - i0^+} \\ &= -\frac{\alpha_s C_F\, n\cdot\bar n}{2\pi}\frac{\left(4\pi\mu^2\right)^\epsilon}{\Gamma(1-\epsilon)}\int_{\mathcal V} {\rm d}k^+ {\rm d}k^- (k^+k^-)^{-1-\epsilon}\,, \end{aligned} \qquad (3.46)$$

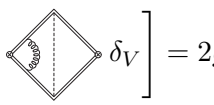

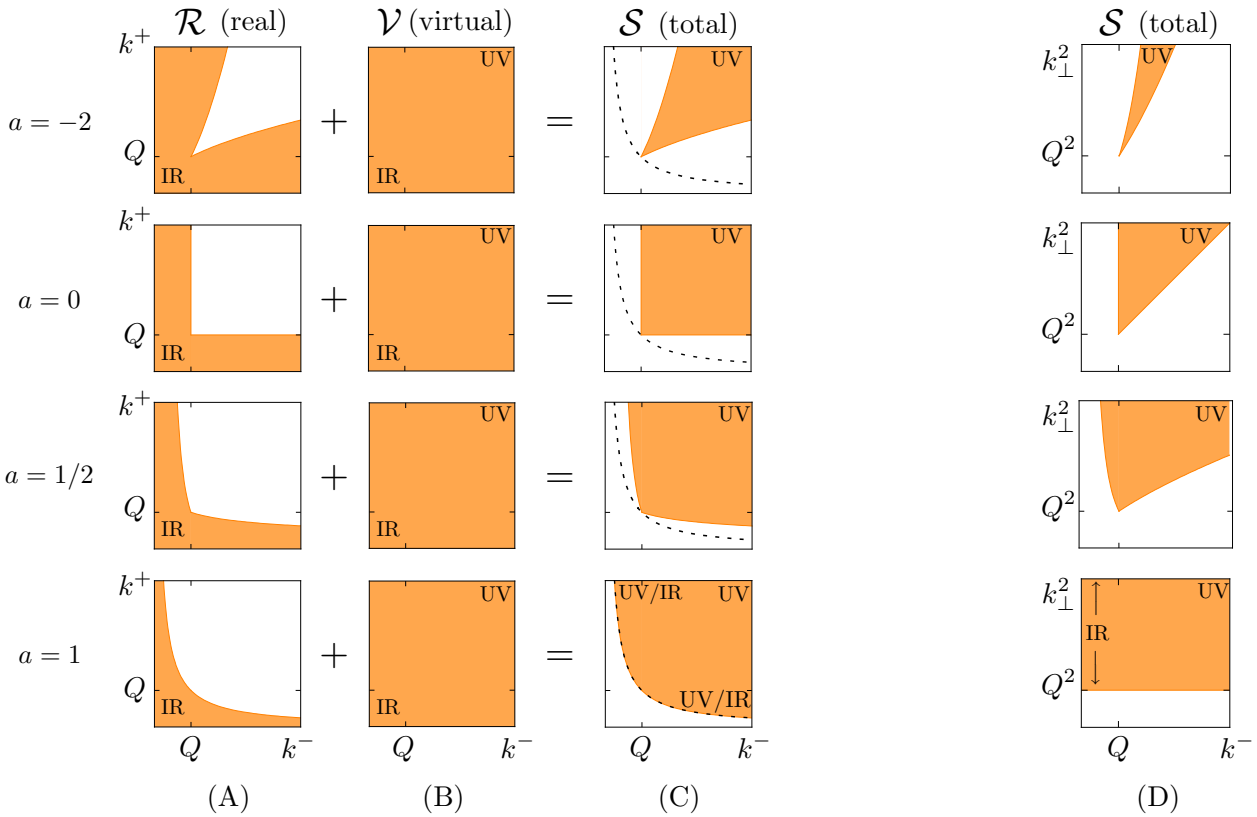

Figure 3.2: The regions of integration for the coefficent of $\delta(\tau_a^s)$ in $S_a^{(0)}(\tau_a^s)$ in the (A), (B), (C) k^-, k^+ and (D) $k^-, \mathbf{k}_\perp^2$ planes. The regions of integration for both (A) the real contribution $\mathcal{R}$ and (B) the virtual contribution $\mathcal{V}$ contain both UV and IR divergences. Since the integrands for the two contributions differ only by an overall minus sign, (C) the region resulting in their sum $\mathcal{S}$, is the complement of $\mathcal{R}$ and contains only UV divergences for $a < 1$. The dashed line in (C) represents the line of constant $k^+k^- = Q^2$.

where $\mathcal{V}$ is the entire positive k^+, k^- quadrant, plotted in Fig. 3.2B.

The two contributions to $\delta(\tau_a^s)$, Eqs. (3.44) and (3.46), are each both UV and IR divergent, but as we will show, their sum is convergent for $\epsilon > 0$ and so is only UV divergent. Since the form of the integrand is the same and the virtual contribution differs only by an overall minus sign, it converts the region of integration of the real contribution, $\mathcal{R}$, into the complementary part of the positive k^+, k^- quadrant (see Fig. 3.2) which does not include the IR divergent regions $k^\pm \to 0$. Note that as $a \to 1$, the boundary of the region of integration $\mathcal{R}$ approaches the curve of constant $k^+k^- = Q^2$. With this boundary, the integral over the region $\mathcal{S}$ does not converge for either positive or negative ϵ, implying that both IR and UV divergences are present.

That the region $\mathcal{S}$ has only UV divergence for $a < 1$ and has both UV and IR divergence for $a = 1$ is perhaps more clearly seen in the $k^-, \mathbf{k}_\perp^2$ plane. The integral of the soft diagrams over

τ_a^s in terms of these variables is given by

$$\int_0^1 \mathrm{d}\tau_a^s \left[2 \; \delta_R + 2 \; \delta_V \right] = -\frac{\alpha_s C_F \, n\cdot\bar{n}}{2\pi} \frac{\left(4\pi\mu^2\right)^\epsilon}{\Gamma(1-\epsilon)} \int_{\mathcal{S}} \frac{\mathrm{d}k^- \mathrm{d}\mathbf{k}_\perp^2}{k^- (\mathbf{k}_\perp^2)^{1+\epsilon}} \,,$$

and the resulting region $\mathcal{S}$ in terms of k^- and $\mathbf{k}_\perp^2$ for $a \leq 1$ is

$$\left(\frac{\mathbf{k}_\perp^2}{Q^2}\right)^{-\frac{a}{2(1-a)}} < \left(\frac{k^-}{Q}\right) < \left(\frac{\mathbf{k}_\perp^2}{Q^2}\right)^{\frac{2-a}{2(1-a)}} \quad \text{with} \quad \mathbf{k}_\perp^2 > Q^2 \,. \tag{3.47}$$

The region $\mathcal{S}$ is plotted for several values of a in Fig. 3.2D. The limiting case $a = 1$ clearly includes the IR divergent region $k^- \to 0$ for all $\mathbf{k}_\perp^2 > Q^2$.

Performing the integral over $\mathcal{S}$ we obtain

$$\int_0^1 \mathrm{d}\tau_a^s \, S_a^{(0)}(\tau_a^s;\mu) = 1 - \frac{\alpha_s C_F \, n\cdot\bar{n}}{2\pi(1-a)} \left(\frac{4\pi\mu^2}{Q^2}\right)^\epsilon \frac{1}{\epsilon^2 \, \Gamma(1-\epsilon)} \,. \tag{3.48}$$

After expanding Eq. (3.48) in ϵ, we find that the coefficient of $\delta(\tau_a^s)$ in Eq. (3.42) is unchanged, except that for $a < 1$ all the $1/\epsilon$ poles are unambiguously of UV origin.

A lesson from this analysis is that in pure dimensional regularization, the coefficient of $(1/\epsilon_{\mathrm{UV}} - 1/\epsilon_{\mathrm{IR}})$ in a virtual diagram cannot be determined from the virtual diagram alone, but only together with the real diagram whose IR divergence it is supposed to cancel. The reason that the virtual subtraction can depend on a even though by itself it is independent of a is that the area of overlap between the integration regions of real and virtual diagrams depends on a.

3.5 Calculation of the jet functions to NLO

Now we proceed to calculate the jet functions given by Eqs. (3.21) and (3.22). The diagrams that contribute to J_a^n are shown in Fig. 3.3, and the Feynman rules necessary to calculate these diagrams are found in [14]. The total momentum flowing through each diagram is $Qn/2 + l$, with the label component $Qn/2$ specified by the labels on the jet fields in the matrix elements in Eq. (3.22a), and l the residual momentum. The total momentum of the gluon in each loop is q, which has both label and residual components. All results for the anti-quark jet function $J_a^{\bar{n}}$ can be found from those for the quark jet function J_a^n with the replacement $n \leftrightarrow \bar{n}$ and so we calculate explicitly only J_a^n.

Cutting the diagrams in Fig. 3.3 in all possible places, we can cut through the gluon loops or through one of the individual quark propagators connected to a current. We naturally call these classes of cut diagrams "real" and "virtual" respectively. The real and virtual diagrams contain the delta functions,

$$\begin{aligned} \delta_R &\equiv \delta_R(\tau_a^n, q, l^+) \equiv \delta\Big(\tau_a^n - \frac{1}{Q}\Big[(q^-)^{\frac{a}{2}}(q^+)^{1-\frac{a}{2}} + (Q-q^-)^{\frac{a}{2}}(l^+-q^+)^{1-\frac{a}{2}}\Big]\Big) \,, \\ \delta_V &\equiv \delta_V(\tau_a^n, l^+) \equiv \delta\Big(\tau_a^n - \big(l^+/Q\big)^{1-\frac{a}{2}}\Big) \,, \end{aligned} \tag{3.49}$$

which are obtained using Eq. (3.34). In this case we simply consider the contribution to τ_a from a final state with a single on-shell collinear quark of momentum l for δ_V and from a final state

Figure 3.3: Diagrams contributing to the angularity jet function $\mathcal{J}_a^n(\tau_a^n, l^+)$ with incoming momentum $l = \frac{n}{2}Q + \frac{\bar{n}}{2}l^+$ and gluon momentum q: (A) Wilson line emission diagram and (B) its mirror; (C) sunset and (D) tadpole QCD-like diagrams. The contributions to the jet function $J_a^n(\tau_a^n)$ are given by the integrals of these diagrams over the + component of the incoming momentum, $\int \mathrm{d}l^+ \mathcal{J}_a^n(\tau_a^n, l^+) = 2\pi J_a^n(\tau_a^n)$.

consisting of an on-shell collinear gluon of momentum q together with an on-shell collinear quark of momentum $l - q$ for δ_R, and use that the '$-$' component of momentum is always larger than the '+' component for on-shell collinear particles. The momentum l flowing through the diagrams in Fig. 3.3 has a label component which is fixed to be $Qn/2$ by the labels on the collinear fields in the matrix element in Eq. (3.22a).

Before turning to evaluate the diagrams in Fig. 3.3, we first perform a few simplifications to facilitate the computation. First, we note that the Wilson line emission diagram, Fig. 3.3A, and its mirror, Fig. 3.3B, give identical contributions. Second, we employ the fact that the number and complexity of jet function diagrams needed in loop calculations is reduced by noticing that the QCD-like diagrams can be computed using ordinary QCD Feynman rules with appropriate insertions of the projection operators $P_n = \not{n}\not{\bar{n}}/4$ and $P_{\bar{n}} = \not{\bar{n}}\not{n}/4$ [28, 9]. In particular, for our one-loop example we use that the sum of Fig. 3.3C and Fig. 3.3D reduces to

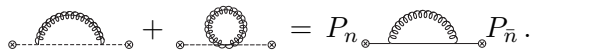

(3.50)

Next, we relate the τ_a^n-discontinuity to the ordinary discontinuity,

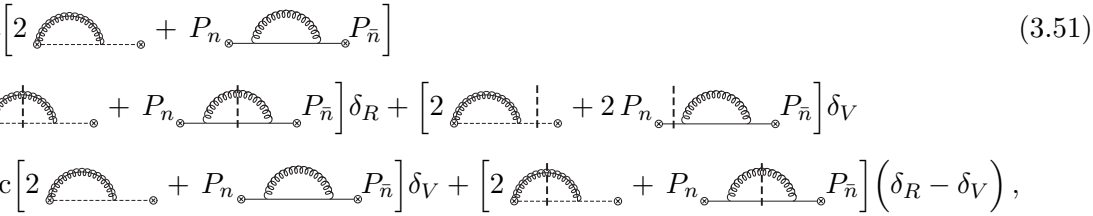

(3.51)

where in the third line the we used that the real diagrams induced by taking the discontinuity in the first term cancel the coefficient of δ_V in the second term.

Now, since $\delta_V(\tau_a^n, l^+)$ has no dependence on the loop momentum q, it factors out of the $\mathrm{d}^d q$ integrand. This implies that, after adding the tree-level contribution to the one-loop τ_a^n-discontinuity in Eq. (3.51), we can write the NLO jet function as

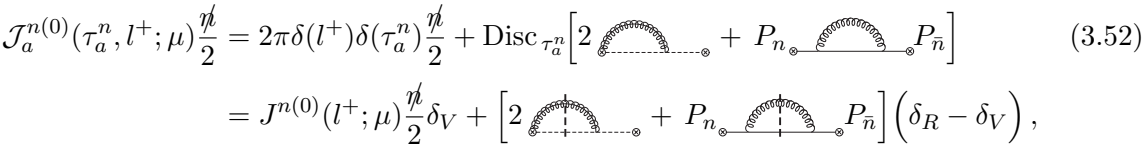

(3.52)

where $J_n^{(0)}(l^+;\mu)$ is the standard jet function [21],

$$J^{n(0)}(l^+;\mu)\frac{\not{n}}{2} \equiv \frac{1}{N_C}\mathrm{Disc}\left[\int \mathrm{d}^4x\, e^{il\cdot x}\,\mathrm{Tr}\left\langle 0\right|\mathrm{T}\,\chi_{n,Q}(x)\,\bar{\chi}_{n,Q}(0)\left|0\right\rangle\right]$$
$$= 2\pi\delta(l^+)\frac{\not{n}}{2} + \mathrm{Disc}\Big[2$$ 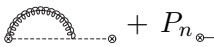 $$+\ P_n$$ 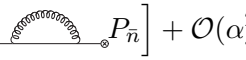 $$P_{\bar{n}}\Big] + \mathcal{O}(\alpha_s^2)\,, \qquad (3.53)$$

containing no additional operator insertions. Each term on the second line of Eq. (3.52) is then well-defined[4] and straightforwardly calculable. In fact, $J^n(l^+;\mu)$ has been calculated to two loops [28], and we expect that the techniques we employed above are the most practical way to extend our results to two loops. The additional term on the second line of Eq. (3.52) is a sum of real emission diagrams containing a difference of the delta functions δ_R and δ_V. Note that for the special case $a = 0$, $\delta_V(\tau_a^n, l^+) = \delta_R(\tau_a^n, q, l^+)$ and this additional term vanishes, so $J^n = J^n_{a=0}$. This is why only the standard jet function is needed when $a = 0$.

To find the angularity jet function $J_a^n(\tau_a^n;\mu)$, we must integrate Eq. (3.52) over l^+ as in Eq. (3.21),

$$J_a^{n(0)}(\tau_a^n;\mu) = \int\frac{\mathrm{d}l^+}{2\pi}\mathcal{J}_a^{n(0)}(\tau_a^n, l^+;\mu)\,. \qquad (3.54)$$

By integrating the known one-loop expression for $J_n^{(0)}(l^+;\mu)$ (see, e.g., [18, 45]), we find that the contribution of the first term in Eq. (3.52) is

$$\int\frac{\mathrm{d}l^+}{2\pi}J^{n(0)}(l^+;\mu)\,\delta_V = \delta(\tau_a^n)\Bigg\{1 + \frac{\alpha_s C_F}{4\pi}\left[\frac{4}{\epsilon^2} + \frac{3}{\epsilon} + \frac{4}{\epsilon}\ln\frac{\mu^2}{Q^2} + 2\ln^2\frac{\mu^2}{Q^2}\right.$$
$$\left. + 3\ln\frac{\mu^2}{Q^2} + 7 - \pi^2\right]\Bigg\}$$
$$- \frac{1}{1-a/2}\left[\left(\frac{4}{\epsilon} + 3 + 8\ln\frac{\mu}{Q(\tau_a^n)^{1/(2-a)}}\right)\left(\frac{\theta(\tau_a^n)}{\tau_a^n}\right)\right]_+ . \qquad (3.55)$$

It is well known that all $1/\epsilon$ poles in this expression are of UV origin.

[4] By this we mean that had we evaluated the individual cut virtual QCD-like diagrams contained in the first line of Eq. (3.52) directly, we would have encountered the complication of cutting one lone quark propagator and thus putting the second lone, uncut quark propagator on shell also.

We find that the term involving the real QCD-like diagram in Eq. (3.52) is

$$\int \frac{\mathrm{d}l^+}{2\pi}\Big[\, P_n \otimes \!\!\smile\!\!\otimes P_{\bar n}\Big]\Big(\delta_R - \delta_V\Big) \tag{3.56}$$
$$= -g^2\mu^{2\epsilon} C_F (d-2)\frac{\not{n}}{2}\int\frac{\mathrm{d}l^+}{2\pi}\left(\frac{1}{l^+}\right)^2\int\frac{\mathrm{d}^d q}{(2\pi)^d}(l^+ - q^+)$$
$$\times\Big((-2\pi i)\delta(q^+q^- - |\mathbf{q}_\perp|^2)\theta(q^-)\Big)\frac{1}{q^-}\Big(\delta_R(\tau_a^n, q, l^+) - \delta_V(\tau_a^n, l^+)\Big)$$
$$\times\Big((-2\pi i)\delta\big((Q-q^-)(l^+-q^+) - |\mathbf{q}_\perp|^2\big)\theta(Q-q^-)\Big)$$
$$= \frac{\alpha_s C_F}{2\pi(2-a)}\frac{\not{n}}{2}\left(\frac{4\pi\mu^2}{Q^2}\right)^\epsilon\frac{2(1-\epsilon)}{\Gamma(1-\epsilon)}\left(\frac{1}{\tau_a^n}\right)^{1+\frac{\epsilon}{1-a/2}}$$
$$\times\int_0^1 \mathrm{d}x\, x\left[\big(x^{a-1}+(1-x)^{a-1}\big)^{\frac{\epsilon}{1-a/2}} - \big(x(1-x)\big)^{-\epsilon}\right],$$

where we defined $x \equiv q^-/Q$. This expression is finite as $\epsilon \to 0$.

For the term involving the real Wilson line diagram, we find

$$\int \frac{\mathrm{d}l^+}{2\pi}\Big[\, \smile\!\!\otimes\Big]\Big(\delta_R - \delta_V\Big) \tag{3.57}$$
$$= -g^2\mu^{2\epsilon} C_F\, n\cdot\bar n\frac{\not{n}}{2}\int\frac{\mathrm{d}l^+}{2\pi}\frac{1}{l^+}\int\frac{\mathrm{d}^d q}{(2\pi)^d}\frac{1}{q^-}\Big((-2\pi i)\delta(q^+q^- - |\mathbf{q}_\perp|^2)\theta(q^-)\Big)$$
$$\times\Bigg[(Q-q^-)\Big((-2\pi i)\delta\big((Q-q^-)(l^+-q^+) - |\mathbf{q}_\perp|^2\big)\theta(Q-q^-)\Big)$$
$$- Q\Big((-2\pi i)\delta\big(Q(l^+-q^+)\big)\Big)\Bigg]\Big(\delta_R(\tau_a^n, q, l^+) - \delta_V(\tau_a^n, l^+)\Big).$$

The piece with δ_R can be written as

$$\int \frac{\mathrm{d}l^+}{2\pi}\Big[\, \smile\!\!\otimes\Big]\delta_R = \theta(\tau_a^s)\frac{\alpha_s C_F n\cdot\bar n}{2\pi(2-a)}\frac{\not{n}}{2}\left(\frac{4\pi\mu^2}{Q^2}\right)^\epsilon\frac{1}{\Gamma(1-\epsilon)}\left(\frac{1}{\tau_a^n}\right)^{1+\frac{\epsilon}{1-a/2}} \tag{3.58}$$
$$\times\left[\int_0^1\frac{\mathrm{d}x}{x}(1-x)\big(x^{a-1}+(1-x)^{a-1}\big)^{\frac{\epsilon}{1-a/2}} - \int_0^\infty\frac{\mathrm{d}x}{x}x^{-\epsilon\frac{1-a}{1-a/2}}\right],$$

and the piece with δ_V is

$$\int \frac{\mathrm{d}l^+}{2\pi}\Big[\, \smile\!\!\otimes\Big]\delta_V = \theta(\tau_a^s)\frac{\alpha_s C_F n\cdot\bar n}{2\pi(2-a)}\frac{\not{n}}{2}\left(\frac{4\pi\mu^2}{Q^2}\right)^\epsilon\frac{1}{\Gamma(1-\epsilon)}\left(\frac{1}{\tau_a^n}\right)^{1+\frac{\epsilon}{1-a/2}}$$
$$\times\left[\int_0^1\frac{\mathrm{d}x}{x}(1-x)\big(x(1-x)\big)^{-\epsilon} - \int_0^\infty\frac{\mathrm{d}x}{x}x^{-\epsilon}\right]. \tag{3.59}$$

The second term in brackets in each of Eqs. (3.57), (3.58), and (3.59) corresponds to the zero-bin subraction [129] needed to avoid the double counting of soft modes [119, 105, 104]. Note that from the expressions in both Eqs. (3.58) and (3.59), the zero-bin contributions are scaleless and hence

formally zero. Their role is to convert the IR divergence ($q^- \to 0$) in each integrand into a UV divergence ($q^- \to \infty$) for $a < 1$. After this subtraction, both of the integrals over x in brackets are convergent for $\epsilon > 0$.

Subtracting Eq. (3.59) from Eq. (3.58) and performing the integral over x we find that

$$\int \frac{\mathrm{d}l^+}{2\pi} \mathrm{Disc}\Big[2 \quad + \; P_n \quad P_{\bar{n}}\Big]\Big(\delta_R - \delta_V\Big) \tag{3.60}$$
$$= -\frac{\alpha_s C_F}{2\pi(2-a)} \frac{\not{n}}{2} \left(\frac{4\pi\mu^2}{Q^2}\right)^{\epsilon} \frac{1}{\Gamma(1-\epsilon)} \frac{1}{\epsilon} \left(\frac{1}{\tau_a^n}\right)^{1+\frac{\epsilon}{1-a/2}} \left[\frac{2a}{1-a} + \epsilon^2 \frac{2a(\pi^2-9)}{3(2-a)}\right.$$
$$\left. - \epsilon^2 \frac{4}{1-a/2} \int_0^1 \mathrm{d}x \frac{1-x+x^2/2}{x} \ln[(1-x)^{1-a} + x^{1-a}] + \mathcal{O}(\epsilon^3)\right],$$

where the overall $1/\epsilon$ pole is of UV origin from the discussion above.

Applying the relation Eq. (3.39) to Eq. (3.60) and adding the result to Eq. (3.55), we arrive at our final expression for the (bare) NLO angularity jet function,

$$J_a^{n(0)}(\tau_a^n;\mu) = \int \mathrm{d}\tau_a^{n\prime}\, Z_J(\tau_a^n - \tau_a^{n\prime};\mu) J_a^n(\tau_a^{n\prime};\mu)\,, \tag{3.61}$$

where the renormalized jet function, J_a^n, is

$$J_a^n(\tau_a^n;\mu) = \delta(\tau_a^n)\left\{1 + \frac{\alpha_s C_F}{\pi}\left[\frac{1-a/2}{2(1-a)} \ln^2 \frac{\mu^2}{Q^2} + \frac{3}{4} \ln \frac{\mu^2}{Q^2} + f(a)\right]\right\}$$
$$- \frac{\alpha_s C_F}{\pi}\left[\left(\frac{3}{4}\frac{1}{1-a/2} + \frac{2}{1-a} \ln \frac{\mu}{Q(\tau_a^n)^{1/(2-a)}}\right)\left(\frac{\theta(\tau_a^n)}{\tau_a^n}\right)\right]_+, \tag{3.62}$$

where we defined

$$f(a) \equiv \frac{1}{1-a/2}\left(\frac{7-13a/2}{4} - \frac{\pi^2}{12}\frac{3-5a+9a^2/4}{1-a}\right.$$
$$\left. - \int_0^1 \mathrm{d}x \frac{1-x+x^2/2}{x} \ln[(1-x)^{1-a} + x^{1-a}]\right), \tag{3.63}$$

and the Z-factor is given by

$$Z_J(\tau_a^n;\mu) = \delta(\tau_a^n)\left[1 + \frac{\alpha_s C_F}{\pi}\left(\frac{1-a/2}{1-a}\left(\frac{1}{\epsilon^2} + \frac{1}{\epsilon}\ln\frac{\mu^2}{Q^2}\right) + \frac{3}{4\epsilon}\right)\right] - \frac{1}{\epsilon}\frac{\alpha_s C_F}{\pi(1-a)}\left[\frac{\theta(\tau_a^n)}{\tau_a^n}\right]_+. \tag{3.64}$$

3.6 IR structure of the jet functions

As we showed in Sec. 3.5, the $1/\epsilon$ pole in front of the plus-distribution corresponds to a UV divergence. However, as we discussed for the case of the soft function in Sec. 3.4, the use of Eq. (3.39) means that we can not immediately make the same claim for the poles in the coefficient of $\delta(\tau_a^n)$. We now perform an analysis similar to that in Sec. 3.4 by integrating over $0 < \tau_a^n < 1$ to isolate this coefficient and study its divergent structure in the resulting q^-, $\mathbf{q}_\perp^2$ integration regions, complementing our discussion in [102].

The diagrams (C) and (D) in Fig. 3.3, being equivalent to diagrams in full QCD as noted above, are manifestly infrared-finite and do not need to be analyzed in further detail. The Wilson line graphs (A) and (B) potentially contain infrared divergences that we must identify more carefully.

If the jet function is infrared-safe, infrared divergences in virtual and real diagrams, with proper zero-bin subtractions taken, should cancel and leave purely UV divergent integrals. The contribution of the sum of the real and virtual Wilson line diagrams to the coefficient of $\delta(\tau_a^n)$ in the jet function $J_a^{n(0)}(\tau_a^n)$ is

$$2\int_0^1 \mathrm{d}\tau_a \int \frac{\mathrm{d}l^+}{2\pi}\Big[\delta_V + \delta_R\Big] \tag{3.65}$$
$$= -\frac{\alpha_s C_F}{\pi}\frac{(4\pi\mu^2)^\epsilon}{\Gamma(1-\epsilon)}\left[\int_{\tilde{\mathcal{J}}} \mathrm{d}q^-\mathrm{d}\mathbf{q}_\perp^2 \frac{1}{(\mathbf{q}_\perp^2)^{1+\epsilon}}\left(\frac{1}{q^-}-\frac{1}{Q}\right) - \int_{\mathcal{J}_0} \mathrm{d}q^-\mathrm{d}\mathbf{q}_\perp^2 \frac{1}{(\mathbf{q}_\perp^2)^{1+\epsilon}}\frac{1}{q^-}\right],$$

where the last integral is the zero-bin subtraction of the naïve collinear integral in the first term. The naïve integration region $\tilde{\mathcal{J}}$ is shown in Fig. 3.4 and is given by $0 < q^- < Q$ and

$$\mathbf{q}_\perp^2 > \left\{ Q\left[\frac{1}{(Q-q^-)^{1-a}} + \frac{1}{(q^-)^{1-a}}\right]^{-1}\right\}^{\frac{1}{1-a/2}} . \tag{3.66}$$

The zero-bin region $\mathcal{J}_0$ is given by $q^- > 0$ and

$$\mathbf{q}_\perp^2 > \left[Q(q^-)^{1-a}\right]^{\frac{1}{1-a/2}} . \tag{3.67}$$

The resulting integral for the total contribution of the zero-bin-subtracted Wilson line diagrams to the coefficient of $\delta(\tau_a^n)$ in the jet function is

$$2\int_0^1 \mathrm{d}\tau_a \int \frac{\mathrm{d}l^+}{2\pi}\left[\delta_V + \delta_R\right] \tag{3.68}$$
$$= -\frac{\alpha_s C_F}{\pi}\frac{(4\pi\mu^2)^\epsilon}{\Gamma(1-\epsilon)}\left[\int_{\mathcal{J}} \mathrm{d}q^-\mathrm{d}\mathbf{q}_\perp^2 \frac{1}{(\mathbf{q}_\perp^2)^{1+\epsilon}}\frac{\mathrm{sgn}(q^--Q)}{q^-} - \int_{\tilde{\mathcal{J}}} \mathrm{d}q^-\mathrm{d}\mathbf{q}_\perp^2 \frac{1}{(\mathbf{q}_\perp^2)^{1+\epsilon}}\frac{1}{Q}\right],$$

where the region $\mathcal{J}$ resulting from combining $\tilde{\mathcal{J}}$ and $\mathcal{J}_0$, with a relative minus sign in the integrands, is also shown in Fig. 3.4.

The shape of the final integration region $\mathcal{J}$ in Fig. 3.4 demonstrates that the scaleless virtual and zero-bin integrals succeed in converting IR divergences in the real diagram contributions into UV divergences for all $a < 1$. The integral over $\mathcal{J}$ in Eq. (3.68) converges for $\epsilon > 0$ if and only if $a < 1$. The result of performing this integration, after including the contributions of the QCD-like diagrams in Fig. 3.3C and D, agrees with the coefficient of $\delta(\tau_a^n)$ that is obtained by (naïvely) using the relation Eq. (3.39) in Eq. (3.60).

3.7 Infrared safety, factorizability, and the effective theory

In the one-loop calculations of soft and jet functions above, we observed that infrared safety of these functions, and, thus, factorizability of the angularity distributions, required $a < 1$.

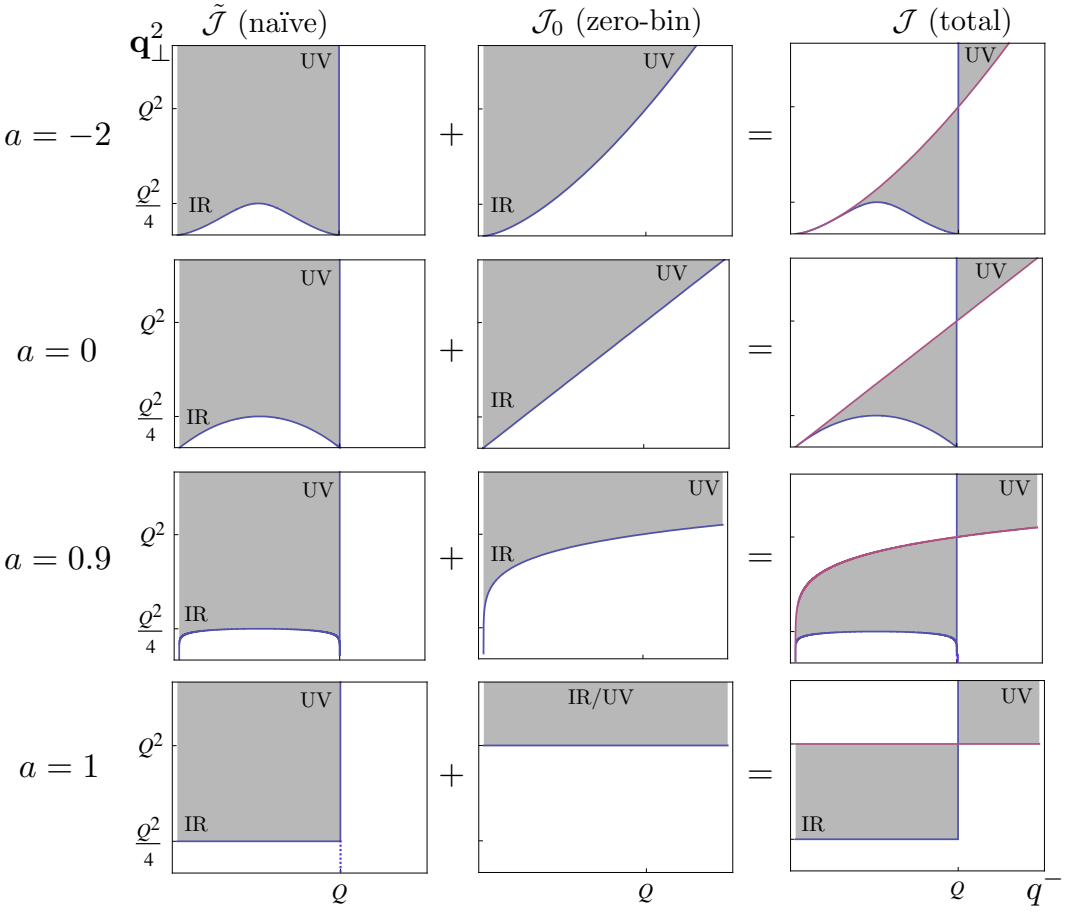

Figure 3.4: Regions of integration for the coefficient of $\delta(\tau_a^n)$ in the jet function $J_a^{n(0)}(\tau_a^n)$. The sum of naïve real and virtual Wilson line diagrams are integrated over the region $\tilde{\mathcal{J}}$ in the $q^-, \mathbf{q}_\perp^2$ plane. The sum of real and virtual zero-bin subtractions are integrated over $\mathcal{J}_0$, and the resulting sum of naïve diagrams and zero-bin subtractions over the region $\mathcal{J}$. Integrals over $\mathcal{J}$ have only UV divergences as long as $a < 1$. For $a = 1$, an IR divergent region remains.

By analyzing explicitly the regions of integration over loop momenta in real and virtual graphs, we were able to identify when the loop integrals contained infrared or ultraviolet divergences. Cancellations of regions in real gluon diagrams sensitive to IR divergences relied crucially not only on the addition of virtual diagrams but also on zero-bin subtractions from collinear diagrams (see also examples in [129, 105, 104, 57]).

The shape of the momentum regions contributing to the one-loop soft function in Fig. 3.2 suggest a simple physical interpretation of the breakdown of factorization as $a \to 1$. In the $k^\pm$ plane, the region of integration in the sum of real and virtual graphs for $a = 1$ is the region above the line $k^+k^- = Q^2$. For angularity soft functions with $a < 1$, as $k^\pm \to \infty$, the loop integral goes over a region with k^+k^- strictly greater than Q^2, and in fact, $k^+k^- \to \infty$, while for $a > 1$, the loop integral enters the region with $k^+k^- < Q^2$, and in fact, $k^+k^- \to 0$. But this latter region, $k^+ \to \infty$ while $k^- \to 0$ or vice versa, is the region where collinear modes live, illustrated in Fig. 3.5.

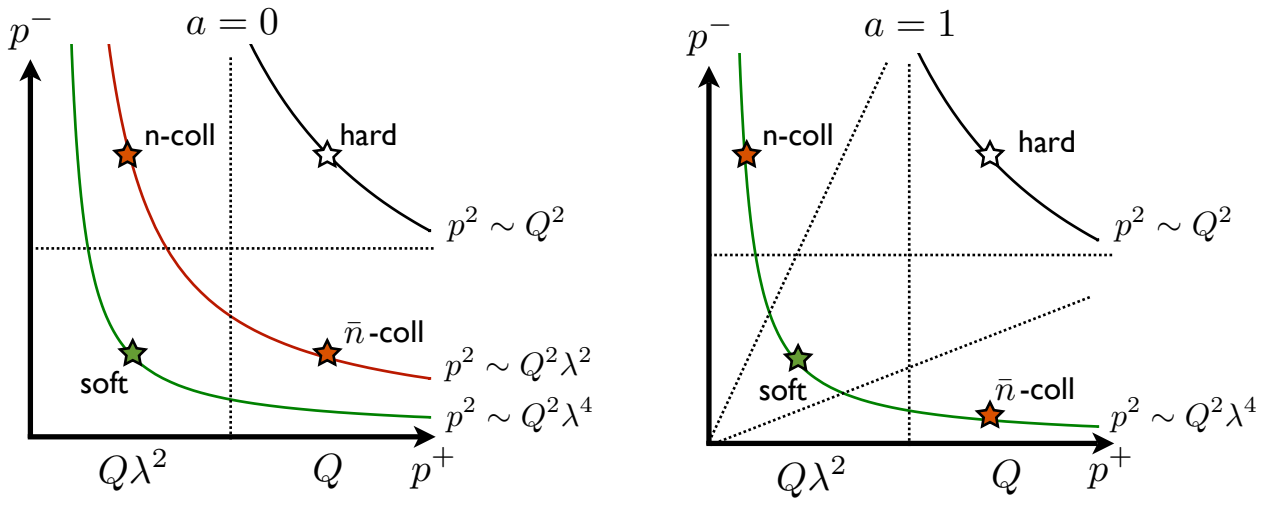

Figure 3.5: Scaling of SCET modes appropriate for angularities τ_a, $a = 0, 1$. For $a = 0$, the collinear modes dominating the τ_a distribution have virtualities $p^2 \sim (Q\lambda)^2$, parametrically separated from the soft scale $p^2 \sim (Q\lambda^2)^2$. These scalings correspond to the effective theory known as SCET$_{\rm I}$. For $a = 1$, the collinear modes in the distribution have typical $p^2 \sim (Q\lambda^2)^2$, coinciding with the soft scale. The collinear and soft modes are no longer separated by virtuality but instead by rapidity. These scalings correspond to SCET$_{\rm II}$. Collinear modes dominating angularity distributions for other values of a between 0 and 1 live at scales intermediate between these limits.

This means that collinear modes still contribute to the soft function even after the attempted factorization.

This suggests that for $a \geq 1$, the contributions of SCET$_{\rm I}$ soft and collinear modes to the angularity distribution have not actually been separated. In SCET$_{\rm I}$, soft, collinear, and hard modes can be distingushed by their well-separated virtualities, namely, $p_S^2 \sim (Q\lambda^2)^2$, $p_J^2 \sim (Q\lambda^{1/(1-a/2)})^2$, and $p_H^2 \sim Q^2$. At $a = 1$, the virtualities of soft and collinear modes contributing to the τ_a distribution coincide, and SCET$_{\rm I}$ must be matched onto SCET$_{\rm II}$ where collinear and soft modes both have virtualities $p^2 \sim (Q\lambda^2)^2$. In this case, the modes are no longer distinguished by their virtuality, but instead by their rapidity, as illustrated in Fig. 3.5. Ref. [129] suggested a modified version of the factorization theorem Eq. (3.1) in which soft and jet functions are defined either with cutoffs on rapidity or in dimensional regularization with the scale μ separated into two light-cone scales $\mu^\pm$, which must satisfy $\mu^+\mu^- = \mu^2$, with each of the two jet functions depending on one of these scales, and the soft function on both. However, in the present paper we do not pursue such a strategy and limit our analysis to angularities with strictly $a < 1$. For arbitrary values of a, the virtuality of collinear modes $p_J^2 \sim (Q\lambda^{1/(1-a/2)})^2$ suggests an interpretation as the modes of an effective theory "SCET$_{1+a}$."[5] Since our analysis and calculations utilize the framework of SCET$_{\rm I}$, we may expect non-negligible corrections to our results to arise for values of a less than but approaching 1, and for reasonable criteria for when corrections are negligible, our analysis is reliable for values of $a \lesssim 1/2$ [119].

[5]We would like to thank M. Strassler for suggesting this terminology to CL.

4 NLL Resummation of Logarithms and Fixed-order Matching to QCD

The fixed-order NLO cross-section, obtained by using the fixed-order expressions for the hard, jet, and soft functions in Eqs. (3.29), (3.42), and (3.62) in the factorization formula Eq. (3.18), contain logarithms of μ divided by the scales Q, $Q\tau_a$, and the intermediate scale $Q\tau_a^{1/(2-a)}$. This means that there is no single choice for the scale μ that will simultaneously set all of the logarithms in the NLO cross-section to zero. For small τ_a, these scales become widely separated and the logarithms of ratios of these scales become large, which causes the perturbative series to break down. In Sec. 4.1 and Sec. 4.2, we take advantage of the effective theory framework separating the hard, jet, and soft contributions by evolving each of them separately through renormalization-group (RG) evolution which resums these logarithms. We then combine these RG-evolved functions into the full cross-section accurate to NLO at fixed order in α_s and resummed to NLL accuracy in Sec. 4.3.

Since our final result for the NLL/NLO resummed distribution is derived using an effective theory which is valid only in the small-τ_a limit, it does not get the larger-τ_a region as accurately as QCD at $\mathcal{O}(\alpha_s)$. To arrive at a result that retains NLL/NLO accuracy in the small-τ_a region while retaining the accuracy of QCD at $\mathcal{O}(\alpha_s)$ in the larger-τ_a region, we need to match our distribution onto QCD. This matching is constructed such that if we turn off the resummation, the distributions should agree with full QCD to $\mathcal{O}(\alpha_s)$. We perform this matching in Sec. 4.4.

4.1 Hard function at NLL

The anomalous dimension of the hard function in Eq. (3.29) can be found by requiring that matrix elements of the bare two-jet operator in Eq. (3.30) are independent of the scale μ, and is given by

$$\gamma_H(\mu) = -\gamma_{\mathcal{O}}(Qn/2, -Q\bar{n}/2; \mu) - \gamma_{\mathcal{O}}^*(Qn/2, -Q\bar{n}/2; \mu)\,, \tag{3.69}$$

where

$$\gamma_{\mathcal{O}}(\tilde{p}_n, \tilde{p}_{\bar{n}}; \mu) = -Z_{\mathcal{O}}^{-1}(\tilde{p}_n, \tilde{p}_{\bar{n}}; \mu)\mu\frac{\mathrm{d}}{\mathrm{d}\mu}Z_{\mathcal{O}}(\tilde{p}_n, \tilde{p}_{\bar{n}}; \mu) = \frac{\alpha_s C_F}{2\pi}\left(2\ln\frac{\mu^2}{2\tilde{p}_n\cdot\tilde{p}_{\bar{n}}} + 3\right)\,, \tag{3.70}$$

so that

$$\gamma_H(\mu) = -\frac{\alpha_s C_F}{\pi}\left(2\ln\frac{\mu^2}{Q^2} + 3\right)\,, \tag{3.71}$$

which is the first term in the expansion of the anomalous dimension to all orders in α_s,

$$\gamma_H(\mu) = \Gamma_H[\alpha_s]\ln\frac{\mu^2}{Q^2} + \gamma_H[\alpha_s]\,. \tag{3.72}$$

Solving the RG equation,

$$\mu\frac{\mathrm{d}}{\mathrm{d}\mu}H(Q;\mu) = \gamma_H(\mu)H(Q;\mu)\,, \tag{3.73}$$

for $H(Q;\mu)$ gives

$$H(Q;\mu) = H(Q;\mu_0)e^{K_H}\left(\frac{\mu_0}{Q}\right)^{\omega_H}\,, \tag{3.74}$$

where ω_H and K_H are defined as

$$\omega_H \equiv \omega_H(\mu,\mu_0) \equiv \frac{8C_F}{\beta_0}\left[\ln r + \left(\frac{\Gamma^1_{\rm cusp}}{\Gamma^0_{\rm cusp}} - \frac{\beta_1}{\beta_0}\right)\frac{\alpha_s(\mu_0)}{4\pi}(r-1)\right] \tag{3.75a}$$

$$\begin{aligned} K_H \equiv K_H(\mu,\mu_0) \equiv{}& \frac{6C_F}{\beta_0}\ln r + \frac{16\pi C_F}{(\beta_0)^2}\left[\frac{r-1-r\ln r}{\alpha_s(\mu)}\right. \\ &\left. + \left(\frac{\Gamma^1_{\rm cusp}}{\Gamma^0_{\rm cusp}} - \frac{\beta_1}{\beta_0}\right)\frac{1-r+\ln r}{4\pi} + \frac{\beta_1}{8\pi\beta_0}\ln^2 r\right]. \end{aligned} \tag{3.75b}$$

Here $r = \frac{\alpha_s(\mu)}{\alpha_s(\mu_0)}$, and β_0, β_1 are the one-loop and two-loop coefficients of the beta function,

$$\beta[\alpha_s] = \mu\frac{{\rm d}\alpha_s}{{\rm d}\mu} = -2\alpha_s\left[\beta_0\left(\frac{\alpha_s}{4\pi}\right) + \beta_1\left(\frac{\alpha_s}{4\pi}\right)^2 + \cdots\right], \tag{3.76}$$

where

$$\beta_0 = \frac{11C_A}{3} - \frac{2n_f}{3} \qquad \text{and} \qquad \beta_1 = \frac{34C_A^2}{3} - \frac{10C_An_f}{3} - 2C_Fn_f\,. \tag{3.77}$$

The two-loop running coupling $\alpha_s(\mu)$ at any scale is given by

$$\frac{1}{\alpha_s(\mu)} = \frac{1}{\alpha_s(M_Z)} + \frac{\beta_0}{2\pi}\ln\left(\frac{\mu}{M_Z}\right) + \frac{\beta_1}{4\pi\beta_0}\ln\left[1 + \frac{\beta_0}{2\pi}\alpha_s(M_Z)\ln\left(\frac{\mu}{M_Z}\right)\right]. \tag{3.78}$$

In Eq. (3.74), we have used the fact that to all orders in perturbation theory, $\Gamma_H[\alpha_s]$ is proportional to $\Gamma_{\rm cusp}[\alpha_s]$, where

$$\Gamma_{\rm cusp}[\alpha_s] = \left(\frac{\alpha_s}{4\pi}\right)\Gamma^0_{\rm cusp} + \left(\frac{\alpha_s}{4\pi}\right)^2\Gamma^1_{\rm cusp} + \cdots\,. \tag{3.79}$$

The ratio of the one-loop and two-loop coefficients of $\Gamma_{\rm cusp}$ is [111]

$$\frac{\Gamma^1_{\rm cusp}}{\Gamma^0_{\rm cusp}} = \left(\frac{67}{9} - \frac{\pi^2}{3}\right)C_A - \frac{10n_f}{9}\,. \tag{3.80}$$

$\Gamma^1_{\rm cusp}$ and β_1 are needed in the expressions of ω_H and K_H for complete NLL resummation since we formally take $\alpha_s^2\ln\tau_a \sim \mathcal{O}(\alpha_s)$.

4.2 Jet and soft functions at NLL

The jet and soft functions obey the RG equation

$$\mu\frac{d}{d\mu}F(\tau;\mu) = \int_{-\infty}^{+\infty}{\rm d}\tau'\,\gamma_F(\tau-\tau';\mu)F(\tau';\mu)\,, \tag{3.81}$$

where $F = J, S$. The anomalous dimensions γ_F can be found from the Z-factors (given in Eqs. (3.43) and (3.64)) via the relation

$$\gamma_F(\tau - \tau'; \mu) = -\int \mathrm{d}\tau''\, Z_F^{-1}(\tau - \tau''; \mu)\, \mu \frac{\mathrm{d}}{\mathrm{d}\mu} Z_F(\tau'' - \tau'; \mu)\,. \tag{3.82}$$

We find that

$$\gamma_J(\tau - \tau'; \mu) = \frac{2\alpha_s C_F}{\pi} \left\{ \delta(\tau - \tau') \left(\frac{1 - a/2}{1 - a} \ln \frac{\mu^2}{Q^2} + \frac{3}{4} \right) - \frac{1}{1 - a} \left[\frac{\theta(\tau - \tau')}{\tau - \tau'} \right]_+ \right\}, \tag{3.83}$$

and

$$\gamma_S(\tau - \tau'; \mu) = \frac{2\alpha_s C_F}{\pi(1 - a)} \left\{ -\delta(\tau - \tau') \ln \frac{\mu^2}{Q^2} + 2 \left[\frac{\theta(\tau - \tau')}{\tau - \tau'} \right]_+ \right\}. \tag{3.84}$$

Both anomalous dimensions are the first terms in the perturbative expansion of the general form to all orders in α_s [87, 95],

$$\gamma_F(\tau - \tau'; \mu) = -\Gamma_F[\alpha_s] \left(\frac{2}{j_F} \left[\frac{\theta(\tau - \tau')}{(\tau - \tau')} \right]_+ - \ln \frac{\mu^2}{Q^2}\, \delta(\tau - \tau') \right) + \gamma_F[\alpha_s] \delta(\tau - \tau')\,, \tag{3.85}$$

where the coefficients $\Gamma_F[\alpha_s], \gamma_F[\alpha_s]$ have the expansions

$$\Gamma_F[\alpha_s] = \left(\frac{\alpha_s}{4\pi} \right) \Gamma_F^0 + \left(\frac{\alpha_s}{4\pi} \right)^2 \Gamma_F^1 + \cdots \tag{3.86}$$

and

$$\gamma_F[\alpha_s] = \left(\frac{\alpha_s}{4\pi} \right) \gamma_F^0 + \left(\frac{\alpha_s}{4\pi} \right)^2 \gamma_F^1 + \cdots\,. \tag{3.87}$$

We summarize the coefficients Γ_F^0 and γ_F^0 and the j_F-values for the jet and soft functions in Table 3.1.

The solution of the RG equation Eq. (3.81) with the anomalous dimension γ_F of the form given in Eq. (3.85) with particular values of j_F was developed in the series of papers [30, 110, 5, 134]. Later, it was solved for arbitrary j_F in [87] using a convolution variable $t = Q^j \tau$ with mass dimension $j = j_F$. The resulting evolution equation for F is

$$F(\tau; \mu) = \int \mathrm{d}\tau'\, U_F(\tau - \tau'; \mu, \mu_0) F(\tau'; \mu_0)\,, \tag{3.88}$$

where the evolution kernel U_F is given to all orders in α_s by the expression

$$U_F(\tau - \tau'; \mu, \mu_0) = \frac{e^{\tilde{K}_F + \gamma_E \tilde{\omega}_F}}{\Gamma(-\tilde{\omega}_F)} \left(\frac{\mu_0}{Q} \right)^{j_F \tilde{\omega}_F} \left[\frac{\theta(\tau - \tau')}{(\tau - \tau')^{1 + \tilde{\omega}_F}} \right]_+, \tag{3.89}$$

where γ_E is the Euler constant and where $\tilde{\omega}_F$ and $\tilde{K}_F$ are defined as

$$\tilde{\omega}_F(\mu, \mu_0) \equiv \frac{2}{j_F} \int_{\alpha_s(\mu_0)}^{\alpha_s(\mu)} \frac{d\alpha}{\beta[\alpha]} \Gamma_F[\alpha]\,, \tag{3.90a}$$

$$\tilde{K}_F(\mu, \mu_0) \equiv \int_{\alpha_s(\mu_0)}^{\alpha_s(\mu)} \frac{d\alpha}{\beta[\alpha]} \gamma_F[\alpha] + 2 \int_{\alpha_s(\mu_0)}^{\alpha_s(\mu)} \frac{d\alpha}{\beta[\alpha]} \Gamma_F[\alpha] \int_{\alpha_s(\mu_0)}^{\alpha} \frac{d\alpha'}{\beta[\alpha']}\,. \tag{3.90b}$$

The plus function in Eq. (3.89) for all $\omega < 1$ and $\omega \neq 0$ is defined as[6]

$$\begin{aligned}\left[\frac{\theta(x)}{x^{1+\omega}}\right]_+ &\equiv \lim_{\beta\to 0}\left[\frac{\theta(x-\beta)}{x^{1+\omega}} - \frac{\beta^{-\omega}}{\omega}\delta(x-\beta)\right] \\ &= -\frac{\delta(x)}{\omega} + \sum_{n=0}^{\infty}(-\omega)^n\left[\frac{\theta(x)\ln^n x}{x}\right]_+ ,\end{aligned} \tag{3.91}$$

with the latter plus functions defined in Eq. (3.40).

For the NLL parameters of the evolution kernel U_F, Eq. (3.90) gives

$$\omega_F(\mu,\mu_0) = -\frac{\Gamma_F^0}{j_F\,\beta_0}\left[\ln r + \left(\frac{\Gamma^1_{\rm cusp}}{\Gamma^0_{\rm cusp}} - \frac{\beta_1}{\beta_0}\right)\frac{\alpha_s(\mu_0)}{4\pi}(r-1)\right] , \tag{3.92a}$$

$$\begin{aligned}K_F(\mu,\mu_0) = &-\frac{\gamma_F^0}{2\beta_0}\ln r + \frac{-2\pi\Gamma_F^0}{(\beta_0)^2}\bigg[\frac{r-1-r\ln r}{\alpha_s(\mu)} \\ &+ \left(\frac{\Gamma^1_{\rm cusp}}{\Gamma^0_{\rm cusp}} - \frac{\beta_1}{\beta_0}\right)\frac{1-r+\ln r}{4\pi} + \frac{\beta_1}{8\pi\beta_0}\ln^2 r\bigg] ,\end{aligned} \tag{3.92b}$$

where we have used the fact that $\Gamma_F \propto \Gamma_{\rm cusp}$. This proportionality is well known for the $a = 0$ jet and soft functions. In Appendix B we verify that it remains true for all $a < 1$.

From Eq. (3.88) we can write explicit formulas for the resummed jet and soft functions at any scale μ. Details of evaluating the integral over the convolution variable τ' are given in Appendix C. For the soft function, we plug the fixed-order NLO result Eq. (3.42) at the scale μ_0 into Eq. (3.88), and obtain at the scale μ,

$$\begin{aligned}S_a(\tau_a;\mu) = &\frac{e^{K_S+\gamma_E\omega_S}}{\Gamma(-\omega_S)}\left(\frac{\mu_0}{Q}\right)^{j_S\omega_S} \\ &\times\bigg[\bigg\{1 - \frac{\alpha_s(\mu_0)C_F}{2\pi}\frac{1}{1-a}\bigg(\ln^2\frac{\mu_0^2}{(Q\tau_a)^2} + 4H(-1-\omega_S)\ln\frac{\mu_0^2}{(Q\tau_a)^2} \\ &+ \frac{\pi^2}{2} + 4\Big[[H(-1-\omega_S)]^2 - \psi^{(1)}(-\omega_S)\Big]\bigg)\bigg\}\left(\frac{\theta(\tau_a)}{\tau_a^{1+\omega_S}}\right)\bigg]_+ ,\end{aligned} \tag{3.93}$$

and for the jet function, plug in the fixed-order NLO result Eq. (3.62) at μ_0 into Eq. (3.88), and obtain at μ,

$$\begin{aligned}J_a^n(\tau_a;\mu) = &\frac{e^{K_J+\gamma_E\omega_J}}{\Gamma(-\omega_J)}\left(\frac{\mu_0}{Q}\right)^{j_J\omega_J} \\ &\times\bigg[\bigg\{1 + \frac{\alpha_s(\mu_0)C_F}{4\pi}\bigg(\frac{2-a}{1-a}\ln^2\frac{\mu_0^2}{Q^2\tau_a^{\frac{2}{2-a}}} + \Big(3 + \frac{4H(-1-\omega_J)}{1-a}\Big)\ln\frac{\mu_0^2}{Q^2\tau_a^{\frac{2}{2-a}}} \\ &+ 4f(a) + \frac{4}{(1-a)(2-a)}\Big[\frac{\pi^2}{6} + [H(-1-\omega_J)]^2 - \psi^{(1)}(-\omega_J)\Big]\bigg)\bigg\}\left(\frac{\theta(\tau_a)}{\tau_a^{1+\omega_J}}\right)\bigg]_+ ,\end{aligned} \tag{3.94}$$

where in the above two equations $K_F \equiv K_F(\mu,\mu_0)$, $\omega_F \equiv \omega_F(\mu,\mu_0)$, $H(z)$ is the harmonic number function, and $\psi^{(\nu)}(z)$ is the polygamma function.

[6]Note that from the definition in Eq. (3.91), for $\omega < 0$ the '+' label can be dropped and so Eq. (3.91) is consistent with the distribution relation Eq. (3.39).

4.3 Full distribution at NLL

By running the hard, jet, and soft functions from the scales $\mu_0 = \mu_H$, μ_J, and μ_S, respectively, to the common factorization scale μ and performing the convolution in Eq. (3.18) (see Appendix C for details), we find for the final resummed expression for the two-jet angularity distribution with NLL/NLO perturbative accuracy

$$\frac{1}{\sigma_0}\frac{\mathrm{d}\sigma_2{}^{\mathrm{PT}}}{\mathrm{d}\tau_a}\bigg|_{\mathrm{NLL/NLO}} = \left[\left(1 + f_H + 2f_J + f_S\right)U_a^\sigma(\tau_a;\mu,\mu_H,\mu_J,\mu_S)\right]_+ , \tag{3.95}$$

where we defined

$$U_a^\sigma(\tau_a;\mu,\mu_H,\mu_J,\mu_S) \equiv \frac{e^{K+\gamma_E\Omega}}{\Gamma(-\Omega)}\left(\frac{\mu_H}{Q}\right)^{\omega_H}\left(\frac{\mu_J}{Q}\right)^{2j_J\omega_J}\left(\frac{\mu_S}{Q}\right)^{j_S\omega_S}\left(\frac{\theta(\tau_a)}{{\tau_a}^{1+\Omega}}\right), \tag{3.96}$$

where

$$\Omega \equiv 2\,\omega_J(\mu,\mu_J) + \omega_S(\mu,\mu_S) \tag{3.97}$$

$$K \equiv K_H(\mu,\mu_H) + 2K_J(\mu,\mu_J) + K_S(\mu,\mu_S)\,, \tag{3.98}$$

with ω_H, K_H given by Eq. (3.75) and $\omega_{J,S}$ and $K_{J,S}$ given by Eq. (3.92) and

$$f_H = \frac{\alpha_s(\mu_H)C_F}{\pi}\left(-4 + \frac{7\pi^2}{12} - 2\ln^2\frac{\mu_H}{Q} - 3\ln\frac{\mu_H}{Q}\right) \tag{3.99a}$$

$$f_J = \frac{\alpha_s(\mu_J)C_F}{\pi}\left[f(a) + \frac{3/4}{1-a/2}H(-1-\Omega) + \frac{\frac{\pi^2}{6} + H(-1-\Omega)^2 - \psi^{(1)}(-\Omega)}{2(1-a)(1-a/2)}\right. \tag{3.99b}$$
$$\left. + \frac{2-a}{1-a}\ln^2\frac{\mu_J}{Q{\tau_a}^{1/(2-a)}} + \left(\frac{3}{2} + \frac{2}{1-a}H(-1-\Omega)\right)\ln\frac{\mu_J}{Q{\tau_a}^{1/(2-a)}}\right]$$

$$f_S = \frac{\alpha_s(\mu_S)C_F}{\pi}\left[\frac{1}{1-a}\left(-\frac{\pi^2}{4} - 2H(-1-\Omega)^2 + 2\psi^{(1)}(-\Omega)\right)\right. \tag{3.99c}$$
$$\left. - 2\ln^2\frac{\mu_S}{Q\tau_a} - 4H(-1-\Omega)\ln\frac{\mu_S}{Q\tau_a}\right],$$

and $f(a)$ was defined in Eq. (3.63).

From these expressions, it is clear that the logarithms are minimized by choosing μ_H, μ_J, and μ_S of order Q, $Q{\tau_a}^{1/(2-a)}$, and $Q\tau_a$, respectively. We will describe in more detail precisely which values we choose for these scales when we plot the full distributions in Sec. 6.

4.4 Matching to QCD

One way to achieve matching onto QCD is to include three-jet operators in the matching of the QCD current onto the SCET operators in Eq. (3.13) [24, 133]. For the scope of this paper, however, we simply adopt the matching procedure described by [48], as implemented in [32].

To $\mathcal{O}(\alpha_s)$ the full QCD distribution will take the form

$$\frac{1}{\sigma_0}\frac{\mathrm{d}\sigma}{\mathrm{d}\tau_a} = \delta(\tau_a) + \left(\frac{\alpha_s}{2\pi}\right)A_a(\tau_a) + \mathcal{O}(\alpha_s^2)\,. \tag{3.100}$$

In Appendix D we describe how to calculate $A_a(\tau_a)$ numerically. Meanwhile, the fixed-order two-jet angularity distribution in SCET at $\mathcal{O}(\alpha_s)$ is given by the convolution Eq. (3.18) of the fixed-order hard, jet, and soft functions Eqs. (3.29), (3.42), and (3.62). The result is independent of μ (except through $\alpha_s \equiv \alpha_s(\mu)$), and is given by

$$\frac{1}{\sigma_0}\frac{\mathrm{d}\sigma_2}{\mathrm{d}\tau_a} = \delta(\tau_a) D_a^\delta + \frac{\alpha_s}{2\pi}[D_a(\tau_a)]_+ \,, \tag{3.101}$$

where

$$D_a^\delta = 1 - \frac{\alpha_s C_F}{2\pi}\frac{1}{2-a}\bigg\{2 + 5a - \frac{\pi^2}{3}(2+a) + 4\int_0^1 \mathrm{d}x \frac{x^2-2x+2}{x}\ln[x^{1-a} + (1-x)^{1-a}]\bigg\} \tag{3.102}$$

$$D_a(\tau_a) = -\frac{2C_F}{2-a}\frac{\theta(\tau_a)(3+4\ln\tau_a)}{\tau_a} \,. \tag{3.103}$$

The two-jet fixed-order SCET distribution Eq. (3.101) reproduces the most singular parts of the full QCD distribution[7] Eq. (3.100), that is, the coefficient of the $\delta(\tau_a)$, $1/\tau_a$ and $(1/\tau_a)\ln\tau_a$ pieces. The expression for $D_a(\tau_a)$ in Eq. (3.103) makes explicit that the angularities are not infrared-safe for $a = 2$.

The difference of the two fixed-order distributions Eq. (3.100) and Eq. (3.101) away from $\tau_a = 0$ is a purely integrable function,

$$r_a(\tau_a) \equiv \frac{1}{\sigma_0}\left(\frac{\mathrm{d}\sigma}{\mathrm{d}\tau_a} - \frac{\mathrm{d}\sigma_2}{\mathrm{d}\tau_a}\right) = \left(\frac{\alpha_s}{2\pi}\right)[A_a(\tau_a) - D_a(\tau_a)] \,. \tag{3.104}$$

By adding this remainder function to the NLL resummed SCET distribution, we obtain a result which both agrees with QCD to $\mathcal{O}(\alpha_s)$ and resums large logarithmic terms in the entire perturbative series with NLL/NLO accuracy. The matched distributions are thus defined as

$$\frac{1}{\sigma_0}\frac{\mathrm{d}\sigma}{\mathrm{d}\tau_a}^{\mathrm{PT}}\bigg|_{\mathrm{NLL/NLO}} = \frac{1}{\sigma_0}\frac{\mathrm{d}\sigma_2}{\mathrm{d}\tau_a}^{\mathrm{PT}}\bigg|_{\mathrm{NLL/NLO}} + r_a(\tau_a) \,. \tag{3.105}$$

To find $r_a(\tau_a)$, we numerically obtain $A_a(\tau_a)$ from an analysis of the full QCD distributions away from $\tau_a = 0$ using the procedure described in Appendix D, and then subtract out the expression for $D_a(\tau_a)$ given in Eq. (3.103).

For the case $a = 0$ (thrust), the analytic form of $\mathrm{d}\sigma^{\mathrm{PT}}/\mathrm{d}\tau_0$ is known [74], with which our formula Eq. (D.10) for $A_0(\tau_0)$ agrees. Using Eqs. (D.10) and (3.103), we obtain the remainder function

$$r_0(\tau_0) = \frac{\alpha_s C_F}{2\pi}\left[\frac{2(2-3\tau_0+3\tau_0^2)}{1-\tau_0}\frac{\ln(1-2\tau_0)}{\tau_0} - \frac{2(1-3\tau_0)}{1-\tau_0}\ln\tau_0 + 6 + 9\tau_0\right] \,, \tag{3.106}$$

which we see is integrable down to $\tau_0 = 0$.

[7] Technically, we mean that the difference of the two distributions integrated from 0 to ϵ vanishes as $\epsilon \to 0$.

As a consistency check of this matching technique, we calculated the total integral[8] of our fixed-order result,

$$\sigma_{\text{total}} = \int_0^{\tau_a^{\max}} \mathrm{d}\tau_a \left(\frac{1}{\sigma_0} \frac{\mathrm{d}\sigma_2^{\text{PT}}}{\mathrm{d}\tau_a} + r_a(\tau_a) \right) , \tag{3.107}$$

and compared with the total inclusive cross-section, $\sigma(e^+e^- \to X) = \sigma_0(1 + \alpha_s/\pi)$. We found that our results agreed to any arbitrary precision which could be achieved by our numerical computation.

5 Nonperturbative Model for the Soft Function

In this section we adapt the model for the soft function used in jet mass and thrust distributions as constructed in [100] to work for all angularities with $a < 1$. This model is designed to describe the small-τ_a region where perturbation theory breaks down, while leaving the perturbatively reliable large- and intermediate-τ_a regions unaffected. The gap parameter in this model is designed to turn off the soft function at energies below a minimum hadronic threshold. Such a parameter is known to have renormalon ambiguities [100], which must cancel those in the perturbative soft function (which we denote in this section as S^{PT}) to yield a renormalon-free total soft function S. To ensure perturbative stability, a scheme is needed to explicitly enforce this cancellation order-by-order in perturbation theory. Recently, the position-mass scheme developed in Ref. [106] was used to define a renormalon-free gap parameter for hemisphere jet masses in Ref. [98]. This gap parameter obeys transitive RG evolution and has a well-behaved perturbative expansion. We implement this scheme generalized to arbitrary angularity.

5.1 Review of hemisphere and thrust soft function models

To motivate the functional form of the model function that we will use for all angularity distributions, we begin with the model hemisphere soft function constructed in [113]. This model is a function of two variables which can be chosen to be l^+ and l^-, defined as the $+$ and $-$ components of the momentum in the n and $\bar{n}$ hemispheres, respectively. It takes the form

$$f^{\text{exp}}(l^+, l^-) = \theta(l^+)\theta(l^-) \frac{\mathcal{N}(A,B)}{\Lambda^2} \left(\frac{l^+ l^-}{\Lambda^2} \right)^{A-1} \exp\left(\frac{-(l^+)^2 - (l^-)^2 - 2Bl^+l^-}{\Lambda^2} \right) . \tag{3.108}$$

The parameter A controls how steeply the soft function falls as $l^\pm \to 0$, and B contains information about the cross-correlation of the soft particles in the two hemispheres. f^{exp} is normalizable for $A > 0$ and $B > -1$. Λ is an $\mathcal{O}(\Lambda_{\text{QCD}})$ parameter that describes the range that hadronic effects can smear the soft function around a given l^+, l^-. Finally, $\mathcal{N}(A,B)$ is chosen such that f^{exp} is normalized to unity, $\int_{-\infty}^{+\infty} \mathrm{d}l^+ \mathrm{d}l^- f^{\text{exp}}(l^+, l^-) = 1$.

In Ref. [87], this model was used to relate the total hemisphere soft function $S_{\text{hemi}}(l^+, l^-)$ to the perturbative hemisphere soft function $S_{\text{hemi}}^{\text{PT}}(l^+, l^-)$ via the convolution

$$S_{\text{hemi}}(l^+, l^-; \mu) = \int_{-\infty}^{+\infty} \mathrm{d}\tilde{l}^+ \mathrm{d}\tilde{l}^- S_{\text{hemi}}^{\text{PT}}(l^+ - \tilde{l}^+, l^- - \tilde{l}^-; \mu) f^{\text{exp}}(\tilde{l}^+ - \Delta, \tilde{l}^- - \Delta) . \tag{3.109}$$

[8] The upper limit on τ_a in Eq. (3.107), $\tau_a^{\max}$, is that of the maximally symmetric three-jet configuration, $\tau_{\text{sym}}(a) = 1/3^{1-a/2}$ [40], but only for $a \gtrsim -2.6$ (see Appendix D).

where Δ is the gap parameter. This method of implementing the model function ensures a smooth continuation between the nonperturbative, model-dominated and the perturbative regions of the cross-section.

To use this expression in our formalism, we first relate the $a = 0$ soft function, $S_0(\tau_0, \mu)$, and the hemisphere soft function, $S_{\text{hemi}}(l^+, l^-, \mu)$. Using that $\tau_0 = (l^+ + l^-)/Q$, we find

$$\begin{aligned} S_0(\tau_0; \mu) &= \int \mathrm{d}l^+ \mathrm{d}l^- S_{\text{hemi}}(l^+, l^-; \mu)\, \delta\left(\tau_0 - \frac{l^+ + l^-}{Q}\right) \\ &= Q \int \mathrm{d}l\, S_{\text{hemi}}(l, Q\tau_0 - l; \mu)\,. \end{aligned} \tag{3.110}$$

This gives the model function convolution for $S_0(\tau_0; \mu)$ as

$$\begin{aligned} S_0(\tau_0; \mu) &= Q \int \mathrm{d}l \int \mathrm{d}l^+ \mathrm{d}l^-\, S^{\text{PT}}_{\text{hemi}}(l - l^+, Q\tau_0 - l - l^-; \mu) f^{\text{exp}}(l^+ - \Delta, l^- - \Delta) \\ &= \int \mathrm{d}\tau_0'\, S_0^{\text{PT}}(\tau_0 - \tau_0'; \mu) f^{\text{exp}}\left(\tau_0' - \frac{2\Delta}{Q}\right), \end{aligned} \tag{3.111}$$

where (absorbing A and B dependent constants into the normalization $\mathcal{N}$)

$$\begin{aligned} f^{\text{exp}}(\tau) &\equiv Q^2 \int \mathrm{d}\tau'\, f^{\text{exp}}(Q\tau - Q\tau', Q\tau') \\ &= \theta(\tau)\, \mathcal{N}(A, B) \frac{Q}{\Lambda} \left(\frac{Q\tau}{\Lambda}\right)^{2A-1} {}_1F_1\left(\frac{1}{2}, \frac{1}{2} + A, (B-1)\frac{(Q\tau)^2}{2\Lambda^2}\right) e^{-(B+1)\frac{(Q\tau)^2}{2\Lambda^2}}\,. \end{aligned} \tag{3.112}$$

$f^{\text{exp}}(\tau)$ inherits its normalization from $f^{\text{exp}}(l^+, l^-)$, $\int_{-\infty}^{\infty} \mathrm{d}\tau f^{\text{exp}}(\tau) = 1$.

5.2 Adaptation to all angularities

For nonzero a, we still want to use a convolution of the form

$$S_a(\tau_a; \mu) = \int \mathrm{d}\tau_a'\, S_a^{\text{PT}}(\tau_a - \tau_a'; \mu)\, f_a^{\text{exp}}\left(\tau_a' - \frac{2\Delta_a}{Q}\right). \tag{3.113}$$

Moreover, we would like to retain the functional form of f^{exp} since it has had relatively good success in describing different event shapes with the same values of A and B [113]. However, we must at a minimum modify f^{exp} so that the first moment of $S_a(\tau_a; \mu)$ satisfies the scaling relation given in Eqs. (3.24) and (3.27). In terms of the first moment of $S_a^{\text{PT}}(\tau_a; \mu)$ and f_a^{exp}, the first moment of $S_a(\tau_a; \mu)$ is

$$\begin{aligned} \int \mathrm{d}\tau_a\, \tau_a\, S_a(\tau_a; \mu) &= \int \mathrm{d}\tau_a\, \tau_a \int \mathrm{d}\tau_a'\, S_a^{\text{PT}}(\tau_a - \tau_a'; \mu)\, f_a^{\text{exp}}\left(\tau_a' - \frac{2\Delta_a}{Q}\right) \\ &= S_a^{\text{PT}[1]}(\mu) + \left[\int \mathrm{d}\tau_a\, S_a^{\text{PT}}(\tau_a; \mu)\right]\left(\frac{2\Delta_a}{Q} + f_a^{\text{exp}[1]}\right) \\ &= S_a^{\text{PT}[1]}(\mu) + \frac{2\Delta_a}{Q} + f_a^{\text{exp}[1]}\,, \end{aligned} \tag{3.114}$$

where here $S_a^{\rm PT[1]}(\mu)$ and $f_a^{\rm exp[1]}$ are the first moments of $S_a^{\rm PT}(\tau_a;\mu)$ and $f_a^{\rm exp}(\tau_a)$, respectively, and in the third line we dropped α_s corrections to the $\mathcal{O}(\Lambda_{\rm QCD}/Q)$ power corrections Δ_a/Q and $f_a^{\rm exp[1]}$.

Since the first moment of the perturbative soft function, $S_a^{\rm PT[1]}$, already obeys the proper scaling (cf. Eq. (3.42)) we simply rescale the gap parameter,

$$\Delta_a = \frac{\Delta}{1-a}\,, \tag{3.115}$$

and require that the parameters of $f_a^{\rm exp}$ vary from those in $f^{\rm exp}$ such that

$$f_a^{\rm exp[1]} \equiv \int \mathrm{d}\tau_a\, \tau_a\, f_a^{\rm exp}(\tau_a) = \frac{1}{1-a}\int \mathrm{d}\tau\, \tau\, f^{\rm exp}\,(\tau) = \frac{1}{1-a} f^{\rm exp[1]}\,. \tag{3.116}$$

This latter condition is most easily satisfied by fixing A and B to their value at $a=0$ and allowing $\Lambda \to \Lambda_a$ to vary accordingly. Note from the definition of $f^{\rm exp}$, Eq. (3.112), $\Lambda f^{\rm exp}(\Lambda\tau/Q)$ is independent of Λ and hence $\Lambda_a f_a^{\rm exp}(\Lambda_a\tau/Q) = \Lambda f^{\rm exp}(\Lambda\tau/Q)$ when A and B are fixed. This implies that

$$f_a^{\rm exp[1]} = \left(\frac{\Lambda_a}{Q}\right)^2 \int \mathrm{d}\tau_a\, \tau_a\, f_a^{\rm exp}\left(\frac{\Lambda_a}{Q}\tau_a\right) = \left(\frac{\Lambda_a\Lambda}{Q^2}\right)\int \mathrm{d}\tau\, \tau\, f^{\rm exp}\left(\frac{\Lambda}{Q}\tau\right) = \left(\frac{\Lambda_a}{\Lambda}\right) f^{\rm exp[1]}\,, \tag{3.117}$$

and so to satisfy Eq. (3.116) we take $f_a^{\rm exp}$ to be defined as in Eq. (3.112) but with Λ replaced with Λ_a where

$$\Lambda_a = \frac{\Lambda}{1-a}\,. \tag{3.118}$$

5.3 Renormalon cancellation

We want to ensure that the $1/Q$ renormalon ambiguity in $S^{\rm PT}(\tau_a;\mu)$ is cancelled order-by-order in perturbation theory. To implement the position-mass renormalon cancellation scheme defined in Ref. [106] for jet-masses and applied to the $a=0$ gap parameter in Ref. [98], we first take the Fourier transform of $S_a(\tau_a;\mu)$ with respect to $Q\tau_a$,

$$\begin{aligned}
S_a(x_a;\mu) &\equiv \int \mathrm{d}\tau_a\, e^{-iQ\tau_a x_a} S_a(\tau_a;\mu) \\
&= \int \mathrm{d}\tau_a\, e^{-iQ\tau_a x_a} \int \mathrm{d}\tau_a'\, S_a^{\rm PT}(\tau_a-\tau_a';\mu)\, f_a^{\rm exp}\Big(\tau_a' - \frac{2\Delta_a}{Q}\Big) \\
&= S_a^{\rm PT}(x_a;\mu)\, f^{\rm exp}(x_a) e^{-2i\Delta_a x_a} \\
&= \Big[S_a^{\rm PT}(x_a;\mu) e^{-2i\delta_a(\mu)x_a}\Big]\Big[f_a^{\rm exp}(x_a) e^{-2i\bar\Delta_a(\mu)x_a}\Big]\,,
\end{aligned} \tag{3.119}$$

where in the second line we used Eq. (3.113) and in fourth line we split Δ_a into two μ dependent pieces, $\Delta_a = \bar\Delta_a(\mu) + \delta_a(\mu)$. Note that since Δ_a is μ-independent, $S_a^{\rm PT}$ and S_a obey the same RG equation.

Next, we demand that for some value R, the term in the first pair of brackets in the last line of Eq. (3.119) satisfies

$$\frac{\mathrm{d}}{\mathrm{d}(ix_a)} \ln[S_a^{\rm PT}(x_a;\mu) e^{-2i\delta_a(\mu)x_a}]_{ix_a=(Re^{\gamma_E})^{-1}} = 0\,, \tag{3.120}$$

a condition which guarantees no ambiguity in $S_a^{\rm PT}$ at order $1/Q$. This gives $\delta_a(\mu)$ to all orders in terms of $S_a^{\rm PT}(\tau_a;\mu)$ as

$$\delta_a(\mu) = -\frac{Q}{2}\frac{\int \mathrm{d}\tau_a\, \tau_a\, e^{-Q\tau_a/(Re^{\gamma_E})} S_a^{\rm PT}(\tau_a;\mu)}{\int \mathrm{d}\tau_a\, e^{-Q\tau_a/(Re^{\gamma_E})} S_a^{\rm PT}(\tau_a;\mu)}\,, \tag{3.121}$$

which to leading order is given by the expression

$$\delta_a^1(\mu) = -Re^{\gamma_E}\frac{8C_F}{1-a}\left(\frac{\alpha_s(\mu)}{4\pi}\right)\ln\frac{\mu}{R}\,. \tag{3.122}$$

Since $\Delta_a = \bar\Delta_a(\mu) + \delta_a(\mu)$ is μ-independent we find that to $\mathcal{O}(\alpha_s)$,

$$\mu\frac{\mathrm{d}}{\mathrm{d}\mu}\bar\Delta_a(\mu) = -\mu\frac{\mathrm{d}}{\mathrm{d}\mu}\delta_a(\mu) = Re^{\gamma_E}\left[\frac{8C_F}{1-a}\left(\frac{\alpha_s(\mu)}{4\pi}\right)\right] \equiv -Re^{\gamma_E}\left[\Gamma_S^0\left(\frac{\alpha_s(\mu)}{4\pi}\right)\right]. \tag{3.123}$$

Using that $\Gamma_{\bar\Delta}[\alpha_s] \propto \Gamma_S[\alpha_s]$ (cf. Refs. [98, 106]) to all orders, we find that the NLL expression for $\mu\,\mathrm{d}\bar\Delta_a/\mathrm{d}\mu$ is and that, for arbitrary a, $\Gamma_S[\alpha_s] \propto \Gamma_{\rm cusp}[\alpha_s]$ (cf. App. B)

$$\mu\frac{\mathrm{d}}{\mathrm{d}\mu}\bar\Delta_a(\mu) = -Re^{\gamma_E}\left[\Gamma_S^0\left(\frac{\alpha_s(\mu)}{4\pi}\right)\left(1+\frac{\Gamma^1_{\rm cusp}}{\Gamma^0_{\rm cusp}}\frac{\alpha_s(\mu)}{4\pi}\right)\right], \tag{3.124}$$

which has the solution

$$\bar\Delta_a(\mu) = \bar\Delta_a(\mu_0) - \frac{Re^{\gamma_E}}{2}\omega_S(\mu,\mu_0)\,, \tag{3.125}$$

where $\omega_S(\mu,\mu_0)$ is given in Eq. (3.92). Note that since $\delta_a^1(\mu)$ and $\bar\Delta_a(\mu) - \bar\Delta_a(\mu_0)$ are proportional to $1/(1-a)$, Eq. (3.115) suggests that we should choose $\bar\Delta_a(\mu_0)$ to be $\bar\Delta(\mu_0)/(1-a)$, where $\bar\Delta(\mu_0)$ is the best choice for $a=0$.

Expanding Eq. (3.113) in powers of α_s to $\mathcal{O}(\alpha_s)$ gives

$$S_a(\tau_a;\mu) = \int \mathrm{d}\tau_a'\left[S_a^{\rm PT}(\tau_a-\tau_a';\mu) + \frac{2\delta_a^1(\mu)}{Q}\frac{\mathrm{d}}{\mathrm{d}\tau_a'}S_a^{\rm PT}(\tau_a-\tau_a';\mu)\right] f^{\rm exp}\left(\tau_a' - \frac{2\bar\Delta_a(\mu)}{Q}\right), \tag{3.126}$$

where $S_a^{\rm PT}$ at NLO in the first term in brackets and at LO in the second term should be used since δ_a^1 is $\mathcal{O}(\alpha_s)$. Using the fixed-order expression $S_a^{\rm PT}(\tau_a;\mu) = \delta(\tau_a) + \mathcal{O}(\alpha_s)$ in the second term and integrating this term by parts gives

$$S_a(\tau_a;\mu) = \int \mathrm{d}\tau_a'\left[S_a^{\rm PT}(\tau_a-\tau_a';\mu)\, f_a^{\rm exp}\left(\tau_a' - \frac{2\bar\Delta_a(\mu)}{Q}\right)\right] - \frac{2\delta_a^1(\mu)}{Q}\frac{\mathrm{d}}{\mathrm{d}\tau_a} f_a^{\rm exp}\left(\tau_a - \frac{2\bar\Delta_a(\mu)}{Q}\right). \tag{3.127}$$

Evolving $S_a(\tau_a;\mu_S)$ to the scale μ with $U_S(\tau_a-\tau_a';\mu,\mu_S)$ as in Eq. (3.88) gives

$$\begin{aligned} S_a(\tau_a;\mu) = \int \mathrm{d}\tau_a'\Bigg[&S_a^{\rm PT}(\tau_a-\tau_a';\mu)\, f_a^{\rm exp}\left(\tau_a' - \frac{2\bar\Delta_a(\mu_S)}{Q}\right) \\ &- \frac{2\delta_a^1(\mu_S)}{Q}\, U_S(\tau_a-\tau_a';\mu,\mu_S)\,\frac{\mathrm{d}}{\mathrm{d}\tau_a'} f_a^{\rm exp}\left(\tau_a' - \frac{2\bar\Delta_a(\mu_S)}{Q}\right)\Bigg]. \end{aligned} \tag{3.128}$$

Here we keep $\bar{\Delta}_a$ and δ_a at the scale μ_S which is needed to achieve the $1/Q$ renormalon cancellation [99].

Finally, Eq. (3.128) implies that the total resummed distribution at NLL convoluted with the model function $f_a^{\rm exp}$ is

$$\begin{aligned}\frac{1}{\sigma_0}\frac{\mathrm{d}\sigma}{\mathrm{d}\tau_a}\bigg|_{\rm NLL/NLO} = \int \mathrm{d}\tau_a' \bigg\{ &\frac{1}{\sigma_0}\frac{\mathrm{d}\sigma^{\rm PT}}{\mathrm{d}\tau_a}(\tau_a-\tau_a';\mu)\bigg|_{\rm NLL/NLO} f_a^{\rm exp}\bigg(\tau_a' - \frac{2\bar{\Delta}_a(\mu_S)}{Q}\bigg) \\ &- \frac{2\delta_a^1(\mu_S)}{Q}\Big[U_a^\sigma(\tau_a-\tau_a';\mu,\mu_H,\mu_J,\mu_S)\Big]_+ \frac{\mathrm{d}}{\mathrm{d}\tau_a'} f_a^{\rm exp}\bigg(\tau_a' - \frac{2\bar{\Delta}_a(\mu_S)}{Q}\bigg)\bigg\}\,,\end{aligned} \tag{3.129}$$

where the resummed two-jet distribution matched to QCD, $\mathrm{d}\sigma^{\rm PT}/\mathrm{d}\tau_a|_{\rm NLL/NLO}$, is given in Eq. (3.105) and U_a^σ is given in Eq. (3.96).

5.4 Numerical results for the soft function

By plugging the partonic soft function Eq. (3.42) into the model Eq. (3.127), we obtain for the full convoluted model soft function to $\mathcal{O}(\alpha_s)$,

$$\begin{aligned}S_a(\tau_a;\mu) = &\bigg\{1 - \frac{\alpha_s C_F}{2\pi}\frac{1}{1-a}\bigg[\ln^2\bigg(\frac{\mu^2}{Q^2(\tau_a^\Delta)^2}\bigg) - \frac{\pi^2}{6}\bigg]\bigg\} f_a^{\rm exp}\left(\tau_a^\Delta\right) - \frac{2\delta_1^a(\mu)}{Q}\frac{\mathrm{d}}{\mathrm{d}\tau_a} f^{\rm exp}(\tau_a^\Delta) \\ &+ \frac{2\alpha_s C_F}{\pi}\frac{1}{1-a}\int_0^{\tau_a^\Delta}\mathrm{d}\tau'\frac{1}{\tau'}\ln\bigg(\frac{\mu^2}{Q^2\tau'^2}\bigg)\left[f_a^{\rm exp}\left(\tau_a^\Delta-\tau'\right) - f_a^{\rm exp}\left(\tau_a^\Delta\right)\right]\,,\end{aligned} \tag{3.130}$$

where $\tau_a^\Delta \equiv \tau_a - 2\bar{\Delta}_a(\mu)/Q$. To integrate against the plus distributions in Eq. (3.42), we used the prescription

$$\int_0^a \mathrm{d}x \left[\frac{\theta(x)}{x}\right]_+ f(x) = \int_0^a \mathrm{d}x \frac{\theta(x)}{x}[f(x)-f(0)] + f(0)\ln a \tag{3.131a}$$

$$\int_0^a \mathrm{d}x \left[\frac{\theta(x)\ln x}{x}\right]_+ f(x) = \int_0^a \mathrm{d}x \frac{\theta(x)\ln x}{x}[f(x)-f(0)] + \frac{1}{2}f(0)\ln^2 a\,, \tag{3.131b}$$

which correspond to the definition of plus-functions given in Eq. (3.40). To minimize the logarithms in the peak region of the soft function while also avoiding the Landau pole in α_s, it is natural to choose the scale to be of order $\mu \gtrsim \Lambda_{\rm QCD}$. To minimize the logarithms for larger values of τ_a, it is natural to choose $\mu \sim Q\tau_a$. A scale choice that interpolates between these two regions is

$$\mu = \sqrt{\theta(Q\tau_a - \mu_S^{\rm min})(Q\tau_a-\mu_S^{\rm min})^2 + (\mu_S^{\rm min})^2}\,, \tag{3.132}$$

where the minimum scale is $\mu_S^{\rm min} \gtrsim \Lambda_{\rm QCD}$.

In Fig. 3.6, we plot $S_a(\tau_a;\mu)$ for six values of a between -2 and $1/2$. In each plot, we show the tree-level (LO) soft function with a gap parameter (solid gray), the one-loop (NLO) soft function with a gap parameter but without renormalon subtraction (dashed green), and the one-loop soft function with a gap and renormalon subtraction (solid blue). For the parameters in the model function Eq. (3.112) we take $A = 2.5, B = -0.4, \Lambda = 0.55$ GeV, as extracted from a fit to the jet mass distribution [113]. For the scale dependence of the gap parameter, we choose

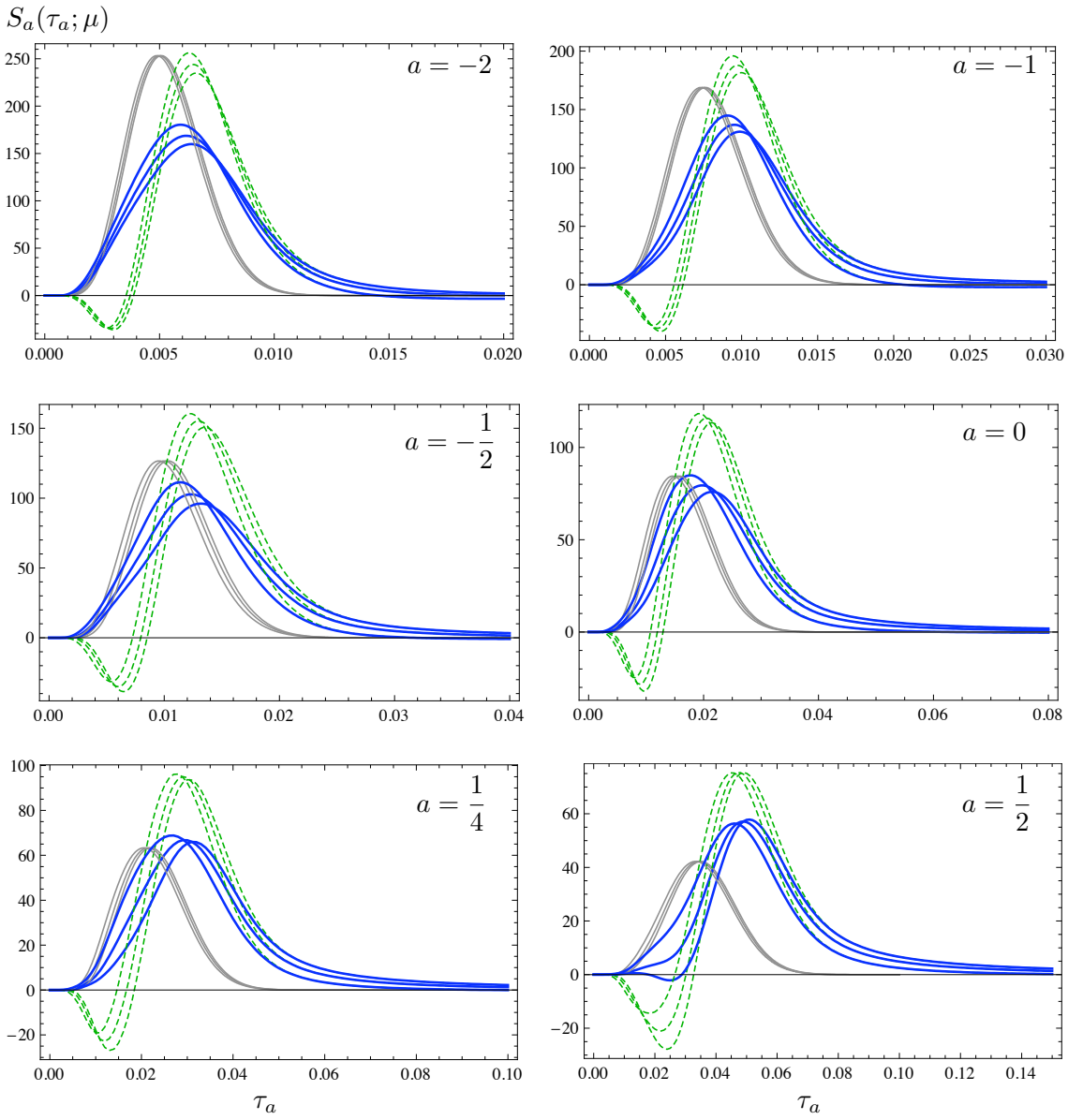

Figure 3.6: Angularity soft functions with a gap parameter, at tree-level (solid gray) and at one-loop with (solid blue) and without (dashed green) renormalon subtraction, for $Q = 100$ GeV, for several values of a as labeled on each plot. The variation of the soft functions with the scale μ is illustrated by first setting $\mu_S^{\min} = 1.0$ GeV in Eq. (3.132) and choosing μ to be $(0.8, 1, 1.2)$ times the formula in Eq. (3.132), with the plots for smaller values of μ_S peaking earlier in τ_a. For the model parameters we take $A = 2.5, B = -0.4, \Lambda = 0.55$ GeV. In the renormalon subtraction Eq. (3.122), we have chosen $R = 200$ MeV.

$\bar{\Delta}_0(1\text{ GeV}) = 100$ MeV and use Eq. (3.125) to evolve to other scales. We choose $R = 200$ MeV in the renormalon subtraction Eq. (3.122) and the minimum value of the scale in Eq. (3.132) to be $\mu_S^{\min} = 1$ GeV. We illustrate the variation of $S_a(\tau_a;\mu)$ with the scale μ by varying it between 0.8 and 1.2 times the formula in Eq. (3.132). The tree-level soft functions depend on μ only through the gap parameter $\bar{\Delta}_a(\mu)$ and thus artificially have smaller scale variation than the one-loop soft functions, at which order the nontrivial μ dependence is first probed.

The one-loop soft functions in Fig. 3.6 display unphysical behavior near $\tau_a = 0$ by taking negative values, due to the renormalon ambiguity in the perturbative series for the partonic soft function. By cancelling the renormalon ambiguity between the partonic soft function and the nonperturbative gap parameter Δ_a through Eq. (3.127), we obtain the renormalon-free one-loop soft functions. One of the plots of the soft function for $a = 1/2$ still exhibits a small negative dip after renormalon subtraction, but it is nevertheless much smaller than the original negative dip, and from its size may be expected to an effect of higher-order power corrections. The dip does not appear in the total cross-section calculated below in Sec. 6.

6 Numerical Results for the Full Distribution

In this section we plot the angularity distributions $\mathrm{d}\sigma/\mathrm{d}\tau_a$ which include LO and NLO perturbative hard, jet, and soft function contributions, resummation of large logarithmic terms to NLL accuracy, matching to QCD at $\mathcal{O}(\alpha_s)$, and the effects of the nonperturbative gapped soft functions.

In Fig. 3.7 we plot the angularity distributions given by Eq. (3.129), plugging in the NLL resummed partonic distribution given by Eq. (3.95) and matched according to Eq. (3.105). We keep the same soft model function parameters as in the previous section. As noted earlier, the logarithms in the hard, jet, and soft functions are minimized by choosing $\mu_H = Q$, $\mu_J \sim Q\tau_a^{1/(2-a)}$, and $\mu_S \sim Q\tau_a$. In order to avoid the Landau pole in α_s as $\tau_a \to 0$, we choose the scales as in Eq. (3.132),

$$\mu_S = \sqrt{\theta(Q\tau_a - \mu_S^{\min})(Q\tau_a - \mu_S^{\min})^2 + (\mu_S^{\min})^2} \tag{3.133a}$$

$$\mu_J = \sqrt{\theta(Q\tau_a^{1/(2-a)} - \mu_J^{\min})(Q\tau_a^{1/(2-a)} - \mu_J^{\min})^2 + (\mu_J^{\min})^2}\,. \tag{3.133b}$$

We may vary $\mu_{S,J}^{\min}$ independently, or choose them in a correlated fashion suggested by their natural scaling $\mu_S \sim Q\lambda, \mu_J \sim Q\lambda^{1/(2-a)}$, that is,

$$\mu_J^{\min} = Q^{(1-a)/(2-a)}(\mu_S^{\min})^{1/(2-a)}\,. \tag{3.134}$$

In Fig. 3.7 we have done the latter. The NLL/NLO distributions exhibit negative values for small τ_a as a result of the renormalon ambiguity. Performing the renormalon subtraction in the soft function removes this pathology.

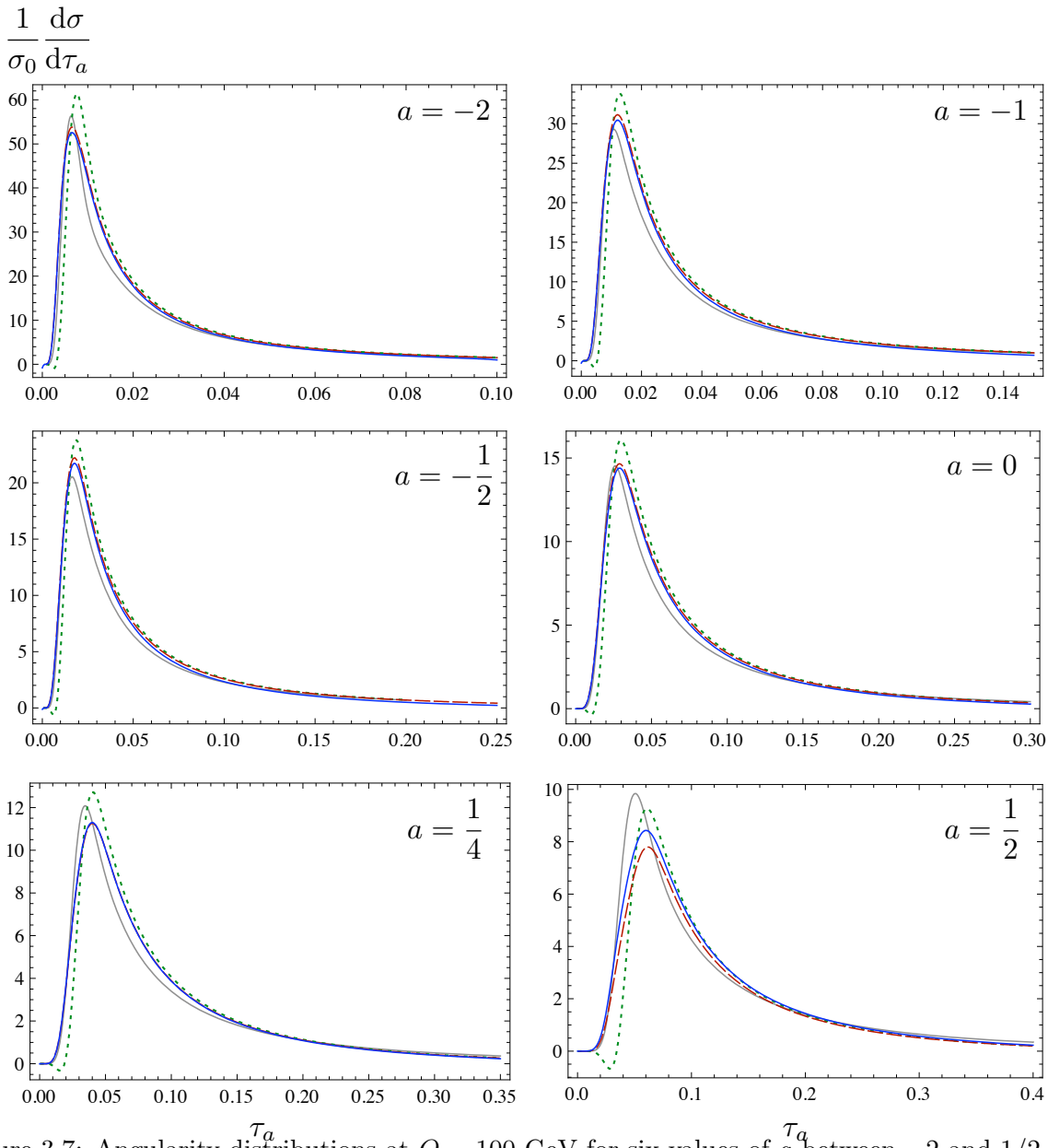

Figure 3.7: Angularity distributions at $Q = 100$ GeV for six values of a between -2 and $1/2$. The solid gray curves are the LO partonic distributions resummed to NLL and convoluted with the gapped soft model function. The dotted green curves are NLL/NLO convoluted with the gapped soft function but without renormalon subtraction. The dashed red curves are the same as the green but with renormalon subtraction, and the solid blue curves are the same as the red but matched to fixed-order QCD at $\mathcal{O}(\alpha_s)$. We choose the scales $\mu = Q, \mu_S^{\min} = 1$ GeV, and $\mu_J^{\min}$ given by Eq. (3.134). For the gap parameter we take $\bar{\Delta}_0(1\text{ GeV}) = 100$ MeV and in the renormalon subtraction $R = 200$ MeV.

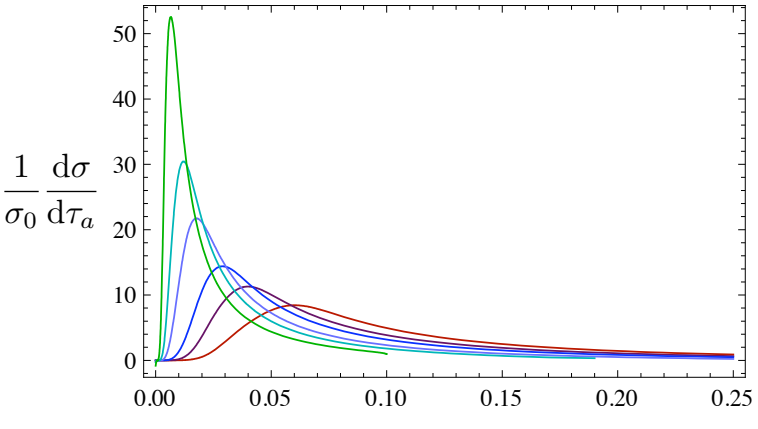

Figure 3.8: Angularity distributions at $Q = 100$ GeV. The full, NLL/NLO resummed, renormalon-subtracted distributions in Fig. 3.7 are here shown all on the same scale. The parameters are chosen the same as in Fig. 3.7. From highest to lowest peak value, the curves are for $a = -2, -1, -\frac{1}{2}, 0, \frac{1}{4}, \frac{1}{2}$.

	$F = S$	$F = J$
j_F	1	$2 - a$
Γ_F^0	$-8C_F\frac{1}{1-a}$	$8C_F\frac{1-a/2}{1-a}$
γ_F^0	0	$6C_F$

Table 3.1: Γ_F^0, γ_F and j_F for the jet and soft functions.

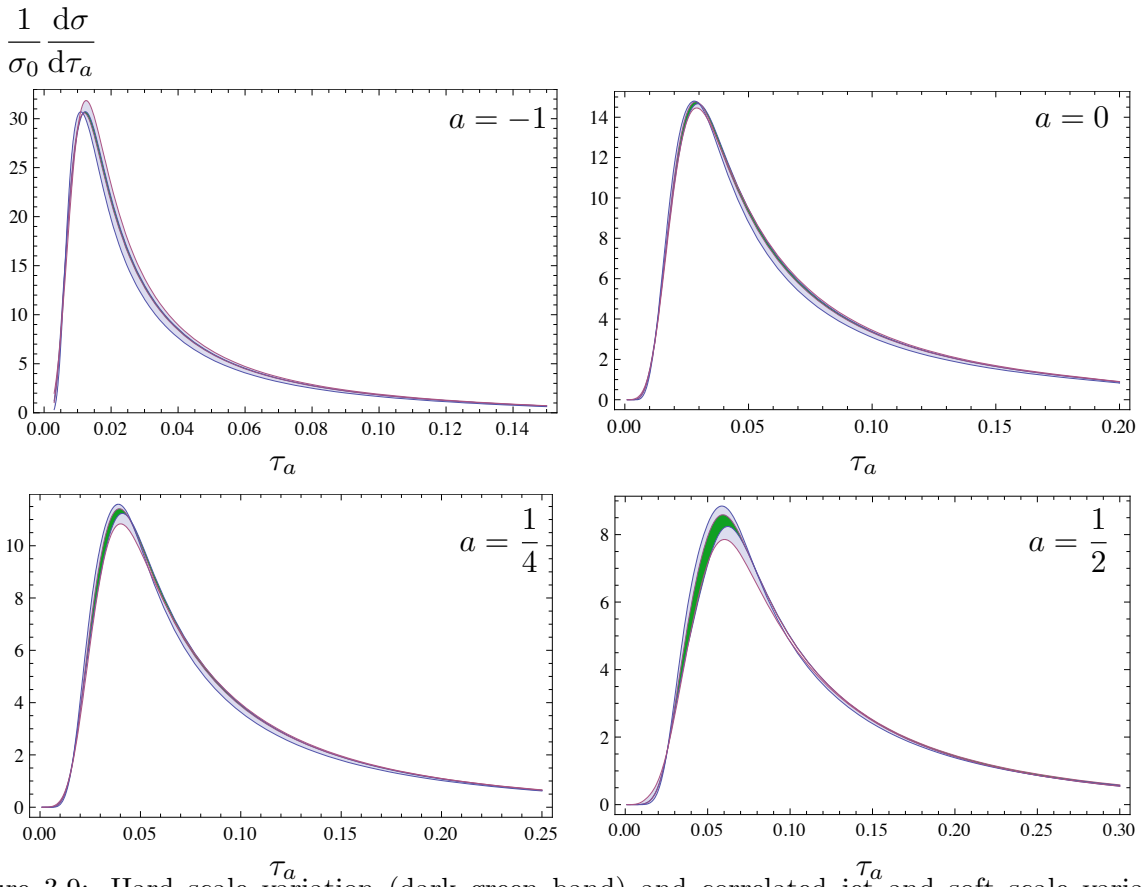

Figure 3.9: Hard scale variation (dark green band) and correlated jet and soft scale variation (light blue band) of the NLL/NLO resummed, renormalon-subtracted angularity distributions at $Q = 100$ GeV for $a = -1$, $a = 0$, $a = 1/4$, and $a = 1/2$. For the hard scale variation, μ_H varied between $Q/2$ and $2Q$ and for the correlated scale variation, μ_J and μ_S are varied between half the values given in Eq. (3.133) and twice these values.

In Fig. 3.8 we plot angularity distributions for the values of a used in Fig. 3.7 on the same figure to illustrate clearly how they change with a. The range of τ_a populated by two-jet-like events grows with increasing a, so that the peak regions are populated by jets of increasing narrowness with increasing a. This is reflected in the scales $\mu_{J,S}$ in Eq. (3.133) drawing closer as a grows to 1.

In Fig. 3.9 we vary the hard, jet, and soft scales and plot the resulting variation of our final predictions for the distributions. First we vary the hard scale μ_H between $Q/2$ and $2Q$, plotting the result in the dark green band. Then we vary the collinear and soft scales $\mu_{J,S}$ between half and twice the values we chose in Eq. (3.133) and plot the result in the light blue band.

Although published data on e^+e^- angularity distributions for $a \neq 0$ are not yet available, data for the $a = 0$ (thrust) distribution are of course plentiful. The remaining difference between our prediction in Fig. 3.7 and existing measurements of the $a = 0$ distribution can be accounted for by higher-order perturbative corrections (see, for example, Fig. 6 in Ref. [32]), which are known but have not been included here, since we calculated the other angularity distributions only to NLL/NLO. For a sufficiently smaller than 1, we expect our predictions of all angularity distributions to agree with data to the same accuracy that the NLL/NLO $a = 0$ prediction agrees with the thrust data.

7 Comparison to Previous Results and Classic Resummation

To compare to previous predictions of angularity distributions [37, 40] and focus more generally on the differences between SCET and alternative approaches to factorization and resummation, in this section we restrict our attention to the perturbative distribution both before matching, Eq. (3.95), and after matching, Eq. (3.105), leaving out the nonperturbative model of Sec. 5.

Our result for the unmatched NLL resummed distribution Eq. (3.95) involves an evolution factor U_a^σ, which resums all leading and next-to-leading logarithms (for example the $(1/\tau_a)\ln\tau_a$ and $1/\tau_a$ terms in the fixed-order $D_a(\tau)$ of Eq. (3.103)), and a multiplicative NLO prefactor $1 + f_H + 2f_J + f_S = 1 + \mathcal{O}(\alpha_s)$. Both the evolution factor and the NLO prefactor are sensitive to physics at the three distinct scales μ_H, μ_J, and μ_S. Keeping these scales arbitrary until after solving the RG equations in Sec. 4 and retaining the freedom to choose them only at the end provides a flexibility which is indispensable in achieving reliable predictions in the SCET approach. This approach has significant advantages over what we refer to as the classic approach to resummation in QCD [48].

To illustrate these advantages, we compare our results for angularity distributions to those obtained in full QCD [37, 40]. The analysis in Ref. [37] used a formalism of factorization and resummation of logarithms through renormalization-group evolution paralleling that of SCET, in principle containing all the advantages that we emphasize here, but which were not fully realized. Before arriving at the explicit prediction for the NLL resummed distribution $\mathrm{d}\sigma/\mathrm{d}\tau_a$ given in Ref. [40], the factorized result of Ref. [37] was first converted into the form of a resummed event shape distribution that would be obtained using the classic approach (and has been for $a = 0$).

One major advantage of the SCET approach over the classic approach is the presence of Landau pole singularities in the results of the classic approach that are not in the results from SCET, as also found in the cases of DIS and Drell-Yan [126, 27, 30]. We can illustrate why SCET avoids this for the case of angularities by returning to our results for the resummed jet and soft functions and for the final resummed distribution. From the expressions for the resummed soft

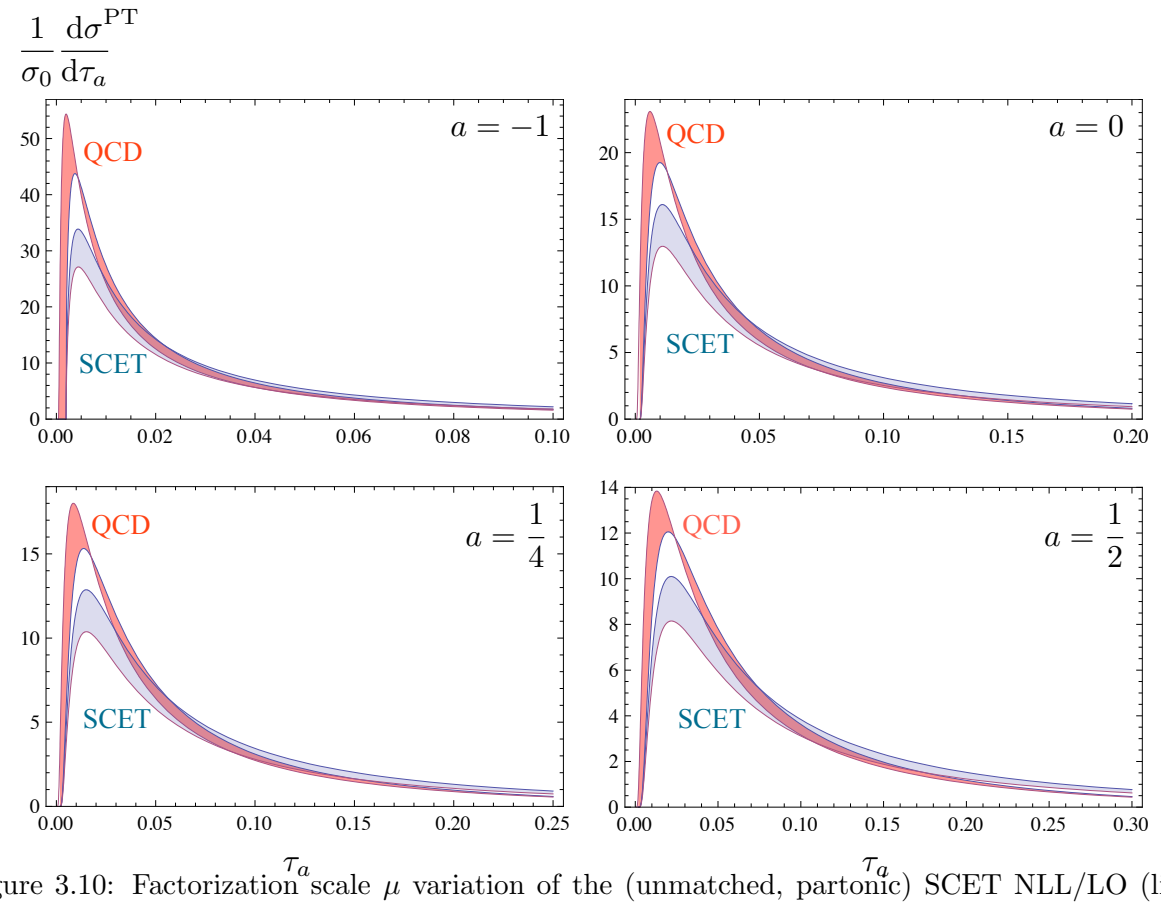

Figure 3.10: Factorization scale μ variation of the (unmatched, partonic) SCET NLL/LO (light blue band) and the classic QCD NLL/LO (red band) resummed results for angularity distributions. μ is varied over the range $\frac{Q}{2} \leq \mu \leq 2Q$ with $Q = 100$ GeV for the cases $a = -1$, $a = 0$, $a = 1/4$, and $a = 1/2$. To make a direct comparison to the QCD results, the scales in the SCET results have been chosen as $\mu = \mu_H = Q$, $\mu_J = Q\tau_a^{1/(2-a)}$, and $\mu_S = Q\tau_a$.

function $S_a(\tau_a^s)$, Eq. (3.93), and for the resummed jet function $J_a^n(\tau_a^n)$, Eq. (3.94), one might be tempted to set $\mu_S = Q\tau_a^s$ and $\mu_J = Q(\tau_a^n)^{1/(2-a)}$, since the logarithms in Eqs. (3.93) and (3.94) are minimized for these choices. The problem with this choice is that the soft and jet functions still enter the convolution in the factorization theorem Eq. (3.1) and thus the scales in $\alpha_s(\mu_{J/S})$ run below $\tau_a^{n,s} = \Lambda_{\mathrm{QCD}}/Q$ even for $\tau_a > \Lambda_{\mathrm{QCD}}/Q$ (where $\tau_a = \tau_a^n + \tau_a^{\bar{n}} + \tau_a^s$) if these $\tau_a^{n,s}$-dependent scales are chosen. However, for a τ_a^s-independent choice of μ_S in the case of the soft function, for instance, the full functional dependence of the resummed $S(\tau_a^s;\mu)$ on τ_a^s and μ_S is such that after the integrals over τ_a^s, τ_a^n, and $\tau_a^{\bar{n}}$ needed to get to the final resummed distribution, Eq. (3.95), are performed, the resulting dependence on μ_S only comes in the combination $\mu_S/Q\tau_a$ in logarithms (and similarly for the jet functions). The proper choice is thus $\mu_S \sim Q\tau_a$ (and $\mu_J \sim Q\tau_a^{1/(2-a)}$) and not $\mu_S \sim Q\tau_a^s$. With this choice, Landau pole singularites never affect our result for $\tau_a > \Lambda_{\mathrm{QCD}}/Q$. Setting $\mu_S = Q\tau_a^s$ before doing the convolution Eq. (3.1) is equivalent to setting $\mu_S = Q/\nu$ in the Laplace transform with respect to ν of the distribution, which is the scale choice made in Ref. [37] needed to reproduce the classic result for $a = 0$. Thus, when transforming back to get $\mathrm{d}\sigma/\mathrm{d}\tau_a$,

one inevitably runs into spurious Landau pole singularities with this scale choice[9], confirming the similar observation of [30].

Another difference between the explicit results we give and those given in [37] is that while both achieved resummation of logarithms to NLL accuracy, the latter does not include a full NLO calculation of the jet and soft functions in the distribution $\mathrm{d}\sigma/\mathrm{d}\tau_a$, that is, effectively does not have the prefactors $f_{H,J,S}$. As with our SCET results, the results of [37] are not as accurate as fixed-order QCD in the large-τ_a region and need to be matched. This matching was subsequently performed numerically to at $\mathcal{O}(\alpha_s^2)$ in Ref. [40]. We summarize this by saying that we have resummed logarithms of τ_a to NLL/NLO with $\mathcal{O}(\alpha_s)$ matching and Ref. [40] has resummed to NLL/LO with $\mathcal{O}(\alpha_s^2)$ matching.

The explicit dependence of the NLO prefactor on the separate scales $\mu_{H,J,S}$ makes it distinct from what is obtained by NLO matching to QCD in the large-τ_a region where the three scales are comparable. Specifically, it improves the accuracy in the smaller-τ_a region where the distribution depends on physics at the three widely disparate scales separately, as revealed by the factorization theorem. We emphasize that even though the effects of including this NLO piece are formally of next-to-next-to-leading logarithmic (NNLL) accuracy (using the counting $\alpha_s \ln \tau_a \sim \mathcal{O}(1)$), it *is* natural to include it in our NLL resummed result since the dependence on the arbitrary scales $\mu_{H,J,S}$ is cancelled to order α_s in our NLL/NLO calculation.[10]

Finally, we point out that while SCET can incorporate $\mathcal{O}(\alpha_s^2)$ matching with, for example, an $\mathcal{O}(\alpha_s^2)$ QCD calculation or an event generator, the classic approach by itself is less easily generalized to achieve full NLL/NLO accuracy. The reason for this difference is that SCET predicts the evolution boundary conditions for the hard, jet, and soft functions, $H(Q;\mu_H)$ and $F(\tau_a;\mu_F)$ ($F = J, S$) in Eq. (3.88), for arbitrary scales $\mu_{H,J,S}$ order by order in perturbation theory. On the other hand, as discussed in Ref. [140], the classic approach in contrast must effectively use the evolution boundary conditions $F(\tau_a;\mu_0) = \delta(\tau_a)$, which are LO in the SCET point of view. An implication of this difference is that, since our NLO prefactor is formally part of the NNLL series, full NNLL resummation is a nontrivial task in the classic approach (e.g. [46, 73]) whereas it is straightforward in SCET, using no new techniques additional to the ones described above.

In Fig. 3.10, we compare our result with the classic result obtained in [37]. To make this comparison, we truncate our result to NLL/LO accuracy and make the scale choices that are equivalent to those that were made in Ref. [37] for the purpose of arriving at the classic resummed form. Namely, we run the jet and soft functions from their respective natural scales, $\mu_J = Q\tau_a^{1/(2-a)}$ and $\mu_S = Q\tau_a$, to the hard scale set to $\mu_H = Q$. In addition, in Ref. [37] the factorization scale μ was also chosen to be $\mu = \mu_H$, effectively turning off running between μ_H and μ. Thus, to make a genuine comparison, we vary μ both in the classic result given in [40] and in our result Eq. (3.95) over the range $Q/2$ to $2Q$, fixing $\mu_H = \mu$ in our result. Notice from the plots that the peak position appears to be more stable in the SCET results relative to the classic results and that there is a discrepancy in the overall normalization in the peak region, both of which may be attributed to

[9] There are also inherent Landau pole singularities in the classic approach before transforming back to τ_a-space and thus not associated with making ν-dependent scale choices for $\mu_{J,S}$. In the classic approach, a prescription to avoid both types of Landau pole singularities is employed, but at the expense of introducing unphysical power corrections [48, 52]. The results of [40] plotted in Fig. 3.10 used the prescription of [48].

[10] More generally, in an $\mathrm{N}^n\mathrm{LL}/\mathrm{N}^m\mathrm{LO}$ calculation, the dependence on $\mu_{H,J,S}$ cancels up to order $\alpha_s^{\min\{n,m\}}$, as the $\mu_{H,J,S}$ derivative of the logarithm of the distribution receives contributions from the prefactor at order α_s^m and from the anomalous dimension at order α_s^n.

power corrections arising from the spurious Landau poles present in the classic result.

8 Conclusions

We have calculated angularity distributions in e^+e^- collisions for $a < 1$ to $\mathcal{O}(\alpha_s)$ in fixed-order accuracy, resummed leading and next-to-leading large logarithms in the perturbative series, incorporated the effects of a nonperturbative model for the soft function with a gap parameter, and cancelled the leading renormalon ambiguities in the perturbative expansion of the distribution and the gap parameter. Our new results for the one-loop jet and soft functions for all $a < 1$ and the NLL resummation of logarithms of τ_a with explicit analytical dependence on the scales $\mu_{H,J,S}$ made possible what we believe are the most precise predictions of angularity distributions to date.

These predictions, especially after extension to higher orders in perturbation theory and resummation of logarithms, can prove useful in improving extraction of the strong coupling α_s or the parameters of nonperturbative models for the soft function. At the present time, in the absence of a new linear collider, such extractions would require the re-analysis of LEP data to extract the angularity distributions.

We also gain insight into the steps that will be required to predict jet observables in hadronic collisions, a broad range of which have been studied in [7, 6] using the classic approach. An SCET-based framework to factorize jet observables in this environment was developed in [15]. Our analysis of angularities suggests that the study of any set of jet observables which vary in their sensitivity to narrower or wider jets or which depend on a jet algorithm picking out narrower or wider jets should be scrutinized in the same way as we did for angularities to determine whether the contributions of collinear and soft modes to each observable can be clearly separated. Also, our calculations of light quark angularity distributions in e^+e^- collisions can be extended to calculating individual jet shapes for jets of various origins to higher accuracy, contributing to strategies to use such jet shapes to distinguish experimentally different types of jets [3, 2].

While we have used SCET to calculate and explore the behavior of angularity distributions, the variation in behavior of the angularities has in turn shed light on the behavior and applicability of the effective theory. Varying a essentially varies the collinear scale of SCET, in effect interpolating between (and extrapolating beyond) SCET_I and SCET_II , and so angularities provide an ideal testing ground for the behavior of these effective theories.

It is natural and straightforward to consider further improvement of our predictions to higher perturbative accuracy and reduced nonperturbative uncertainty. We believe by using the cut diagram methods described above to obtain the angularity distributions to $\mathcal{O}(\alpha_s)$ we can extend our results to $\mathcal{O}(\alpha_s^2)$ in a straightforward manner. Also, all of the ingredients necessary for NNLL resummation at $a = 0$ are already known [32], and we would only need to calculate those pieces which change with a. The three-loop $\Gamma_{J,S}$ part of the jet and soft anomalous dimensions for arbitrary a can be obtained from the known three-loop Γ_{cusp} [30] and the all-orders proportionality $\Gamma_{J,S} \propto \Gamma_{\text{cusp}}$ which we verified in Appendix B. The only unknown ingredients are the two-loop non-cusp part of the jet and soft anomalous dimensions. These can be obtained solely from the UV divergences of the two-loop graphs, and would immediately extend our results to NNLL accuracy. As for nonperturbative effects in the angularity distributions, we have treated these effects in the soft function in the simplest manner possible, adapting the $a = 0$ soft model function to all a by rescaling its first moment. Comparison of these predictions to e^+e^- data can shed light on the

reliability of this choice.

Angularities and other event shapes have proven to be powerful probes of QCD and its effective theories, and promise to play a key role in the new era of collider physics searching for signals of new physics amid a sea of jets and strong interactions.

Chapter 4

On Glauber Gluons in SCET

1 Introduction

Factorization of QCD hard scattering cross-sections into calculable high-energy and universal non-perturbative parts plays vital role in our theoretical understanding of strong interactions. In practice one should derive a factorization formula on a process by process basis. Then, one could extract the hadron Parton-Distribution Function (PDF) say from the Deeply Inelastic Scattering (DIS) and use it in the factorized Drell-Yan (DY) [82] cross-section as an input to make theoretical prediction that can be compared to data.

Glauber gluons play special role in DY like processes where they threaten Factorization [44, 65]. They are low-energy momentum exchanges involving remnants in hadronic collisions, where the transferred momentum is almost entirely in the direction perpendicular to the beam axis. The presence of this transverse interaction causes the factorization to be broken in the usual sense of PDF's and the generalized Transverse Momentum Dependant PDF's (TMDPDF) should be introduced for the exclusive in Q_{T} DY cross-section [67]. However, in the inclusive cross-section, i.e. after integrating over the Q_{T}, the effects from Glauber gluons cancel, and Factorization holds [43, 66].

The modern approach to Factorization proofs, which has the advantage of straightforward resummation of large logarithms of multiple physical scales, is using one or more effective field theories. In this approach the ingredients of a Factorization formula are identified with Wilson coefficients and matrix elements of operators in these field theories, see e.g. [124].

Soft-collinear effective theory (SCET) [12, 14, 25, 21] plays an important role and has been employed in proofs of Factorization for many jet-involving processes. It is thus of particular interest how Glauber gluons can be accounted for in SCET. The straightforward approach is to assign a momentum scaling of $(\lambda^2, \lambda^2, \lambda)$ for the $(+, -, \perp)$ light-cone components and treat them as propagating fields, at least for book-keeping purposes. Since these fields are off-shell and cannot appear as external particles in perturbation theory, they may be integrated out of the effective theory, leading to a potential between pairs of collinear fields in opposite directions.

An attempt to include Glauber gluons into SCET was done in [122], where the factorization of DY cross-section in the presence of Glauber mode was reconsidered. However in this attempt the overlaps between modes which we find to play a very important role is completely ignored.

Inclusion of Glauber gluons into SCET lagrangian has been phenomenologically suitable

for description of jet broadening in dense QCD matter [103, 75].

The purpose of the present Chapter is to motivate the inclusion of Glauber gluons into SCET to have a consistent effective theory for the DY cross-section. The proven cancelation [43, 66] of Glauber interactions in the inclusive DY cross-section needs to be understood from the effective theory point of view.

The plan of the Chapter is as follows. In Section 2 we perform a one-loop matching calculation within SCET involving DY amplitude topologies and show that the effective theory breaks down, while in SCET+Glauber mode we get the consistency back into effective theory. In Section 3 we perform the pinch analysis of DY amplitudes at one loop and identify the right modes for the effective theory for each topology. In Section 4 we discuss the reconciliation of having an off-shell Glauber pinch and the Coleman and Norton theorem, and finally we conclude in Section 5.

2 Setting up the playground

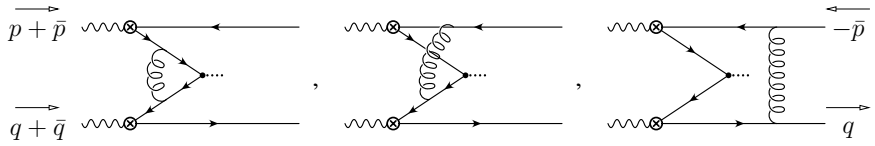

Figure 4.1: One-loop examples of — Left: active-active interactions, Middle: spectator-active interactions, Right: spectator-spectator interactions

The goal of this Chapter is to study interactions that are mediated by a momentum configuration with Glauber scaling, i.e. $l \sim (\lambda^2, \lambda^2, \lambda)$. It is well known that such modes are present between spectators at the amplitude level for Drell-Yan type processes [Collins, Soper, Sterman]. It is helpful to construct an example in SCET in which the conditions that lead to Glauber gluon exchanges are present. To this end we reconsider the well-studied SCET current $O_2 = \bar{\chi}_{\bar{n}} \Gamma \chi_n$, for which the Wilson coefficient C_2 and its anomalous dimension γ_2 are known to high precision [Pecjak et. al.] by explicit calculation using partonic external states of free quarks $\langle \bar{q}q|O_2|0\rangle$. However, since our aim is directed toward spectator interactions, we intentionally choose more complicated external states, namely $\langle \gamma^*\gamma^* \to \bar{q}q\bar{q}q|O_2|\bar{q}q\rangle$, which must yield the same results for C_2 and γ_2 as they are independent of the choice of external states. Examples of Feynman diagrams to consider are depicted in Figure 4.1.

Since we will work backwards from a known result, we may formulate our expectations as follows. Interactions between particles participating in the hard scattering process, called "active" particles, will reproduce the previous results, while the new type of topologies where an active particle interacts with a spectator or purely between spectators will not contribute to C_2 or γ_2 in the matching calculation. In other words, the sum of the full theory graphs in the new topologies must be reproduced in its entirety within SCET.

In the next subsection we will match the full (scalar) theory to SCET at one-loop order, where the field content of the effective theory is given by soft, collinear and anti-collinear momentum

modes. We assign momenta $p+\bar{p}$ and $q+\bar{q}$ to the two inital virtual photons, and $\bar{p}$ and q to the two outgoing partons. Note that the tree-level amplitude is simply given by the $1/(p^2\bar{q}^2)$,

$$\langle\gamma^*\gamma^*|\, O_2\,|\bar{q}q\rangle_{\rm tree} = \frac{1}{p^2\bar{q}^2}\ . \tag{4.1}$$

At one loop order, the full theory amplitude of the matrix element of our interest is equal to sum of three topologies, which we write as I_3, I_4, I_5, namely a triangle graph in the active-active, box graphs in the spectator-active and a pentagon graph in the spectator-spectator topology,

$$\langle\gamma^*\gamma^*|\, O_2\,|\bar{q}q\rangle_{\rm FT} = \frac{1}{p^2\bar{q}^2}I_3 + \frac{1}{\bar{q}^2}I_4^{(n\bar{n})} + \frac{1}{p^2}I_4^{(\bar{n}n)} + I_5\ , \tag{4.2}$$

where the prefactors of $1/p^2$, $1/\bar{q}^2$ take into account the propagators that are independent of the loop-momenta. The notation $I_4^{(n\bar{n})}$ and the one with n, $\bar{n}$ reversed takes into account two spectator-active graphs: firs one with spectator in the n direction and the active quark in the $\bar{n}$ direction, and the second one vise verse.

In the the first effective theory that we consider, which is the usual, unmodified $\mathrm{SCET_I}$, we consider only collinear and ultrasoft modes (which we for brevity call soft everywhere below). The one loop amplitude for this effective theory equals to

$$\langle\gamma^*\gamma^*|\, O_2\,|\bar{q}q\rangle_{\mathrm{EFT}_1} = \frac{1}{p^2\bar{q}^2}(I_3^c + I_3^{\bar{c}} + I_3^s) + \frac{1}{\bar{q}^2}(I_4^{(n\bar{n})c} + I_4^{(n\bar{n})s}) + \frac{1}{p^2}(I_4^{(\bar{n}n)\bar{c}} + I_4^{(\bar{n}n)s}) + I_5^s\ . \tag{4.3}$$

Here we have already used the fact that some graphs, i.e. $I_4^{(n\bar{n})\bar{c}}$, $I_4^{(\bar{n}n)c}$, I_5^c, $I_5^{\bar{c}}$, are power-suppressed.

Finally we will repeat the same calculation in another effective theory in which one additional (Glauber gluon) mode is included, which has momentum scaling $(\lambda^2,\lambda^2,\lambda)$. In this effective theory our matrix element equals

$$\begin{aligned}\langle\gamma^*\gamma^*|\, O_2\,|\bar{q}q\rangle_{\mathrm{EFT}_2} \;=\;& \frac{1}{p^2\bar{q}^2}(I_3^{c'} + I_3^{\bar{c}'} + I_3^g + I_3^s) + \frac{1}{\bar{q}^2}(I_4^{(n\bar{n})c'} + I_4^{(n\bar{n})g} + I_4^{(n\bar{n})s}) \\ &+\frac{1}{p^2}(I_4^{(\bar{n}n)\bar{c}'} + I_4^{(\bar{n}n)g} + I_4^{(\bar{n}n)s}) + I_5^g + I_5^s\ .\end{aligned} \tag{4.4}$$

The primed integrals differ from the unprimed ones pricipally in their "zero-bin subtraction", i.e. their overlap with the other modes present in the theory. For example, the collinear contribution in EFT_1 are given by subtracting the overlap with the soft mode,

$$I_k^c = \tilde{I}_k^c - (I_k^c)_{0s}\ , \tag{4.5}$$

while in EFT_2 all three modes overlap with each other: collinear, Glauber and the soft. The following subtractions avoid the double counting:

$$I_k^{c'} \;=\; \tilde{I}_k^{c'} - ((I_k^{c'})_{0g} - (I_k^{c'})_{0g0s} + (I_k^{c'})_{0s})\ , \tag{4.6}$$

$$I_k^{g} \;=\; \tilde{I}_k^{g} - (I_k^{g})_{0s}\ . \tag{4.7}$$

For completeness we perform below the one-loop analysis of all the integrals in both effective theories and compare the resulting matching coefficient to the one with simple external states, $\langle\bar{q}q|\, O_2\,|0\rangle$.

In that case we have

$$\langle \bar{q}q|\, O_2\, |0\rangle_{\rm FT} = I_3\,, \tag{4.8}$$
$$\langle \bar{q}q|\, O_2\, |0\rangle_{{\rm EFT}_1} = I_3^c + I_3^{\bar{c}} + I_3^s\,, \tag{4.9}$$
$$\langle \bar{q}q|\, O_2\, |0\rangle_{{\rm EFT}_2} = I_3^{c'} + I_3^{\bar{c}'} + I_3^g + I_3^s\,. \tag{4.10}$$

The consistency check on the either of the effective theories is that the matching coefficient is independent of the external states and can be written as follows:

$$(C_2)_{{\rm EFT}_i} = \frac{\langle \bar{q}q|\, O_2\, |0\rangle_{\rm FT} - \langle \bar{q}q|\, O_2\, |0\rangle_{{\rm EFT}_i}}{\langle \bar{q}q|\, O_2\, |0\rangle_{\rm tree}} = \frac{\langle \gamma^*\gamma^*|\, O_2\, |\bar{q}q\rangle_{\rm FT} - \langle \gamma^*\gamma^*|\, O_2\, |\bar{q}q\rangle_{{\rm EFT}_i}}{\langle \gamma^*\gamma^*|\, O_2\, |\bar{q}q\rangle_{\rm tree}}, \tag{4.11}$$

where $i = 1, 2$ for two effective theories under consideration.

We will explicitly show below that one of the effective theories, EFT_1, does not satisfies this consistency check, while EFT_2 does.

2.1 Full Theory one loop calculation

The active-active topology in the full theory is simply a standard scalar triangle integral:

$$I_3 = \mu^{4-D} \int \frac{{\rm d}^D l}{(2\pi)^D} \frac{1}{[l^2+i0][(l+p)^2+i0][(l-\bar{q})^2+i0]} \tag{4.12}$$
$$= \frac{i}{16\pi^2} \cdot \frac{1}{p^+\bar{q}^-} \left(\frac{\pi^2}{3} + \ln\frac{p^2}{p^+\bar{q}^-} \cdot \ln\frac{\bar{q}^2}{p^+\bar{q}^-} \right) + \mathcal{O}\left(\epsilon,\, \lambda^2\right). \tag{4.13}$$

The spectator-active topology is the scalar box integral:

$$I_4^{(n\bar{n})} = \mu^{4-D} \int \frac{{\rm d}^D l}{(2\pi)^D} \frac{1}{[l^2+i0][(l-\bar{p})^2+i0][(l+p)^2+i0][(l-\bar{q})^2+i0]} \tag{4.14}$$
$$= \frac{i}{16\pi^2} \cdot \frac{1}{\bar{q}^-} \cdot \frac{1}{\bar{p}^2 p^+ + p^2 \bar{p}^+} \left(\frac{\pi^2}{3} - 2\,{\rm Li}_2\left(-\frac{p^2\bar{p}^+}{\bar{p}^2 p^+} \right) + \left(\ln\left(\frac{\bar{p}^2 p^+}{p^2 \bar{p}^+} \right) - i\,\pi \right) \ln\left(\frac{\bar{q}^- \left(p^+\bar{p}^2 + \bar{p}^+ p^2 \right)^2}{\bar{q}^2 (p+\bar{p})^2 p^+ \bar{p}^2} \right) \right) + \mathcal{O}\left(\epsilon, \lambda^0\right). \tag{4.15}$$

Similar expression is valid for for the second spectator-active integral $I_4^{(\bar{n}n)}$.

The spectator-spectator topology in the full theory can be calculated via a pentagon integral which by standard procedures can be reduced to sum of five box integrals. The result is:

$$I_5 = \mu^{4-D} \int \frac{{\rm d}^D l}{(2\pi)^D} \frac{1}{[l^2+i0][(l-\bar{p})^2+i0][(l+p)^2+i0][(l-\bar{q})^2+i0][(l+q)^2+i0]} \tag{4.16}$$
$$= \frac{i}{16\pi^2} \left[\frac{M^+M^-}{p^+\bar{p}^+(p+\bar{p})^2 q^-\bar{q}^-(q+\bar{q})^2} \left(\ln\left(\frac{\bar{p}^+p^2}{p^+\bar{p}^2}\right) \ln\left(\frac{q^-\bar{q}^2}{\bar{q}^-q^2}\right) + i\pi \ln\left(\frac{\bar{p}^2 p^2 \bar{q}^2 q^2}{\bar{p}^+ p^+ \bar{q}^- q^- (M^+M^-)^2} \right) + \pi^2 \right) + \right.$$
$$\left. \frac{2\pi i\, M^+M^-}{p^+\bar{p}^+(p+\bar{p})^2 (M^-)^2 - q^-\bar{q}^-(q+\bar{q})^2 (M^+)^2} \left(\frac{(M^-)^2 \ln\left(\frac{M^+(M^-)^3}{q^-\bar{q}^-(q+\bar{q})^2}\right)}{q^-\bar{q}^-(q+\bar{q})^2} - \frac{(M^+)^2 \ln\left(\frac{(M^+)^3 M^-}{p^+\bar{p}^+(p+\bar{p})^2}\right)}{p^+\bar{p}^+(p+\bar{p})^2} \right) \right] + \mathcal{O}\left(\epsilon,\, \frac{1}{\lambda^2}\right).$$

2.2 EFT-1: Soft and collinear gluon exchanges

The loop integrals for the effective theory modes in each topology can be found trivially by expanding the corresponding full theory integrals I_3, I_4, I_5 with the appropriate scaling of the gluon momenta.[1] The zero-bin subtraction integrals can be found similarly by expanding the effective theory loop integrals with the scaling of the overlap mode. All zero-bin integrals are zero in this effective theory, so they behave as a pool up mechanism, converting infrared poles into the ultraviolet ones.

The results for all modes in EFT_1 are given below:

$$I_3^c = \frac{i}{16\pi^2}\cdot\frac{1}{p^+\bar{q}^-}\left(-\frac{1}{\epsilon^2}-\frac{\ln\frac{\mu^2}{p^2}+i\pi}{\epsilon}-\frac{1}{2}\left(\ln\frac{\mu^2}{p^2}+i\pi\right)^2+\frac{\pi^2}{12}\right), \tag{4.17}$$

$$I_3^{\bar{c}} = \frac{i}{16\pi^2}\cdot\frac{1}{p^+\bar{q}^-}\left(-\frac{1}{\epsilon^2}-\frac{\ln\frac{\mu^2}{\bar{q}^2}+i\pi}{\epsilon}-\frac{1}{2}\left(\ln\frac{\mu^2}{\bar{q}^2}+i\pi\right)^2+\frac{\pi^2}{12}\right), \tag{4.18}$$

$$I_3^s = \frac{i}{16\pi^2}\cdot\frac{1}{p^+\bar{q}^-}\left(\frac{1}{\epsilon^2}+\frac{1}{\epsilon}\ln\frac{\mu^2p^+\bar{q}^-}{p^2\bar{q}^2}+\frac{i\,\pi}{\epsilon}+\frac{1}{2}\ln^2\frac{\mu^2p^+\bar{q}^-}{p^2\bar{q}^2}+i\,\pi\ln\frac{\mu^2p^+\bar{q}^-}{p^2\bar{q}^2}-\frac{\pi^2}{4}\right), \tag{4.19}$$

$$\begin{aligned} I_4^{(n\bar{n})c} = \frac{i}{16\pi^2}\cdot\frac{1}{\bar{q}^-}\cdot\frac{1}{\bar{p}^2p^+ + p^2\bar{p}^+}\Bigg(&\frac{\ln\frac{p^2\bar{p}^+}{\bar{p}^2p^+}+i\pi}{\epsilon}-\frac{7\pi^2}{6}-2\,\text{Li}_2\left(-\frac{p^2\bar{p}^+}{\bar{p}^2p^+}\right)+i\pi\ln\frac{\mu^2p^2(p+\bar{p})^2(\bar{p}^+)^2}{(\bar{p}^2p^+ + p^2\bar{p}^+)^2\bar{p}^2}+, \\ &\ln\frac{\bar{p}^2p^+}{p^2\bar{p}^+}\left(\ln\frac{(\bar{p}^2p^+ + p^2\bar{p}^+)^2}{(p+\bar{p})^2p^+\bar{p}^+\bar{p}^2}-\frac{1}{2}\ln\frac{\mu^4p^+}{p^2\bar{p}^2\bar{p}^+}\right)\Bigg), \end{aligned} \tag{4.20}$$

$$I_4^{(n\bar{n})s} = \frac{i}{16\pi^2}\cdot\frac{1}{\bar{q}^-}\cdot\frac{1}{\bar{p}^2p^+ + p^2\bar{p}^+}\left(-\frac{\ln\frac{p^2\bar{p}^+}{\bar{p}^2p^+}+i\pi}{\epsilon}+\frac{1}{2}\ln\frac{\bar{p}^2p^+}{p^2\bar{p}^+}\ln\frac{\mu^4p^+\bar{p}^+(\bar{q}^-)^2}{p^2\bar{p}^2(\bar{q}^2)^2}-i\pi\ln\frac{\mu^2p^2(\bar{p}^+)^2\bar{q}^-}{\bar{q}^2(\bar{p}^2)^2p^+}+\frac{3}{2}\pi^2\right),$$

$$I_5^s = \frac{i}{16\pi^2}\frac{M^+M^-}{p^+\bar{p}^+(p+\bar{p})^2q^-\bar{q}^-(q+\bar{q})^2}\left[-\frac{2\,i\pi}{\epsilon}+\ln\left(\frac{\bar{p}^+p^2}{p^+\bar{p}^2}\right)\ln\left(\frac{q^-\bar{q}^2}{\bar{q}^-q^2}\right)+i\pi\ln\left(\frac{\bar{p}^2p^2\bar{q}^2q^2}{\bar{p}^+p^+\bar{q}^-q^-\mu^4}\right)+3\pi^2\right].$$

The contribution to the Wilson coefficient C_2 can be written as sum of three topologies, where the active-active topology gives the same contribution as the final result for C_2, so for the consistency the remaining two topologies should give contributions to C_2 that add up to zero. For the different Wilson coefficient contributions we get:

[1] In the collinear integrals the power counting requires to set the off-shellness regulator to zero when shrinking the propagator to a point. This has one disadvantage, which is that after doing so, the off-shellness does not properly regularize all the infrared physics, and some of the $1/\epsilon$ poles in the dimensional regularization will correspond to infrared origin. If one ignores the power counting and leaves the off-shellness in the shrinked to a point propagator, then the off-shellness regularizes all of the infrared properly. We repeated the calculation for this case too, and all of the conclusions of this section, namely the matching coefficient is identical to the case, which we present below, in which we respect the power counting. We thank Thomas Becher for suggesting to us to do the calculation both ways.

$$\Delta(C_2)^{(\mathrm{AA})}_{\mathrm{EFT}_1} = I_3 - I_3^s - I_3^c - I_3^{\bar{c}} = \frac{1}{\epsilon^2} + \frac{\ln\frac{\mu^2}{p^+\bar{q}^-} + i\pi}{\epsilon} + \frac{1}{2}\ln^2\frac{\mu^2}{p^+\bar{q}^-} + i\pi\ln\frac{\mu^2}{p^+\bar{q}^-} - \frac{7}{12}\pi^2, \tag{4.21}$$

$$\Delta(C_2)^{(\mathrm{SA})}_{\mathrm{EFT}_1} = p^2\left(I_4 - I_4^{(n\bar{n})s} - I_4^{(n\bar{n})c}\right) = 0, \tag{4.22}$$

$$\Delta(C_2)^{(\mathrm{SS})}_{\mathrm{EFT}_1} = p^2\bar{q}^2\left(I_5 - I_5^s\right) = \frac{1}{\epsilon_{\mathrm{UV}}} + \frac{1}{\epsilon_{\mathrm{IR}}} + \text{finite}. \tag{4.23}$$

$$\tag{4.24}$$

We see that EFT_1 breaks down since it fails to reproduce the IR of QCD.

2.3 EFT-2: EFT-1 + Glauber gluons

Having found a serious problem in the EFT_1 we go ahead and do the similar matching calculation to check the consistency for the EFT_2.

In this effective theory the only non vanishing zero-bin subtraction integral turns out to be the overlap between collinear and Glauber modes in the spectator-active topology: $(I_4^{(n\bar{n})c'})_{0g}$. All the rest zero-bin subtractions are scaleless in dimensional regularization.

The explicit results for all the mode contributions in EFT_2 are presented below:

$$I_3^{c'} = I_3^c \tag{4.25}$$

$$I_3^{\bar{c}'} = I_3^{\bar{c}} \tag{4.26}$$

$$I_3^g = 0 \tag{4.27}$$

$$I_4^{(n\bar{n})c'} = I_4^{(n\bar{n})c} - (I_4^{(n\bar{n})c'})_{0g} \tag{4.28}$$

$$I_4^{(n\bar{n})g} = \text{write down explicit formula} \tag{4.29}$$

$$I_5^g = \frac{i}{16\pi^2}\left[\frac{M^+M^-}{p^+\bar{p}^+(p+\bar{p})^2 q^-\bar{q}^-(q+q)^2}\left(\frac{2\pi i}{\epsilon} - 2\pi^2 + 2\pi\, i\,\ln\left(\frac{\mu^2}{M^+M^-}\right)\right) + \right. \tag{4.30}$$

$$\left.\frac{2\pi i\, M^+M^-}{p^+\bar{p}^+(p+\bar{p})^2(M^-)^2 - q^-\bar{q}^-(q+\bar{q})^2(M^+)^2}\left((M^-)^2\frac{\ln\left(\frac{(M^-)^3M^+}{q^-\bar{q}^-(q+\bar{q})^2}\right)}{q^-\bar{q}^-(q+\bar{q})^2} - (M^+)^2\frac{\ln\left(\frac{(M^+)^3M^-}{p^+\bar{p}^+(p+\bar{p})^2}\right)}{p^+\bar{p}^+(p+\bar{p})^2}\right)\right].$$

where the only non-zero zero-bin integral $(I_4^{(n\bar{n})c'})_{0g}$ is identically equal to the Glauber integral in the spectator-active topology:

$$(I_4^{(n\bar{n})c'})_{0g} = I_4^{(n\bar{n})g}. \tag{4.31}$$

The corresponding contributions to the Wilson coefficient C_2 from different topologies are equal to:

$$\Delta(C_2)^{(\mathrm{AA})}_{\mathrm{EFT}_2} = I_3 - I_3^c - I_3^{\bar{c}} - I_3^g - I_3^s = \Delta(C_2)^{(\mathrm{AA})}_{\mathrm{EFT}_1}, \tag{4.32}$$

$$\Delta(C_2)^{(\mathrm{SA})}_{\mathrm{EFT}_2} = p^2 \left(I_4 - I_4^{(n\bar{n})c} - I_4^{(n\bar{n})g} - I_4^{(n\bar{n})s} \right) = 0, \tag{4.33}$$

$$\Delta(C_2)^{(\mathrm{SS})}_{\mathrm{EFT}_2} = p^2 \bar{q}^2 \left(I_5 - I_5^g - I_5^s \right) = 0, \tag{4.34}$$

$$\tag{4.35}$$

We observe that EFT_2 successfully reproduces the IR of QCD and leads to the correct matching coefficient for C_2 given by active-active topology only.

3 Pinch analysis and power counting

In this section we will identify the correct effective theory modes, needed to describe the infrared behavior of the spectator-spectator loop integral:

$$D^{\mathrm{full}}_{(SS)} = \int \frac{d^4 l}{(2\pi)^4} \frac{1}{l^2 + i0} \frac{1}{(l+p)^2 + i0} \frac{1}{(l-\bar{p})^2 + i0} \frac{1}{(l+q)^2 + i0} \frac{1}{(l-\bar{q})^2 + i0} \,. \tag{4.36}$$

Decomposing the loop momentum l into its light-cone components we arrive at the following form, which is suitable for first integrating over the $+$ component by contours and leaving the $\perp$ components as a final integration:

$$D^{\mathrm{full}}_{(SS)} = \frac{1}{2} \int \frac{d^2 l_\perp}{(2\pi)^2} \int \frac{dl^-}{2\pi} N^-(l^-) \int \frac{dl^+}{2\pi} \prod_{i=0}^{4} \frac{1}{l^+ - z_i(l^-, l_\perp)} \,, \tag{4.37}$$

where $1/N^-(l^-) = l^-(l^- + p^-)(l^- - \bar{p}^-)(l^- + q^-)(l^- - \bar{q}^-)$. The singularities in the complex l^+ plane are functions of l^- and $l_\perp$, as well as the external momentum components. Explicitly they are given by

$$z_0(l^-, l_\perp) = \frac{l_\perp^2 - i0}{l^-} \,, \tag{4.38}$$

$$z_1(l^-, l_\perp) = \frac{(l_\perp + p_\perp)^2 - i0}{l^- + p^-} - p^+ \,, \qquad z_3(l^-, l_\perp) = \frac{(l_\perp + q_\perp)^2 - i0}{l^- + q^-} - q^+ \,, \tag{4.39}$$

$$z_2(l^-, l_\perp) = \frac{(l_\perp - \bar{p}_\perp)^2 - i0}{l^- - \bar{p}^-} + \bar{p}^+ \,, \qquad z_4(l^-, l_\perp) = \frac{(l_\perp - \bar{q}_\perp)^2 - i0}{l^- - \bar{q}^-} + \bar{q}^+ \,. \tag{4.40}$$

Note that the locations of the poles above or below the real axis changes during the integration over l^- at the transitions $l^- = -q^- \sim \mathcal{O}(1)$, $\bar{q}^- \sim \mathcal{O}(1)$, $-p^- \sim \mathcal{O}(\lambda^2)$, $\bar{p}^- \sim \mathcal{O}(\lambda^2)$ and $l^- = 0$.

In order to identify which modes one should put into the effective theory, we must find all the momentum regions that contain a pinch singularity and which also are of leading power. One way of finding that out is to expand the integrand in equation (4.37) and count the measures and propagators in the appropriate powers of λ. Also one could analyze the pinch structure of the expanded integrals. In our explicit matching calculation we basically did exactly that.

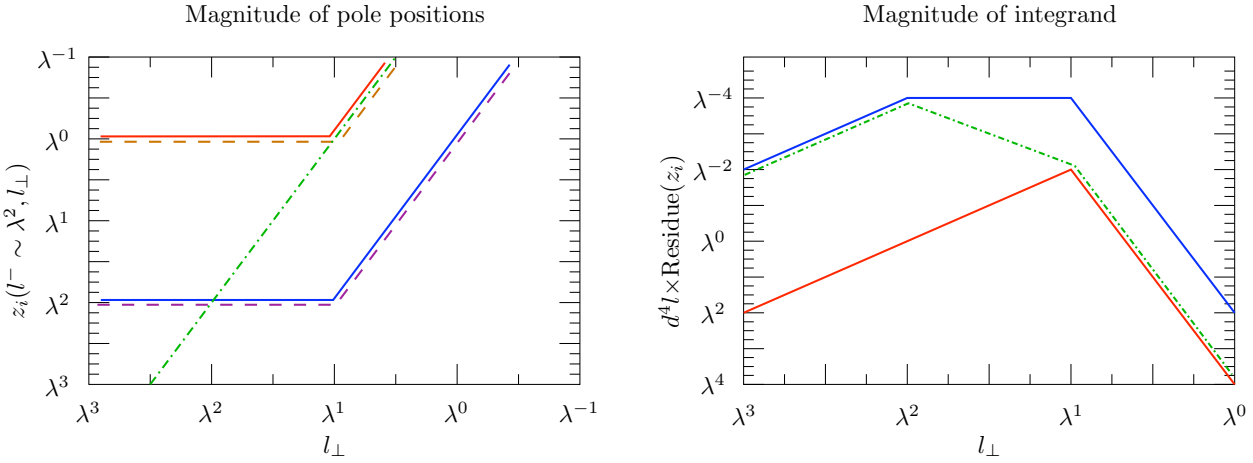

Figure 4.2: Left: magnitude of pole locations as a function of $l_\perp$. Dashed lines denote poles in the lower half plane, while solid ones are in the upper half plane. Right: magnitude of the residues of poles in the upper half plane. The color coding is identical to the one on the left.

Alternatively, it is instructive to choose a countour of integration for l^+, e.g. closing the loop in the upper half plane, and plotting the residues and measures for each of the poles. To that end we define

$$\lambda^{n_j^{\text{Res}}(n_\perp, n^-)} = \lambda^{2n_\perp + n^-} \left| N^-(\lambda^{n^-}) \prod_{i \neq j} \frac{1}{z_j(\lambda^{n^-}, \lambda^{n_\perp}) - z_i(\lambda^{n^-}, \lambda^{n_\perp})} \right| . \tag{4.41}$$

In other words, $n_j^{\text{Res}}(n_\perp, n^-)$ is the power of the jth residual term in the integral (4.37) for a given assignment of $l^- \sim \lambda^{n^-}$ and $l_\perp \sim \lambda^{n_\perp}$.

Now we can answer the question which pinched surfaces are leading order in power counting for the loop integral under consideration, by explicitly plotting the poles in Eq. (4.38)-Eq. (4.40) and the residues in Eq. (4.41). In order to have a two-dimensional visualized picture we have to fix the value for l^-, which we take for both figures to be $l^- \sim \lambda^2$, i.e. $n^- = 2$. This choice limits us to considering only soft, glauber and collinear modes, but not the anti-collinear one. However in our case the anti-collinear is equivalent to collinear under substitutions $p, \bar{p} \leftrightarrow q, \bar{q}$. Thus this choice $n^- = 2$ will still allow us to find all the relevant modes.

In Figure 4.2 we plot the sufficient information needed to identify the set of effective theory modes to describe the spectator-spectator interaction topology. The left graph represents five lines, one for each pole in l^+, given in Eq. (4.38)-Eq. (4.40), which show the dependance of the $\left|z_j(\lambda^2, l_\perp)\right|$ on $l_\perp$. The colors are: green(z_0), orange(z_1), red(z_2), purple(z_3),blue(z_4). Solid lines correspond to poles in the upper complex plane, while the dashed ones to the lower one, thus whenever the solid and dashed lines come close to each other we have a pinched pole. On the right graph of Figure 4.2 we plot the value of the residue $\lambda^{n_j^{\text{Res}}(n_\perp, n^-)}$ including the loop integral measure, according to Eq. (4.41).

The analysis of both graphs in Figure 4.2 in conjunction gives information about the

effective theory modes. Indeed, we can see from the graph on the right that the leading in power counting contribution, which is λ^{-4} in this case, comes from the region where $l_\perp \sim \left(\lambda^2 ... \lambda\right)$ and comes from the residues of the poles z_0 (green) and z_4 (blue). On the other hand, the graph on the left shows that this entire region is pinched, and the value of l^+ is $l^+ \sim \lambda^2$. This means that the general pinched leading order region in the spectator-spectator topology looks like: $\left(\lambda^2, \lambda^2, \lambda^p\right)$, and where $p \in [1...2]$.

We see that choosing $p = 1$ and $p = 2$ in our general pinched leading region obtained above, we observe that the soft and the glauber modes are pinched and leading order, thus should be included into the effective theory.

Another observation that can be made from the left figure above is that there is a pinched pole at $l \sim (\lambda^0, \lambda^2, \lambda)$, which corresponds to the collinear gluon mode. However according to the right figure this mode is contributing at sub-leading order, λ^{-2}, since it is contained exactly in the residues of one of the poles z_0 (green) or z_2(red). Of course the anti-collinear mode, even though it's beyond our consideration because of our choice for l^-, is analogously power suppressed.

Finally we note that it is not wrong to introduce even more modes into the effective theory, for example one with the scaling $l \sim (\lambda^2, \lambda^2, \lambda^{3/2})$, as it passes the test of coming from a pinch singularity and contributing at leading power. This will lead to a scaleless integral again, and the overlap with the soft and glauber modes will subtract its contribution again. This "new" contribution is therefore zero, and the mode not useful. Another way of stating this is that the full theory integrand displays no feature for this momentum scaling. Same is true for all other modes with $1 < p < 2$ in the general leading pinched region that we have found using Figure 4.2.

4 Coleman-Norton theorem and off-shell modes

We established in Section 2 that SCET should be expanded by a Glauber mode in order to consistently describe the exclusive Drell-Yan cross-section. However as it follows from the scaling of the Glauber mode $p_g \sim \left(\lambda^2, \lambda^2, \lambda\right)$, it cannot be made exactly on-shell, since $p_g^2 \sim -\mathbf{p}_\perp^2 \neq 0$. This seems to contradict to the famous Coleman-Norton Theorem (CNT) [60].

The CNT is essentially a physical interpretation of Landau equations [117], see also [137] for a review of this subject. The Landau equations are the necessary conditions for the appearance of a pinch singularity in the arbitrary loop integral. One additional element of the theorem is the proof that Landau equations are also a sufficient conditions for the pinch, if one assumes that the Gram matrix of external loop momenta does not have more than one zero eigenvalue.

Under these rather general assumptions the CNT states that the infrared singularities of any amplitude to any order in perturbation theory come from the configurations of the momentum in the loops such that all intermediate propagators are on-shell, or they are shrinked to a point. Of

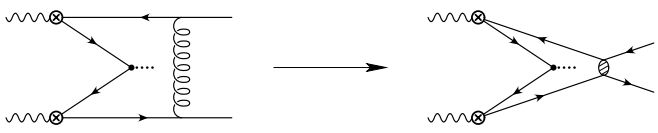

Figure 4.3: Physical picture of both soft and glauber exchange between spectators.

course in that limit the process described by the amplitude becomes a physically observable process with real on-shell particles created and annihilated at the intermediate level.

In our case of three different topologies we showed explicitly that the Glauber region is pinched only in the spectator-spectator topology, while in the remaining topologies usual soft and collinear pinches only occur, which have no problem with the CN interpretation since they can be easily made on-shell because of their momentum scaling.

Let us focus on the spectator-spectator case. The sufficient condition of the CN theorem breaks down for this topology, as the Gram matrix has two additional zero eigenvalues. This can be trivially checked, and the reason for such degeneracy is that most of the products are collinear to each other and thus vanish in the strictly collinear limit $\lambda \to 0$. However, even though formally CN theorem fails for the spectator-spectator graph, the Glauber mode should still satisfy the Landau equations. One of these equations states that the propagating degrees of freedom should be exactly on-shell. Yet, still the Glauber gluon is off-shell, so what is the contradiction that we are facing?

The point is that in the Landau formulation of necessary conditions for the pinch there is no power counting associated. Indeed the goal of the Landau analysis was to identify the cases of the external kinematics when the integral becomes singular. Examples of results from analysis of Landau equations are: finding the threshold singularities in the triangle, box, etc diagrams, also see an interesting application in Higgs physics. Thus the result of solving Landau equations is what external momenta of the given loop integral lead to a singularity. Since these equations involve the loop momentum, they also address the question where in the loop momenta the singularity is located. As an example one can see that both Soft and Collinear pinch for the active-active topology can be found by solving Landau equations (see Sterman's Tasi lectures). However in order to distinguish between Glauber and Soft singularities, one would need to go beyond Landau Equations, and include power counting into the singular region.

Thus the original Landau equations fail to distinguish between Soft pinch and Glauber pinch since both in the limit $\lambda \to 0$ go to the gluon momentum $l^\mu \to 0$. In this limit of course the Glauber gluon becomes on-shell, so if one views the Landau equation in this limit there is no problem with off-shellness, since it goes to zero.

It would be interesting to reformulate the Landau equations in the effective theory friendly language with power counting, i.e. instead of writing down a condition when you get a true pinch singularity, assign off-shellness to external legs and find a condition for pinched poles to occur at distance of say order λ^2 from each other. It should be the case that one would be able to tell the difference between the soft and Glauber pinches in the spectator-spectator diagram, through such Relaxed Landau equations. This is beyond the scope of the present work.

As argued above the formal proof of Coleman and Norton theorem fails for the Glauber diagram, because of the fact that sufficient condition for the pinch is not true. However, since we know from direct pinch analysis and also from the figures above that the Glauber pinch is really there, for this particular case we know that the theorem is still true, and thus Glauber contribution should fit into the CN spacetime picture. If one writes the Landau equations for this case, it is easy to see that solution should satisfy (same for the soft pinch):

$$\alpha_2\, p^+ - \alpha_3\, \bar{p}^+ = 0, \tag{4.42}$$

$$\alpha_4\, \bar{q}^- - \alpha_5\, q^- = 0, \tag{4.43}$$

$$\alpha_i = \mathcal{O}(1), \qquad i = 1, 2, .., 5. \tag{4.44}$$

Equations (4.42) and (4.43) have physical meaning that the active-active collisions occur at the same time and point (along the collision axis) as the interaction of spectators. It makes sense if you think about space-time picture of particles moving at the speed of light and splitting in two and colliding.

5 Conclusions

Our matching calculation shows the necessity of inclusion of Glauber gluons into the SCET lagrangian in order to describe the full infrared physics of Drell-Yan amplitude at one loop order.

Indeed we observed that in SCET (which is same as EFT_1) the consistency check on the effective theory, that the matching coefficient C_2 of the operator O_2 is independent of the external states, failed. However in EFT_2, where we included the contribution of the Glauber mode, the consistency check perfectly works. Even though we didn't directly consider the Drell-Yan process, our choice of external states was such, that contributions of spectator-active and spectator-spectator interactions in addition to active-active one allowed us to make parallels between our conclusion about the consistency of matching and the correct modes for the Drell-Yan amplitude.

For our analysis it was important to avoid double counting between the modes by performing zero-bin subtractions [129] from the collinear and Glauber modes. Especially we want to emphasize the spectator-active case for EFT_2, since in this topology there is an interesting example of non-vanishing in dimensional regularization zero-bin subtraction from the naive collinear mode $(I_4^{(n\bar{n})c'})_{0g} \neq 0$, which makes sure that the inclusion of the Glauber mode for this topology doesn't change the effective theory one loop result compared to EFT_1, which is of course expected from the pinch analyses as explained in section 3.

We explained why the presence of an off-shell mode is in no conflict with the Coleman-Norton theorem for infrared singularities of scattering amplitudes. Our result is that Landau Equations are insensitive in distinguishing Glauber pinch from the Soft one, since they are valid in the limit of strict singularity, when $\lambda = 0$, in which case both regions collapse to $l^\mu = 0$, in which the off-shellness of Glauber gluon becomes exactly zero.

The next important step would be to include Glauber gluons into the SCET lagrangian and study their expected cancelation in the Drell-Yan inclusive in transverse momentum of the lepton pair cross-section. The main challenge in doing so is that the Glauber mode scaling is such that the corresponding particle is always off-shell. One might interpret this mode conveniently as an effective potential, similar to the one in NRQCD.

Bibliography

[1] Riccardo Abbate, Michael Fickinger, Andre H. Hoang, Vicent Mateu, and Iain W. Stewart. Thrust at N^3LL with Power Corrections and a Precision Global Fit for alphas(mZ). 2010.

[2] Leandro G. Almeida et al. Substructure of high-pT Jets at the LHC. *Phys. Rev.*, D79:074017, 2009.

[3] Leandro G. Almeida, Seung J. Lee, Gilad Perez, Ilmo Sung, and Joseph Virzi. Top Jets at the LHC. *Phys. Rev.*, D79:074012, 2009.

[4] Christian M. Arnesen, Joydip Kundu, and Iain W. Stewart. Constraint equations for heavy-to-light currents in SCET. *Phys. Rev.*, D72:114002, 2005.

[5] Christopher Balzereit, Thomas Mannel, and Wolfgang Kilian. Evolution of the light-cone distribution function for a heavy quark. *Phys. Rev.*, D58:114029, 1998.

[6] Andrea Banfi, Gavin P. Salam, and Giulia Zanderighi. Resummed event shapes at hadron - hadron colliders. *JHEP*, 08:062, 2004.

[7] Andrea Banfi, Gavin P. Salam, and Giulia Zanderighi. Principles of general final-state resummation and automated implementation. *JHEP*, 03:073, 2005.

[8] A. Bassetto, M. Dalbosco, I. Lazzizzera, and R. Soldati. Yang-Mills Theories in the Light Cone Gauge. *Phys. Rev.*, D31:2012, 1985.

[9] Christian W. Bauer, Oscar Cata, and Grigory Ovanesyan. On different ways to quantize Soft-Collinear Effective Theory. 2008.

[10] Christian W. Bauer, Matthew P. Dorsten, and Michael P. Salem. Infrared regulators and SCET(II). *Phys. Rev.*, D69:114011, 2004.

[11] Christian W. Bauer, Sean Fleming, Christopher Lee, and George Sterman. Factorization of e+e- Event Shape Distributions with Hadronic Final States in Soft Collinear Effective Theory. *Phys. Rev.*, D78:034027, 2008.

[12] Christian W. Bauer, Sean Fleming, and Michael E. Luke. Summing Sudakov logarithms in $B \to X_s$ gamma in effective field theory. *Phys. Rev.*, D63:014006, 2000.

[13] Christian W. Bauer, Sean Fleming, Dan Pirjol, Ira Z. Rothstein, and Iain W. Stewart. Hard scattering factorization from effective field theory. *Phys. Rev.*, D66:014017, 2002.

[14] Christian W. Bauer, Sean Fleming, Dan Pirjol, and Iain W. Stewart. An effective field theory for collinear and soft gluons: Heavy to light decays. *Phys. Rev.*, D63:114020, 2001.

[15] Christian W. Bauer, Andrew Hornig, and Frank J. Tackmann. Factorization for generic jet production. 2008.

[16] Christian W. Bauer, Bjorn O. Lange, and Grigory Ovanesyan. On glauber gluons in scet. in preparation, 2010.

[17] Christian W. Bauer, Christopher Lee, Aneesh V. Manohar, and Mark B. Wise. Enhanced nonperturbative effects in z decays to hadrons. *Phys. Rev.*, D70:034014, 2004.

[18] Christian W. Bauer and Aneesh V. Manohar. Shape function effects in b $\to$ x/s gamma and b $\to$ x/u l nu decays. *Phys. Rev.*, D70:034024, 2004.

[19] Christian W. Bauer, Aneesh V. Manohar, and Mark B. Wise. Enhanced nonperturbative effects in jet distributions. *Phys. Rev. Lett.*, 91:122001, 2003.

[20] Christian W. Bauer, Dan Pirjol, and Iain W. Stewart. Power counting in the soft-collinear effective theory. *Phys. Rev.*, D66:054005, 2002.

[21] Christian W. Bauer, Dan Pirjol, and Iain W. Stewart. Soft-Collinear Factorization in Effective Field Theory. *Phys. Rev.*, D65:054022, 2002.

[22] Christian W. Bauer, Dan Pirjol, and Iain W. Stewart. On power suppressed operators and gauge invariance in scet. *Phys. Rev.*, D68:034021, 2003.

[23] Christian W. Bauer and Matthew D. Schwartz. Improving jet distributions with effective field theory. *Phys. Rev. Lett.*, 97:142001, 2006.

[24] Christian W. Bauer and Matthew D. Schwartz. Event generation from effective field theory. *Phys. Rev.*, D76:074004, 2007.

[25] Christian W. Bauer and Iain W. Stewart. Invariant operators in collinear effective theory. *Phys. Lett.*, B516:134–142, 2001.

[26] Thomas Becher, Richard J. Hill, and Matthias Neubert. Soft-collinear messengers: A new mode in soft-collinear effective theory. *Phys. Rev.*, D69:054017, 2004.

[27] Thomas Becher and Matthias Neubert. Threshold resummation in momentum space from effective field theory. *Phys. Rev. Lett.*, 97:082001, 2006.

[28] Thomas Becher and Matthias Neubert. Toward a NNLO calculation of the anti-$B \to X_s+$ gamma decay rate with a cut on photon energy. II: Two-loop result for the jet function. *Phys. Lett.*, B637:251–259, 2006.

[29] Thomas Becher and Matthias Neubert. Toward a NNLO calculation of the anti-$B \to X_s$ gamma decay rate with a cut on photon energy. I: Two-loop result for the soft function. *Phys. Lett.*, B633:739–747, 2006.

[30] Thomas Becher, Matthias Neubert, and Ben D. Pecjak. Factorization and momentum-space resummation in deep- inelastic scattering. *JHEP*, 01:076, 2007.

[31] Thomas Becher, Matthias Neubert, and Gang Xu. Dynamical Threshold Enhancement and Resummation in Drell- Yan Production. *JHEP*, 07:030, 2008.

[32] Thomas Becher and Matthew D. Schwartz. A Precise determination of α_s from LEP thrust data using effective field theory. *JHEP*, 07:034, 2008.

[33] Andrei V. Belitsky, G. P. Korchemsky, and G. Sterman. Energy flow in qcd and event shape functions. *Phys. Lett.*, B515:297–307, 2001.

[34] M. Beneke and Vladimir M. Braun. Renormalons and power corrections. 2000.

[35] Carola F. Berger. Higher orders in a(alpha(s))/(1-x)+ of non-singlet partonic splitting functions. *Phys. Rev.*, D66:116002, 2002.

[36] Carola F. Berger, Tibor Kucs, and George Sterman. Energy flow in interjet radiation. *Phys. Rev.*, D65:094031, 2002.

[37] Carola F. Berger, Tibor Kucs, and George Sterman. Event shape / energy flow correlations. *Phys. Rev.*, D68:014012, 2003.

[38] Carola F. Berger, Tibor Kucs, and George Sterman. Interjet energy flow / event shape correlations. *Int. J. Mod. Phys.*, A18:4159–4168, 2003.

[39] Carola F. Berger and Lorenzo Magnea. Scaling of power corrections for angularities from dressed gluon exponentiation. *Phys. Rev.*, D70:094010, 2004.

[40] Carola F. Berger and George Sterman. Scaling rule for nonperturbative radiation in a class of event shapes. *JHEP*, 09:058, 2003.

[41] Carola F. Berger and George Sterman. Power corrections to e+ e- dijet event shapes. *Eur. Phys. J.*, C33:s407–s409, 2004.

[42] Siegfried Bethke. Experimental Tests of Asymptotic Freedom. *Prog. Part. Nucl. Phys.*, 58:351–386, 2007.

[43] Geoffrey T. Bodwin. Factorization of the Drell-Yan Cross-Section in Perturbation Theory. *Phys. Rev.*, D31:2616, 1985.

[44] Geoffrey T. Bodwin, Stanley J. Brodsky, and G. Peter Lepage. Initial State Interactions and the Drell-Yan Process. *Phys. Rev. Lett.*, 47:1799, 1981.

[45] S. W. Bosch, B. O. Lange, M. Neubert, and Gil Paz. Factorization and shape-function effects in inclusive B- meson decays. *Nucl. Phys.*, B699:335–386, 2004.

[46] G. Bozzi, S. Catani, D. de Florian, and M. Grazzini. The q(T) spectrum of the Higgs boson at the LHC in QCD perturbation theory. *Phys. Lett.*, B564:65–72, 2003.

[47] S. Brandt, C. Peyrou, R. Sosnowski, and A. Wroblewski. The principal axis of jets. an attempt to analyze high- energy collisions as two-body processes. *Phys. Lett.*, 12:57–61, 1964.

[48] S. Catani, L. Trentadue, G. Turnock, and B. R. Webber. Resummation of large logarithms in e+ e- event shape distributions. *Nucl. Phys.*, B407:3–42, 1993.

[49] S. Catani, G. Turnock, and B. R. Webber. Jet broadening measures in e+ e- annihilation. *Phys. Lett.*, B295:269–276, 1992.

[50] S. Catani, G. Turnock, B. R. Webber, and L. Trentadue. Thrust distribution in e+ e- annihilation. *Phys. Lett.*, B263:491–497, 1991.

[51] S. Catani and B. R. Webber. Resummed c-parameter distribution in e+ e- annihilation. *Phys. Lett.*, B427:377–384, 1998.

[52] Stefano Catani, Michelangelo L. Mangano, Paolo Nason, and Luca Trentadue. The Resummation of Soft Gluon in Hadronic Collisions. *Nucl. Phys.*, B478:273–310, 1996.

[53] T. Chandramohan and L. Clavelli. Consequences of second order qcd for jet structure in e+ e- annihilation. *Nucl. Phys.*, B184:365, 1981.

[54] Junegone Chay and Chul Kim. Collinear effective theory at subleading order and its application to heavy-light currents. *Phys. Rev.*, D65:114016, 2002.

[55] Junegone Chay, Chul Kim, Yeong Gyun Kim, and Jong-Phil Lee. Soft wilson lines in soft-collinear effective theory. *Phys. Rev.*, D71:056001, 2005.

[56] P. S. Cherzor and N. A. Sveshnikov. Jet observables and energy-momentum tensor. 1997.

[57] Jui-yu Chiu, Andreas Fuhrer, Andre H. Hoang, Randall Kelley, and Aneesh V. Manohar. Soft-Collinear Factorization and Zero-Bin Subtractions. *Phys. Rev.*, D79:053007, 2009.

[58] L. Clavelli. Jet invariant mass in quantum chromodynamics. *Phys. Lett.*, B85:111, 1979.

[59] L. Clavelli and D. Wyler. Kinematical bounds on jet variables and the heavy jet mass distribution. *Phys. Lett.*, B103:383, 1981.

[60] S. Coleman and R. E. Norton. Singularities in the physical region. *Nuovo Cim.*, 38:438–442, 1965.

[61] John C. Collins, Davison E. Soper, and George Sterman. FACTORIZATION FOR ONE LOOP CORRECTIONS IN THE DRELL-YAN PROCESS. *Nucl. Phys.*, B223:381, 1983.

[62] John C. Collins, Davison E. Soper, and George Sterman. ALL ORDER FACTORIZATION FOR DRELL-YAN CROSS-SECTIONS. *Phys. Lett.*, B134:263, 1984.

[63] John C. Collins, Davison E. Soper, and George Sterman. Factorization of Hard Processes in QCD. *Adv. Ser. Direct. High Energy Phys.*, 5:1–91, 1988.

[64] John C. Collins, Davison E. Soper, and George Sterman. Soft gluons and factorization. *Nucl. Phys.*, B308:833, 1988.

[65] John C. Collins, Davison E. Soper, and George F. Sterman. DOES THE DRELL-YAN CROSS-SECTION FACTORIZE? *Phys. Lett.*, B109:388, 1982.

[66] John C. Collins, Davison E. Soper, and George F. Sterman. Factorization for Short Distance Hadron - Hadron Scattering. *Nucl. Phys.*, B261:104, 1985.

[67] John C. Collins, Davison E. Soper, and George F. Sterman. Transverse Momentum Distribution in Drell-Yan Pair and W and Z Boson Production. *Nucl. Phys.*, B250:199, 1985.

[68] John C. Collins and George Sterman. Soft partons in qcd. *Nucl. Phys.*, B185:172, 1981.

[69] Harry Contopanagos, Eric Laenen, and George Sterman. Sudakov factorization and resummation. *Nucl. Phys.*, B484:303–330, 1997.

[70] M. Dasgupta and G. P. Salam. Resummation of non-global qcd observables. *Phys. Lett.*, B512:323–330, 2001.

[71] Mrinal Dasgupta and Gavin P. Salam. Event shapes in e+ e- annihilation and deep inelastic scattering. *J. Phys.*, G30:R143, 2004.

[72] R. A. Davison and B. R. Webber. Non-Perturbative Contribution to the Thrust Distribution in e^+e^- Annihilation. *Eur. Phys. J.*, C59:13–25, 2009.

[73] Daniel de Florian and Massimiliano Grazzini. The back-to-back region in e+ e- energy energy correlation. *Nucl. Phys.*, B704:387–403, 2005.

[74] A. De Rujula, John R. Ellis, E. G. Floratos, and M. K. Gaillard. QCD Predictions for Hadronic Final States in e+ e- Annihilation. *Nucl. Phys.*, B138:387, 1978.

[75] Francesco D'Eramo, Hong Liu, and Krishna Rajagopal. Transverse Momentum Broadening and the Jet Quenching Parameter, Redux. 2010.

[76] G. Dissertori et al. First determination of the strong coupling constant using NNLO predictions for hadronic event shapes in e+e- annihilations. *JHEP*, 02:040, 2008.

[77] Yuri L. Dokshitzer, A. Lucenti, G. Marchesini, and G. P. Salam. On the QCD analysis of jet broadening. *JHEP*, 01:011, 1998.

[78] Yuri L. Dokshitzer, G. Marchesini, and G. P. Salam. Revisiting non-perturbative effects in the jet broadenings. *Eur. Phys. J. direct*, C1:3, 1999.

[79] Yuri L. Dokshitzer, G. Marchesini, and B. R. Webber. Dispersive Approach to Power-Behaved Contributions in QCD Hard Processes. *Nucl. Phys.*, B469:93–142, 1996.

[80] Yuri L. Dokshitzer and B. R. Webber. Calculation of power corrections to hadronic event shapes. *Phys. Lett.*, B352:451–455, 1995.

[81] Yuri L. Dokshitzer and B. R. Webber. Power corrections to event shape distributions. *Phys. Lett.*, B404:321–327, 1997.

[82] S. D. Drell and Tung-Mow Yan. Massive Lepton Pair Production in Hadron-Hadron Collisions at High-Energies. *Phys. Rev. Lett.*, 25:316–320, 1970.

[83] G. Duplancic and B. Nizic. IR finite one-loop box scalar integral with massless internal lines. *Eur. Phys. J.*, C24:385–391, 2002.

[84] G. Duplancic and B. Nizic. Reduction method for dimensionally regulated one-loop N- point Feynman integrals. *Eur. Phys. J.*, C35:105–118, 2004.

[85] R. Keith Ellis, D. A. Ross, and A. E. Terrano. The perturbative calculation of jet structure in e+ e- annihilation. *Nucl. Phys.*, B178:421, 1981.

[86] Edward Farhi. A qcd test for jets. *Phys. Rev. Lett.*, 39:1587–1588, 1977.

[87] Sean Fleming, Andre H. Hoang, Sonny Mantry, and Iain W. Stewart. Top Jets in the Peak Region: Factorization Analysis with NLL Resummation. 2007.

[88] Sean Fleming, Andre H. Hoang, Sonny Mantry, and Iain W. Stewart. Jets from Massive Unstable Particles: Top-Mass Determination. *Phys. Rev.*, D77:074010, 2008.

[89] J. Frenkel and J. C. Taylor. Nonabelian eikonal exponentiation. *Nucl. Phys.*, B246:231, 1984.

[90] Einan Gardi. Suppressed power corrections for moments of event-shape variables in e+ e- annihilation. *JHEP*, 04:030, 2000.

[91] Einan Gardi. Dressed gluon exponentiation. *Nucl. Phys.*, B622:365–392, 2002.

[92] Einan Gardi and Lorenzo Magnea. The c parameter distribution in e+ e- annihilation. *JHEP*, 08:030, 2003.

[93] Einan Gardi and Johan Rathsman. Renormalon resummation and exponentiation of soft and collinear gluon radiation in the thrust distribution. *Nucl. Phys.*, B609:123–182, 2001.

[94] J. G. M. Gatheral. Exponentiation of eikonal cross-sections in nonabelian gauge theories. *Phys. Lett.*, B133:90, 1983.

[95] A. G. Grozin and G. P. Korchemsky. Renormalized sum rules for structure functions of heavy mesons decays. *Phys. Rev.*, D53:1378–1390, 1996.

[96] Richard J. Hill and Matthias Neubert. Spectator interactions in soft-collinear effective theory. ((U)). *Nucl. Phys.*, B657:229–256, 2003.

[97] Andre H. Hoang, Ambar Jain, Ignazio Scimemi, and Iain W. Stewart. Infrared Renormalization Group Flow for Heavy Quark Masses. *Phys. Rev. Lett.*, 101:151602, 2008.

[98] Andre H. Hoang and Stefan Kluth. Hemisphere Soft Function at $O(\alpha_s^2)$ for Dijet Production in e+e- Annihilation. 2008.

[99] Andre H. Hoang and Aneesh V. Manohar. Charm Quark Mass from Inclusive Semileptonic B Decays. *Phys. Lett.*, B633:526–532, 2006.

[100] Andre H. Hoang and Iain W. Stewart. Designing Gapped Soft Functions for Jet Production. *Phys. Lett.*, B660:483–493, 2008.

[101] Andrew Hornig, Christopher Lee, and Grigory Ovanesyan. Effective Predictions of Event Shapes: Factorized, Resummed, and Gapped Angularity Distributions. *JHEP*, 05:122, 2009.

[102] Andrew Hornig, Christopher Lee, and Grigory Ovanesyan. Infrared safety in factorized hard scattering cross-sections. *Phys. Lett.*, B:doi:10.1016/j.physletb.2009.05.039, 2009.

[103] Ahmad Idilbi and Abhijit Majumder. Extending Soft-Collinear-Effective-Theory to describe hard jets in dense QCD media. *Phys. Rev.*, D80:054022, 2009.

[104] Ahmad Idilbi and Thomas Mehen. Demonstration of the Equivalence of Soft and Zero-Bin Subtractions. *Phys. Rev.*, D76:094015, 2007.

[105] Ahmad Idilbi and Thomas Mehen. On the equivalence of soft and zero-bin subtractions. *Phys. Rev.*, D75:114017, 2007.

[106] Ambar Jain, Ignazio Scimemi, and Iain W. Stewart. Two-loop Jet-Function and Jet-Mass for Top Quarks. *Phys. Rev.*, D77:094008, 2008.

[107] Nikolaos Kidonakis, Gianluca Oderda, and George Sterman. Nll resummation for dijet production. 1998.

[108] Nikolaos Kidonakis, Gianluca Oderda, and George Sterman. Threshold resummation for dijet cross sections. *Nucl. Phys.*, B525:299–332, 1998.

[109] G. P. Korchemsky. Shape functions and power corrections to the event shapes. 1998.

[110] G. P. Korchemsky and G. Marchesini. Resummation of large infrared corrections using wilson loops. *Phys. Lett.*, B313:433–440, 1993.

[111] G. P. Korchemsky and A. V. Radyushkin. Renormalization of the wilson loops beyond the leading order. *Nucl. Phys.*, B283:342–364, 1987.

[112] G. P. Korchemsky and A. V. Radyushkin. Infrared factorization, wilson lines and the heavy quark limit. *Phys. Lett.*, B279:359–366, 1992.

[113] G. P. Korchemsky and S. Tafat. On power corrections to the event shape distributions in QCD. *JHEP*, 10:010, 2000.

[114] Gregory P. Korchemsky, Gianluca Oderda, and George Sterman. Power corrections and nonlocal operators. 1997.

[115] Gregory P. Korchemsky and George Sterman. Nonperturbative corrections in resummed cross-sections. *Nucl. Phys.*, B437:415–432, 1995.

[116] Gregory P. Korchemsky and George Sterman. Power corrections to event shapes and factorization. *Nucl. Phys.*, B555:335–351, 1999.

[117] L. D. Landau. On analytic properties of vertex parts in quantum field theory. *Nucl. Phys.*, 13:181–192, 1959.

[118] Bjorn O. Lange and Matthias Neubert. Factorization and the soft overlap contribution to heavy- to-light form factors. *Nucl. Phys.*, B690:249–278, 2004.

[119] Christopher Lee and George Sterman. Momentum flow correlations from event shapes: Factorized soft gluons and soft-collinear effective theory. *Phys. Rev.*, D75:014022, 2007.

[120] Adam K. Leibovich, Zoltan Ligeti, and Mark B. Wise. Comment on quark masses in scet. *Phys. Lett.*, B564:231–234, 2003.

[121] Zoltan Ligeti, Iain W. Stewart, and Frank J. Tackmann. Treating the b quark distribution function with reliable uncertainties. *Phys. Rev.*, D78:114014, 2008.

[122] F. Liu and J. P. Ma. Glauber Gluons in Soft Collinear Effective Theory and Factorization of Drell-Yan Processes. 2008.

[123] Michael E. Luke, Aneesh V. Manohar, and Ira Z. Rothstein. Renormalization group scaling in nonrelativistic qcd. *Phys. Rev.*, D61:074025, 2000.

[124] Aneesh V. Manohar. Effective field theories. 1996.

[125] Aneesh V. Manohar. The HQET/NRQCD Lagrangian to order alpha/m**3. *Phys. Rev.*, D56:230–237, 1997.

[126] Aneesh V. Manohar. Deep inelastic scattering as $x \to 1$ using soft-collinear effective theory. *Phys. Rev.*, D68:114019, 2003.

[127] Aneesh V. Manohar, Thomas Mehen, Dan Pirjol, and Iain W. Stewart. Reparameterization invariance for collinear operators. *Phys. Lett.*, B539:59–66, 2002.

[128] Aneesh V. Manohar and Iain W. Stewart. Renormalization group analysis of the qcd quark potential to order v**2. *Phys. Rev.*, D62:014033, 2000.

[129] Aneesh V. Manohar and Iain W. Stewart. The zero-bin and mode factorization in quantum field theory. *Phys. Rev.*, D76:074002, 2007.

[130] Aneesh V. Manohar and Mark B. Wise. Power suppressed corrections to hadronic event shapes. *Phys. Lett.*, B344:407–412, 1995.

[131] Aneesh V. Manohar and Mark B. Wise. Heavy quark physics. *Camb. Monogr. Part. Phys. Nucl. Phys. Cosmol.*, 10:1–191, 2000.

[132] C. Marcantonini. 2007.

[133] Claudio Marcantonini and Iain W. Stewart. Reparameterization Invariant Collinear Operators. *Phys. Rev.*, D79:065028, 2009.

[134] Matthias Neubert. Advanced predictions for moments of the B $\to$ X/s gamma photon spectrum. *Phys. Rev.*, D72:074025, 2005.

[135] F. R. Ore, Jr. and George Sterman. An Operator Approach to Weighted Cross-Sections. *Nucl. Phys.*, B165:93, 1980.

[136] Dan Pirjol and Iain W. Stewart. A complete basis for power suppressed collinear-ultrasoft operators. *Phys. Rev.*, D67:094005, 2003.

[137] D.I. Olive R.J. Eden, P.V. Landshoff and J.C. Polkinghorne. The Analytic S-Matrix. Reading, Great Britain: Cambridge (1966) pp 39-57.

[138] Ira Z. Rothstein. Factorization, power corrections, and the pion form factor. *Phys. Rev.*, D70:054024, 2004.

[139] L. H. Ryder. QUANTUM FIELD THEORY. Cambridge, Uk: Univ. Pr. (1985) 443p.

[140] Matthew D. Schwartz. Resummation and NLO Matching of Event Shapes with Effective Field Theory. *Phys. Rev.*, D77:014026, 2008.

[141] G. Sterman. Infrared divergences in perturbative qcd. (talk). 1981. In *Tallahassee 1981, Proceedings, Perturbative Quantum Chromodynamics*, 22-40.

[142] George Sterman. Partons, factorization and resummation. . 1995.

[143] N. A. Sveshnikov and F. V. Tkachov. Jets and quantum field theory. *Phys. Lett.*, B382:403–408, 1996.

[144] Gerard t Hooft. A Two-Dimensional Model for Mesons. *Nucl. Phys.*, B75:461, 1974.

[145] Michael Trott. Jets in effective theory: Summing phase space logs. *Phys. Rev.*, D75:054011, 2007.

[146] Andre van Hameren, Jens Vollinga, and Stefan Weinzierl. Automated computation of one-loop integrals in massless theories. *Eur. Phys. J.*, C41:361–375, 2005.

[147] E. V. Veliev. Obtaining gluon propagator with Leibbrandt-Mandelstam prescription. *Phys. Lett.*, B498:199–202, 2001.

[148] Bryan R. Webber. QCD power corrections from a simple model for the running coupling. *JHEP*, 10:012, 1998.

Appendix A

Diagrammatic proof of the equivalence of QCD and SCET with one collinear direction

In the main body of Chapter 2 we have shown that any collinear SCET diagram can be obtained using a gener- ating functional in which the interactions between the fields are equivalent to full QCD, but the external cur- rents are modified to contain projection operators. This relation was first discussed in [14] and used in [28] to calculate jet functions in SCET. In this appendix we want to prove this identity diagrammatically for the correlator containing two collinear fermions and N collinear gluons.

We will accomplish this by working out in both theories the Feynman diagrams for N gluons coupled to a fermion line, from which the correlator can be constructed. Using this result we will then show that both of these calculations lead to equivalent answers. Note that there are $N!$ possible color structures, and for each of them the QCD result has to equal the SCET result. We begin by showing this equivalence for the color structure $T^{a_1} T^{a_2} \ldots T^{a_N}$, and then discuss how the result can be modified to include the other color structures as well.

Define $Q^{(N)}$ and $S^{(N)}$ to be the QCD and SCET cor- relators for this color structure in momentum space, multiplied by a factor of p_i^2 for each internal propagator and with the factor g_s^N removed. This gives

$$Q^{(N)} = P_n \bar{\not{p}}_0 \gamma^{\mu_1} \bar{\not{p}}_1 \ldots \gamma^{\mu_N} \bar{\not{p}}_N P_{\bar{n}} \,, \tag{A.1}$$

$$S^{(N)} = \sum_{k=1}^{N} S^{(N-k)} L_k \,. \tag{A.2}$$

The first equation follows simply from the QCD Feynman rules, while the SCET equation is a recurrence formula, that takes into account all the possibilities of having k out of the N gluons being emitted from a single vertex. L_k is therefore the Feynman rule for k-gluon emissions from a single vertex, multiplied by a factor of $\prod_i p_i^2/g_s$ to account for the removal of the factors p_i^2 and g_s, as discussed above:

$$L_k \frac{\bar{n}\!\!\!/}{2} = i(\bar{n}\cdot p_N) \frac{p_{N-k+1}^2 \cdots p_{N-1}^2}{(-g)^k} V_k \,, \tag{A.3}$$

with

$$V_k = \frac{i(-g)^k \bar{n}^{\mu_{N-k+2}} \dots \bar{n}^{\mu_{N-1}}}{\bar{n}\cdot p_{N-k+1} \dots \bar{n}\cdot p_{N-1}} \frac{\not{\bar{n}}}{2} \times \tag{A.4}$$
$$\times \Big(\gamma_\perp^{\mu_{N-k+1}} \gamma_\perp^{\mu_N} - \bar{n}^{\mu_N} \gamma_\perp^{\mu_{N-k+1}} \frac{\not{p}_N^\perp}{\bar{n}\cdot p_N} +$$
$$+ \frac{\not{p}_{N-k}^\perp \not{p}_N^\perp}{\bar{n}\cdot p_{N-k} \bar{n}\cdot p_N} \bar{n}^{\mu_{N-k+1}} \bar{n}^{\mu_N} - \bar{n}^{\mu_{N-k+1}} \frac{\not{p}_{N-k}^\perp \gamma_\perp^{\mu_N}}{\bar{n}\cdot p_{N-k}} \Big) .$$

We will show the equivalence $Q^{(N)} = S^{(N)}$ by induction. For $N = 0$ it is straightforward:

$$Q^{(0)} = P_n \not{p}_0 P_{\bar{n}} = \frac{\not{n}}{2} \bar{n}\cdot p_0, \tag{A.5}$$

$$S^{(0)} = \frac{\not{n}}{2} \bar{n} p_0 = Q^{(0)} . \tag{A.6}$$

Next, we assume that the statement $Q = S$ holds for $0, 1, \dots N-1$ to show that this leads to $Q^{(N)} = S^{(N)}$. This implies

$$Q^{(N)} = \sum_{k=1}^{N} Q^{(N-k)} L_k . \tag{A.7}$$

To prove Eq. (A.7) we rewrite the general QCD correlator $Q^{(N)}$ by pushing the projection operator P_n in Eq. (A.1) through the $\not{p}_n$ and γ^{μ_n}, to obtain

$$Q^{(N)} = \frac{\not{n}}{2} \sum_{m=0}^{N} \sum_{l=1}^{C_{2N+1}^{2m}} \chi_{i_1 \dots i_{2m}}^{2m,2N+1} , \tag{A.8}$$

where

$$\chi_{i_1 \dots i_{2m}}^{2m,2N+1} = (-1)^{i_1 + \dots + i_{2m} - (1 + \dots + 2m)} \perp_{i_1} \cdots \perp_{i_{2m}}$$
$$\times (\bar{n}_{j_1} n_{j_2} \bar{n}_{j_3} \dots n_{j_{2N-2m}} \bar{n}_{j_{2N+1-2m}}) . \tag{A.9}$$

Here C_k^l denotes the binomial coefficient for l choose k, and we have used a shorthand notation in which $\bar{n}_j$ corresponds to $\bar{n}\cdot p$ for even j and to $\bar{n}^\mu$ for odd j and accordingly $\perp_j$ corresponds to $\not{p}_\perp$ for even j, while $\gamma_\perp^\mu$ for odd j.

We would like to comment on how we obtained this result. Expanding each γ matrix on the right hand side of the Eq. (A.1) according to $\gamma^\alpha = \bar{n}^\alpha \frac{\not{n}}{2} + n^\alpha \frac{\not{\bar{n}}}{2} + \gamma_\perp^\alpha$ will result in terms with fixed number $0 \le N_\perp \le 2N+1$ of $\gamma_\perp$'s, together with $(2N + 1 - N_\perp)$ of $\not{n}$ or $\not{\bar{n}}$. Since the $\not{n}$ and $\not{\bar{n}}$ terms have to alternate, and the projection operator forces the first and last term to be $\not{n}$, $N_\perp$ has to be an even number.

As a next step, we work out the sum on the right hand side of Eq. (A.7). Note that the term L_k contains factors of p_i^2 in the numerators, while there are no such terms on the left hand side of Eq. (A.7). However, both $Q^{(N-k)}$ and L_k contain terms with $\not{p}_\perp$, which can lead to $p_\perp^2 = p^2 - n\cdot p\, \bar{n}\cdot p$. After a straightforward, but lengthy calculation, one can show that

$$\sum_{k=1}^{N} Q^{(N-k)} L_k = \frac{\not{n}}{2} \sum_{m=0}^{N} \sum_{l=1}^{C_{2N+1}^{2m}} \chi_{i_1 \dots i_{2m}}^{2m,2N+1} . \tag{A.10}$$

Thus, both sides of Eq. (A.7) are equal and we have thus shown that $Q^{(N)} = S^{(N)}$ for all values of N.

So far we have only dealt with the term with color structure $T^{a_1} \dots T^{a_N}$. Keeping the general color structure allows us to write

$$Q^{(N)} \to \sum_{l=1}^{N!} Q^{(N)}_{i_1 \dots i_N} T^{a_{i_1}} \dots T^{a_{i_N}} \,, \tag{A.11}$$

$$S^{(N)} \to \sum_{l=1}^{N!} S^{(N)}_{i_1 \dots i_N} T^{a_{i_1}} \dots T^{a_{i_N}} \,. \tag{A.12}$$

What we have shown so far is that $Q^{(N)}_{1,2,\dots,N} = S^{(N)}_{1,2,\dots,N}$. However, it is clear that the proof goes through for any color permutation, with obvious replacements to account for the different orderings of the gluons. Finally, notice that triple or quartic gluon vertices do not change the result, since they are the same in QCD and SCET. This completes the proof.

Appendix B

Relation Among Hard, Jet, Soft, and Cusp Anomalous Dimensions

In Eq. (3.92) we used that the $\Gamma_F[\alpha_s]$ part of the jet or soft function anomalous dimension, defined in Eq. (3.85), is proportional to the cusp anomalous dimension $\Gamma_{\rm cusp}$ to all orders in α_s. This fact is well known for the standard $a = 0$ jet function and soft functions. In this section we verify that this relation remains true for all a. Our strategy will be to show that $\Gamma_{J,S}[\alpha_s]$ must always remain proportional to $\Gamma_H[\alpha_s]$, which is independent of a and is already known to be proportional to $\Gamma_{\rm cusp}$.

The consistency of the factorization theorem Eq. (3.18) requires a relation among the hard, jet, and soft function renormalization counterterms, and, thus, among the anomalous dimensions (see, e.g., [37, 87]). This relation can be derived by requiring that Eq. (3.18) remain true when written in terms of either the bare or renormalized hard, jet, and soft functions on the right-hand side. This requires that

$$Z_H^{-1}(\mu)\delta(\tau_J - \tau_S) = \int \mathrm{d}\tau' \int \mathrm{d}\tau'' Z_J(\tau_J - \tau';\mu) Z_J(\tau' - \tau'';\mu) Z_S(\tau'' - \tau_S;\mu)\,, \tag{B.1}$$

to all orders in α_s. To $\mathcal{O}(\alpha_s)$, we can easily verify this relation using Eqs. (3.31), (3.43), and (3.64) with $Z_H(\mu) = |Z_{\mathcal{O}}(\mu)|^{-2}$. This relation amongst the counterterms requires in turn that the anomalous dimensions satisfy

$$-\gamma_H(\mu)\delta(\tau) = 2\gamma_J(\tau;\mu) + \gamma_S(\tau;\mu)\,. \tag{B.2}$$

To all orders in α_s the hard anomalous dimension takes the form of Eq. (3.72) and the jet and soft anomalous dimensions take the general form of Eq. (3.85) [95] , where the constant j_F is $j_J = 1/(2-a)$ for the jet function and $j_S = 1$ for the soft function. The constraint Eq. (B.2) then requires the three independent relations

$$0 = \frac{4}{j_J}\Gamma_J[\alpha_s] + \frac{2}{j_S}\Gamma_S[\alpha_s]\,, \tag{B.3}$$

$$-\Gamma_H[\alpha_s] = 2\Gamma_J[\alpha_s] + \Gamma_S[\alpha_s]\,, \tag{B.4}$$

$$-\gamma_H[\alpha_s] = 2\gamma_J[\alpha_s] + \gamma_S[\alpha_s]\,, \tag{B.5}$$

to all orders in α_s. These relations can be verified to $\mathcal{O}(\alpha_s)$ from Eq. (3.71) and Table 3.1. The first two relations Eqs. (B.3) and (B.4) taken together imply that

$$\Gamma_S[\alpha_s] = \frac{1}{1-a}\Gamma_H[\alpha_s]\,, \qquad \Gamma_J[\alpha_s] = -\frac{1-a/2}{1-a}\Gamma_H[\alpha_s]\,, \tag{B.6}$$

to all orders in α_s and for all $a < 1$. Since $\Gamma_H[\alpha_s] \propto \Gamma_{\rm cusp}$ and is independent of a, both $\Gamma_{S,J}[\alpha_s] \propto \Gamma_{\rm cusp}$ as well.

Appendix C

Evaluation of Resummed Jet and Soft Functions and Full Distribution

To evaluate the resummed jet and soft functions, we used the following method. First, note that from the expressions for the evolution equation, Eq. (3.88), the form of the evolution kernel, Eq. (3.89), and the generic form of the NLO jet and soft functions,

$$F(\tau;\mu_0) = c_1\delta(\tau) + c_2\left(\frac{1}{\tau}\right)_+ + c_3\left(\frac{\ln\tau}{\tau}\right)_+ , \tag{C.1}$$

the resummed jet and soft functions are proportional to

$$F(\tau;\mu) \propto \int \mathrm{d}\tau' \left[\frac{\theta(\tau-\tau')}{(\tau-\tau')^{1+\omega}}\right]_+ F(\tau';\mu_0) = c_1 W_1 + c_2 W_2 + c_3 W_3 \,, \tag{C.2}$$

where

$$\begin{aligned} W_1 &= \int \mathrm{d}\tau' \left[\frac{\theta(\tau-\tau')}{(\tau-\tau')^{1+\omega}}\right]_+ \delta(\tau') \,, \\ W_2 &= \int \mathrm{d}\tau' \left[\frac{\theta(\tau-\tau')}{(\tau-\tau')^{1+\omega}}\right]_+ \left[\frac{\theta(\tau')}{\tau'}\right]_+ \,, \\ W_3 &= \int \mathrm{d}\tau' \left[\frac{\theta(\tau-\tau')}{(\tau-\tau')^{1+\omega}}\right]_+ \left[\frac{\theta(\tau')\ln(\tau')}{\tau'}\right]_+ . \end{aligned} \tag{C.3}$$

Next, note that from the definitions of the plus functions, Eqs. (3.40) and (3.91), we can find W_i as the coefficient of δ^i in the Taylor series of $W(\delta)$, where $W(\delta)$ is defined as

$$W(\delta) \equiv \int \mathrm{d}\tau' \left[\frac{\theta(\tau-\tau')}{(\tau-\tau')^{1+\omega}}\right]_+ \left[\frac{\theta(\tau')}{\tau'^{1+\delta}}\right]_+ = \frac{\Gamma(-\omega)\Gamma(-\delta)}{\Gamma(-\omega-\delta)} \left[\frac{\theta(\tau)}{\tau^{1+\omega+\delta}}\right]_+ . \tag{C.4}$$

Eq. (C.4) follows from the fact that

$$\int \mathrm{d}\tau'' \left[\frac{\theta(\tau-\tau'')}{(\tau-\tau'')^{1+\omega_1}}\right]_+ \left[\frac{\theta(\tau''-\tau')}{(\tau''-\tau')^{1+\omega_2}}\right]_+ = \frac{\Gamma(-\omega_1)\Gamma(-\omega_2)}{\Gamma(-\omega_1-\omega_2)} \left[\frac{\theta(\tau-\tau')}{(\tau-\tau')^{1+\omega_1+\omega_2}}\right]_+ . \tag{C.5}$$

By expanding both sides of Eq. (C.4) in δ and comparing like powers of δ, we find that

$$W_1 = \left[\frac{\theta(\tau)}{\tau^{1+\omega}}\right]_+, \qquad W_2 = \left[\left(\ln(\tau) - H(-1-\omega)\right)\left(\frac{\theta(\tau)}{\tau^{1+\omega}}\right)\right]_+,$$
$$W_3 = \left[\left(\frac{1}{2}\ln^2(\tau) - \ln(\tau)H(-1-\omega) + \frac{\pi^2}{12} + \frac{1}{2}H(-1-\omega)^2 - \frac{1}{2}\psi^{(1)}(-\omega)\right)\left(\frac{\theta(\tau)}{\tau^{1+\omega}}\right)\right]_+. \tag{C.6}$$

Here, $H(z)$ is the harmonic number function and $\psi^{(\nu)}(z)$ is the polygamma function.

The same technique can be used to analytically calculate the fully resummed cross-section, Eq. (3.18), directly from the unresummed jet and soft functions. The resummed cross-section is of the form

$$\frac{1}{\sigma_0}\frac{\mathrm{d}\sigma}{\mathrm{d}\tau}^{\mathrm{PT}} \propto \prod_{i=1}^{3}\left(\int \mathrm{d}\tau_i\, \mathrm{d}\tau_i'\, F_i(\tau_i';\mu_i)\left[\frac{\theta(\tau_i-\tau_i')}{(\tau_i-\tau_i')^{1+\omega_i}}\right]_+\right)\delta(\tau-\tau_1-\tau_2-\tau_3)\,. \tag{C.7}$$

where the jet and soft functions $F_i(\tau_i,\mu_i)$ are all of the form given in Eq. (C.1). These integrals can be done most easily by replacing the $F_i(\tau_i;\mu_i)$ on the right-hand side of Eq. (C.7) with $\left[\theta(\tau)/\tau^{1+\delta_i}\right]_+$, expanding in δ_i before and after combining all the plus distributions using Eq. (C.5), and comparing like powers of the δ_i. The result for the resummed cross-section Eq. (3.95) then follows.

Appendix D

Angularity Distribution in QCD to $\mathcal{O}(\alpha_s)$

In Sec. 6 we matched the NLL resummed two-jet angularity distributions in SCET onto the $\mathcal{O}(\alpha_s)$ fixed-order distributions in full QCD using the remainder function $r_a(\tau_a)$, defined in Eq. (3.104). In this section we provide some details of how we calculate the QCD contribution to $r_a(\tau_a)$ away from $\tau_a = 0$, $A_a(\tau_a)$. In the process, we show that for $a \lesssim -1.9$ the angularities of events with more two-jet like kinematics become degenerate with those of more three-jet like events and contribute to the same τ_a, and that for $a \lesssim -2.6$ the maximally symmetric three-jet event contributes to a smaller τ_a then some more two-jet like events. Thus, for small enough a, angularities fail to separate two-jet and three-jet like events.

Both the one loop $q\bar{q}$ and tree-level $q\bar{q}g$ final states contribute to $\mathrm{d}\sigma/\mathrm{d}\tau_a$ at $\mathcal{O}(\alpha_s)$. However, the $q\bar{q}$ final states' contribution is proportional to $\delta(\tau_a)$ and hence only contributes to A_a^δ. Thus to find $A_a(\tau_a)$ we only need to consider the tree-level $q\bar{q}g$ final states. Their contribution can be writtten as

$$\frac{1}{\sigma_0}\frac{\mathrm{d}\sigma}{\mathrm{d}\tau_a}^{q\bar{q}g} = \Big(\frac{\alpha_s}{2\pi}\Big)\, A_a(\tau_a)\,, \tag{D.1}$$

where

$$A_a(\tau_a) = C_F \int \mathrm{d}x_1\, \mathrm{d}x_2\, \frac{x_1^2 + x_2^2}{(1-x_1)(1-x_2)} \delta\big(\tau_a - \tau_a(x_1, x_2)\big)\,, \tag{D.2}$$

and where $x_{1,2} \equiv 2E_{1,2}/Q$ are the energy fractions of any two of the three final-state partons. By momentum conservation, $x_1 + x_2 + x_3 = 2$. For a three-particle final state, the thrust axis is given by the direction of the particle with the largest energy. The $x_{1,2}$ phase space can be divided into three regions, as illustrated in Fig. D.1A, according to which parton has the largest energy. In the region in which x_i is larger than $x_{j,k}$, the angularity $\tau_a(x_1, x_2)$ is given by

$$\tau_a(x_1, x_2)\Big|_{x_i > x_{j,k}} = \frac{1}{x_i}(1-x_i)^{1-a/2}\left[(1-x_j)^{1-a/2}(1-x_k)^{a/2} + (1-x_j)^{a/2}(1-x_k)^{1-a/2}\right]. \tag{D.3}$$

At each fixed value of $\tau_a = c$ in the distribution Eq. (D.1), the delta function restricts the integral over $x_{1,2}$ to a linear contour determined by the equation $\tau_a(x_1, x_2) = c$, where $\tau_a(x_1, x_2)$ is given by Eq. (D.3). Examples of these integration contours are shown in Fig. D.1B.

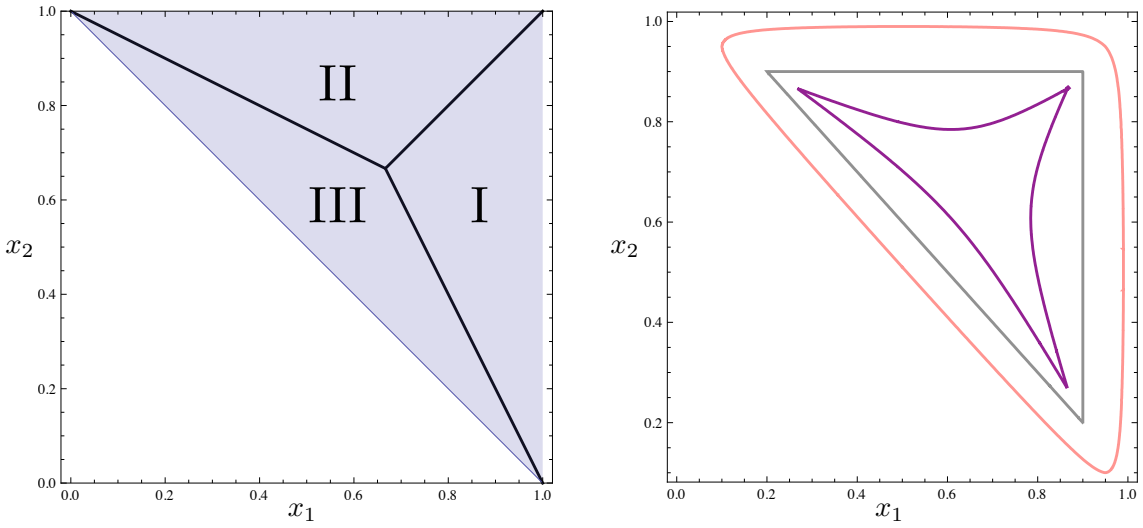

(A) (B)

Figure D.1: (A) Phase space for three-particle $q\bar{q}g$ final state. The energy fractions $x_i = 2E_i/Q$ of the three particles satisfy $x_1 + x_2 + x_3 = 2$. In region I, $x_1 > x_{2,3}$, in region II, $x_2 > x_{1,3}$, and in region III, $x_3 > x_{1,2}$. The thrust axis is in the direction of the particle with the largest energy. (B) Contours of constant $\tau_a = 1/10$ for $a = -1$ (purple), $a = 0$ (gray), and $a = 1$ (pink). The differential cross-section $\mathrm{d}\sigma/\mathrm{d}\tau_a$ is given by integrals over these contours in the $x_{1,2}$ phase space.

It is sufficient to consider the part of the phase space corresponding to region III shown in Fig. D.1, where $x_3 > x_{1,2}$. Integration over the remaining two regions can be related to the integration over region III by a trivial shift of variables of integration. Thus we need to solve

$$c = \frac{1}{2 - x_1 - x_2}(x_1 + x_2 - 1)^{1-a/2}\left[(1-x_1)^{1-a/2}(1-x_2)^{a/2} + (1-x_1)^{a/2}(1-x_2)^{1-a/2}\right], \quad \text{(D.4)}$$

where $x_{1,2}$ lie in region III. To find an explicit one-variable parameterization for $x_{1,2}(w)$ which satisfies Eq. (D.4), we first absorb the factor $1/(2 - x_1 - x_2)$ inside the brackets and define

$$w \equiv \frac{1 - x_1}{2 - x_1 - x_2}. \quad \text{(D.5)}$$

In terms of w, Eq. (D.4) can be written as

$$c = (x_1 + x_2 - 1)^{1-a/2}\left[w^{1-a/2}(1-w)^{a/2} + w^{a/2}(1-w)^{1-a/2}\right]. \quad \text{(D.6)}$$

Solving Eqs. (D.5, D.6) for x_1, x_2 gives:

$$x_1(w) = 1 - w + w\left(\frac{c}{w^{1-a/2}(1-w)^{a/2} + w^{a/2}(1-w)^{1-a/2}}\right)^{\frac{1}{1-a/2}},$$
$$x_2(w) = x_1(1-w). \quad \text{(D.7)}$$

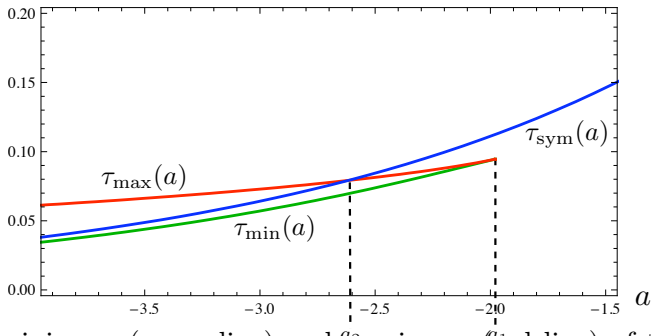

Figure D.2: The local minimum (green line) and maximum (red line) of the function $F_a(w)$ over the range $0 < w < 1/2$ coincide at the point $a \equiv a_1 \approx -1.978$. At $a \equiv a_2 \approx -2.618$, the value of angularity for the maximally symmetric three-jet case, $\tau_{\rm sym}(a) = 1/3^{1-a/2}$ (blue line), intersects the local maximum and so for $a < a_2$, the value of maximum angularity for such a corresponds not to the maximally symmetric case but to a more two-jet like event.

Clearly from Eq. (D.5), w lies in the interval $0 \le w \le 1$. The precise range of values for w is determined from the conditions $x_1(w) \le 2 - x_1(w) - x_2(w)$ and $x_2(w) \le 2 - x_1(w) - x_2(w)$. These inequalities can be simplified to

$$c \le \min\{F_a(w), F_a(1-w)\} = \begin{cases} F_a(w) & \text{for} \quad 0 \le w \le 1/2 \\ F_a(1-w) & \text{for} \quad 1/2 \le w \le 1 \end{cases}, \tag{D.8}$$

where

$$F_a(w) \equiv \frac{w(1-w)^{a/2}}{(1+w)^{1-a/2}}(w^{1-a} + (1-w)^{1-a})\,. \tag{D.9}$$

The function $F_a(w)$ is monotonically increasing over the range $0 < w < 1/2$ only for $2 > a \ge a_1 \approx -1.978$, but for $a < a_1$ turns out to have exactly one local maximum, $\tau_{\rm max}(a)$, and one local minimum, $\tau_{\rm min}(a)$. At $a = a_2 \approx -2.618$, $\tau_{\rm max}(a)$ is equal to the angularity of the symmetric three-jet configuration $x_1 = x_2 = x_3$ (where $w = 1/2$), $\tau_{\rm sym}(a) = 1/3^{1-a/2}$. Thus, the global maximum of τ_a over the whole range $0 \le w \le 1$, defined as $\tau_a^{\rm max}$, is $\tau_{\rm max}(a)$ for $a \le a_2$ and is $\tau_{\rm sym}(a)$ for $a \ge a_2$.

In Fig. D.2, we show how the maximum and minimum of the function $F_a(w)$ depend on a, along with the a dependence of the symmetric three-jet configuration, and plot the special points a_1 and a_2.

In Fig. D.3 we plot the boundary of τ_a ($F_a(w)$ for $0 \le w \le 1/2$ and $F_a(1-w)$ for $1/2 \le w \le 1$) together with the contours of constant $\tau_a(x_1, x_2) = c$ for different values of c in the full x_1-x_2 plane for the cases $a = -1$, $a = -2.3$, and $a = -4$, which qualitatively represent the three cases $a > a_1$, $a_1 > a > a_2$, and $a_2 > a$, respectively. From this analysis we conclude that for $a < a_1$ and especially $a < a_2$ angularities fail to separate two-jet like and three-jet like events.

To obtain $A_a(\tau_a)$, we evaluate the integral in Eq. (D.1) over the appropriate contours in the $x_{1,2}$ phase space numerically, except for $a = 0$, for which the integral can be evaluated

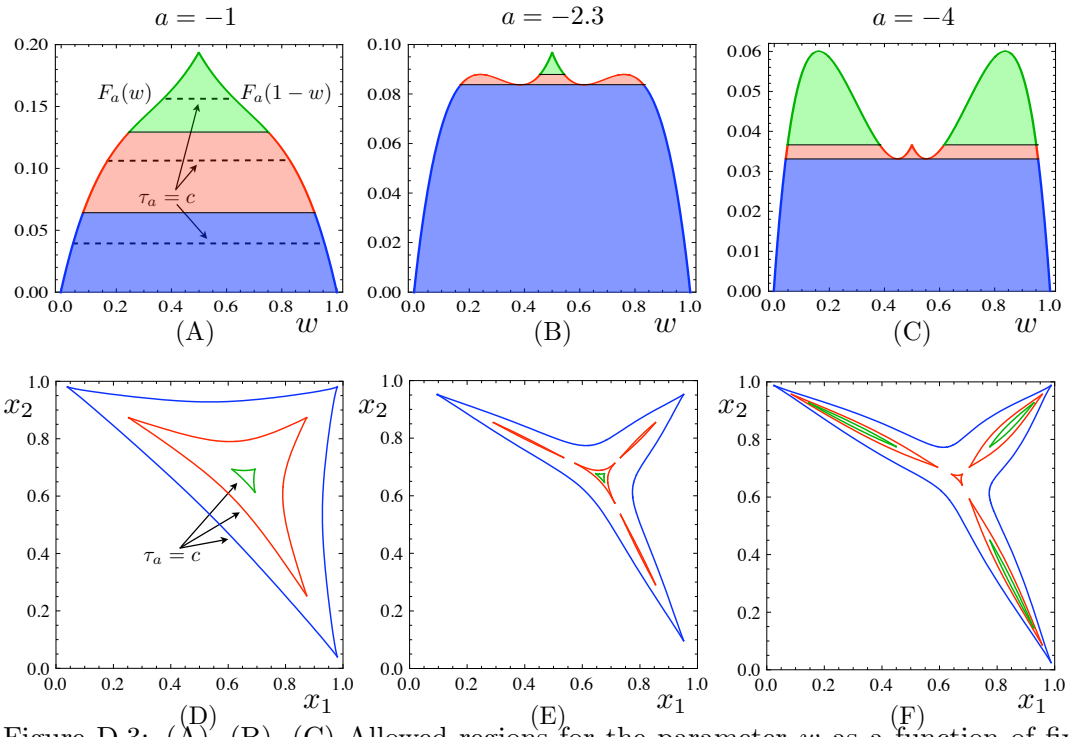

Figure D.3: (A), (B), (C) Allowed regions for the parameter w as a function of fixed $\tau_a = c$ are bounded by the curves $F_a(w)$ and $F_a(1-w)$. For (A), (D) $a = -1$, the integration is over a single, continuous domain for all fixed $\tau_a = c$ but for (B), (E) $a = -2.3$ and (C), (F) $a = -4$, there are multiple disjoint regions of integration for large enough values of c. In (D), (E), and (F), the blue, red, and green curves represent contours of integration for fixed $\tau_a = c$, in order of increasing c, and correspond to integration over a range of w given by the lines of constant $\tau_a = c$ in the regions of the same color in (A), (B) and (C), respectively.

analytically, giving (cf. [74])

$$A_0(\tau_0) = C_F \left[\frac{2(2 - 3\tau_0 + 3\tau_0^2)}{\tau_0(1-\tau_0)} \ln\left(\frac{1-2\tau_0}{\tau_0}\right) - \frac{3(1-3\tau_0)(1+\tau_0)}{\tau_0} \right] . \tag{D.10}$$